Recent and future drying of the Mediterranean region: anthropogenic forcing, natural variability and social impacts

Colin P. Kelley

Submitted in partial fulfillment of the requirements for the degree of
Doctor of Philosophy in the Graduate School of Arts and Sciences

COLUMBIA UNIVERSITY

2014

ABSTRACT

Recent and future drying of the Mediterranean region: anthropogenic forcing, natural variability and social impacts

Colin P. Kelley

The Mediterranean region has experienced persistent drying since the middle of the 20th Century and global climate models project further drying in the future as a consequence of increasing greenhouse gases. The Mediterranean region is also known to oscillate between decades of relatively wet and dry conditions due to the strong influence of multidecadal North Atlantic Oscillation (NAO). It is therefore of great importance to understand the relationship between forced long-term drying resulting from human influences and those due to natural variability. To this end, we used observations, reanalyses and comprehensive global climate models in this thesis research.

The roles of anthropogenic climate change and internal climate variability in causing the Mediterranean region's late 20th Century extended winter drying trend were examined using 20th Century observations as well as 19 coupled climate models from the CMIP3. The drying was strongly influenced by the robust positive trend in the NAO from the 1960s to the 1990s. Model simulations and observations were used to assess the probable relative roles of radiative forcing and internal variability in explaining the circulation trend that drove much of the precipitation change. It was concluded that the radiatively forced trends were a small fraction of the total observed trends. Instead it was argued that the robust trends in the observed NAO and Mediterranean rainfall during this period were largely due to multidecadal internal variability with a small contribution from the external forcing. Differences between the observed and NAO associated precipitation trends are consistent with those expected as a response to radiative forcing. The radiatively forced trends in circulation and precipitation are expected to strengthen in the current century and these results highlight the importance of their contribution to

future precipitation changes in the region.

The Mediterranean precipitation climatology and trend were further examined by comparing the newest generation of global climate models (CMIP5) used in the Intergovernmental Panel on Climate Change (IPCC) Fifth Assessment Report, to the previous generation (CMIP3) and to observations over the latter half of the 20th Century for both the summer and winter half years. The observed drying trend since 1950 was predominantly due to winter drying, with very little contribution from the summer. However, in the CMIP5 multimodel mean, the precipitation trend since 1950 is evenly divided throughout the seasonal cycle. This may indicate that in observation, multidecadal internal variability, particularly that associated with the NAO, dominates the wintertime trend. An estimate of the observed externally forced trend showed that winter drying dominated in observations but the spatial patterns were grossly similar to the multimodel mean trend. The similarity was particularly robust in the eastern Mediterranean region, indicating a radiatively forced component being stronger there. These results also revealed modest improvement for the CMIP5 multimodel ensemble in representation of the observed six-month winter and summer climatology.

We further explored the detailed mechanisms leading to the NAO-associated precipitation change, such as the role of the change in mean circulation versus that of the storm tracks in the regional moisture budget, which had not been investigated previously. We employed a moisture budget analysis using 15 CMIP5 models and the ERA-Interim Reanalysis to investigate the relationship between the NAO and the various moisture budget terms for the six-month winter and summer. Compared with the ERA-Interim, the models performed well in their simulation of the relationship between the naturally varying NAO and the large-scale moisture budget. Our results indicated that the shift in the midlatitude transient eddies induced modest moisture convergence, rather than divergence, over the Mediterranean under a positive NAO. The reduction in precipitation in this region during a positive NAO was dominated by the mean moisture divergence, which opposed the transient contribution. There were significant differences between the patterns of NAO-induced moisture budget anomaly and changes due to external radiative forcing. Under radiative forcing there was enhanced evaporation over the Mediterranean Sea, Italy and eastern Europe and drying by the shift in the wintertime storms over nearly

all of Europe and the Mediterranean. Under a positive phase of the NAO, on the other hand, there was modest reduction in evaporation and wetting by the storms over the Mediterranean, and drying over northern Europe. The dependence of the Mediterranean moisture budget on the NAO was similarly explored in the summer half of the year and in this season the models exhibited more disagreement with observations, but otherwise showed the similar results as winter.

The stronger anthropogenic induced drying signal over the eastern Mediterranean provided a basis to examine the possible cause and impact of the recent severe and persistent drought in Syria that occurred directly prior to the uprising of 2011. The drought devastated Syrian agriculture, resulting in food shortages, widespread unemployment, the collapse of rural social structure and a mass migration of agricultural refugees to Syria's urban areas. Anger at the government's failure to ameliorate conditions was one spark for the uprising that evolved into civil war. We found that though droughts occur periodically in Syria due to natural causes it is likely that the recent drought was more extreme due to the century long drying trend caused by increased radiative forcing. It was estimated that the anthropogenic trend made a drought of such severity several times more likely. Droughts as persistent as the recent one are projected to be commonplace in a future warmer world.

Contents

List of Tables

List of Figures

Commonly used acronyms

NAO - North Atlantic Oscillation

IPCC – Intergovernmental Panel on Climate Change

CMIP3 – Coupled Model Intercomparison Project Three

CMIP5 – Coupled Model Intercomparison Project Five

GCMs – global climate models

GHG – greenhouse gases

CO_2 - carbon dioxide

SST – sea surface temperature

SLP – sea level pressure

Acknowledgements

I owe a tremendous debt of gratitude to my Ph.D. advisors, Dr. Mingfang Ting and Dr. Richard Seager, and to my third committee member Dr. Yochanan Kushnir, for their mentorship, support, encouragement and passion, from the moment I first embarked on my research path to the completion of this dissertation. I also wish to thank Dr. Martin Hoerling and Dr. Ronald Miller for kindly agreeing to serve on my thesis committee.

I would like to extend my kind regards to Dr. Mark Cane for the benefit of his time, knowledge and experience, and for his infectious passion for the applied study of climate and its relationship to society.

I also want to thank the other members of the Division of Ocean and Climate Physics at the Lamont-Doherty Earth Observatory, particularly Naomi Henderson, Lawrence Rosen, Haibo Liu, Yutian Wu, Wenchang Yang, Doug Martinson, and Jennifer Nakamura for their contributions to this work.

I would like to extend my gratitude to those members of the International Research Institute for Climate and Society and the greater Lamont community for their invaluable help and advice. I very much enjoyed working and collaborating with you all.

I would like to acknowledge and thank Shahrzad Mohtadi for her collaboration to the applied portion of this thesis.

Last but not least I wish to express my inestimable appreciation to those family and friends who were so supportive of me during this experience.

To those who encouraged and educated me, with
special dedication to Dorothy Smith.

Chapter 1

Introduction

The Mediterranean is a region of complex coastlines, orography and climate and the spatial and temporal variability of its rainfall are large. The word Mediterranean derives from the Latin *mediterraneus*, meaning "middle of the land," which describes the Mediterranean Sea as it lies between three of the world's continents, Europe, Asia and Africa. The Mediterranean Sea is connected to the Atlantic Ocean via the Strait of Gibraltar in the west and to the Black Sea and Red Sea in the east, via the Sea of Marmara and the Suez Canal, respectively. The climate of the Mediterranean region is characterized as semi-arid, with mild, rainy winters and hot, dry summers. In a given year, evaporation exceeds precipitation over water, while precipitation exceeds evaporation over land. Previous studies have contributed greatly to our understanding of the mechanisms that influence precipitation variability in this region on different timescales (Barnston and Livezey, 1987; Hurrell, 1995; Thompson and Wallace, 2000; Hurrell et al., 2003; Dunkeloh and Jacobeit, 2003; Mariotti and Dell'Aquila, 2012). It is expected that as a consequence of increasing greenhouse gases the Mediterranean region will become drier as the locations of the mean flow and the storm tracks change. In this semi-arid region of stressed water resources future drying is of tremendous importance to those who live in the region. Future decreases in precipitation would have important socio-economic consequences (Schwartz and Ibaraki 2011) for this and other semi-arid regions, such as the American southwest. Our primary tools for projection of future climate are the state-of-the-art global climate models (GCMs). In this thesis we employ two generations of models used in the Intergovernmental Panel on Climate Change

(IPCC) Fourth and Fifth Assessment Reports (AR4 and AR5), the Coupled Model Intercomparison Projects Three (CMIP3) and Five (CMIP5), respectively.

Figure 1.1 compares the projected global precipitation change over the 21st Century for the CMIP3 models, based on the A1B or "middle-of-the-road" scenario, and the CMIP5 models, based on the rcp85 representative concentration pathway, representing increases in radiative forcing of 6 and 8.5 W/m^2 respectively by the end of the 21st Century, for the six-month winter (Nov-Apr) and summer (May-Oct) seasons. All panels represent the multimodel mean, 24 models in the CMIP3 case, and 36 models in the CMIP5, one run for each model. Averaging over a multimodel ensemble gives a measure of the average model response to the imposed forcing. We can easily see a general increase in tropical rainfall and a broad decrease in precipitation over much of the

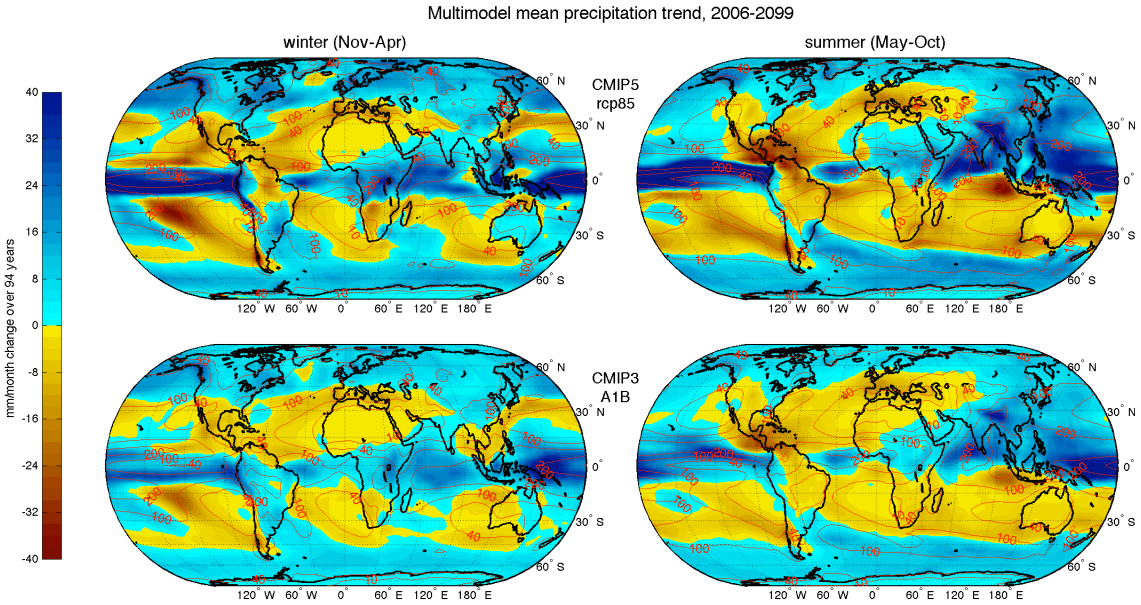

Figure 1.1: Global precipitation change over the 21st Century (2006-2099) based on a linear best fit, for six-month winter and summer. Top panels are the CMIP5 multimodel mean (36 models) under the rcp85 representative concentration pathway, and bottom is the CMIP3 (24 models) under the A1B scenario, using one run from each model. Shading represents precipitation change and red contours the climatology from 2006-2025. Units are in mm/month.

subtropics, in both seasons. The Mediterranean region is predicted to dry strongly in the future, often been referred to as a "hotspot" of future precipitation change (Giorgi, 2006),

and this future drying is clear from the figure. The CMIP5 and CMIP3 projections agree that the Mediterranean will experience robust drying during the 21st Century. The observed Mediterranean drying trend since the middle of the 20th Century leads us to ask: is the observed drying anthropogenic or natural?

The relative contributions of long-term anthropogenic forcing, due to increasing carbon dioxide (CO_2), and multidecadal natural variability to recent and future drying, is complex and not well understood. One purpose of this thesis work is to determine how much of the Mediterranean drying in recent decades was due to natural multidecadal variability associated with the NAO versus the emerging response to increased radiative forcing, how this relationship varies across the region, and how it is projected to change in the future. Drying trends over periods of decades can result from phases of natural multidecadal or longer variability, external forcing or a combination of the two. In a warming world the atmosphere has a greater carrying capacity of water vapor. This intensifies water vapor transports and for purely thermodynamic reasons makes dry regions drier and wet regions wetter (Held and Soden, 2006; Seager et al., 2010). Dynamically it has also been shown that the midlatitude storm tracks and jet streams are expected to shift poleward under global warming (Wu et al., 2011; Yin et al. 2005; Bengtsson et al., 2006), along with an expansion of the global Hadley Cell (Lu et al., 2007, Previdi and Liepert, 2007). Second, previous studies have shown that the North Atlantic Oscillation (NAO), the dominant mode of sea-level pressure (SLP) variability over the North Atlantic domain and the dominant influence over European and Mediterreanean precipitation, exhibits variability on multidecadal timescales, causing decades of relatively wet or dry conditions there (Hurrell, 1995;, Mariotti and Dell'Aquila, 2012; Hurrell et al., 2003; Dunkeloh and Jacobeit, 2003). During positive phases of the NAO the mean flow and the storms shift poleward (Hurrell, 1995) resulting in more rainfall over northern Europe and reduced precipitation over the greater Mediterranean. The multidecadal variability of the NAO is clear in observations and trended steadily negative from the beginning of the 20th Century to the mid-1960s, then trended more sharply positive over the next thirty years, and then reversed again to trend to more negative values.

NAO variability on annual to interdecadal timescales arises from the internal dynamics of the extratropical atmosphere (Thompson et al., 2003). It has been debated whether multidecadal internal NAO variability alone can explain the strength of the recent strongly positive NAO trend from the 1960s to the 1990s (Schneider, 2003; Thompson et al., 2000; Thompson, 2003; Feldstein, 2002; Osborn, 2004; Gillett, et al., 2003), and interaction between the atmosphere and the extratropical and tropical oceans has also been invoked to explain low frequency NAO variability (Kushnir et al. 2006). Theory and model results have suggested that the NAO, as the North Atlantic's manifestation of the Northern Annular Mode, will trend toward its positive phase as a result of forcing by increasing greenhouse gases, and that this anthropogenic trend will be associated with a poleward shift in the midlatitude storm tracks, tropical Hadley Cell expansion and a general drying of the Mediterranean region (Previdi and Liepert, 2007). However, recent studies have shown that the North Atlantic jet and storm track will extend more to the northeast into Europe under radiative forcing, and that although this trend projects onto the NAO in the zonal mean across the basin, it cannot easily be characterized as an NAO shift since it has a different pattern (Simpson et al., 2013). Other model studies that imposed an increase in tropical SSTs, in particular Indian Ocean warming more than the tropical Pacific, explains roughly half of the amplitude of the late 20th Century upswing in the NAO, and produces clear Mediterranean drying (Hoerling et al. 2001, 2013; Hurrell et al. 2006). Hence these studies argued for a substantial role for global warming in Mediterranean region drying over recent decades. Additionally, rising temperatures will greatly impact this region through increased evaporation. The relative strengths of multidecadal natural phases of variability and anthropogenically forced drying thus needs to be thoroughly understood if we are to have a better predictive capacity for future drying in this and other regions.

There have been a number of approaches used to separate internal variability or *noise* from trend or *signal*, using observations, model results or both. One often-used approach is to assume linearity, and to linearly detrend or remove the linear best fit from a variable's timeseries. This does not allow for the possibility of a nonlinear response to the forcing, but the increase in atmospheric CO_2 has been. For such a short period as over several decades the forced trend can easily be obscured, or amplify or oppose a

natural variability trend, making discrimination difficult. Use of a suite of global climate models offers the ability to increase the sample size with which to determine the response to prescribed forcing. These models generate their own internal variability and cannot be expected to reproduce the variability of the real world over the past century. However, by taking the multimodel mean, the out-of-phase intermodel variability is suppressed, leaving behind the common, radiatively-forced signal. However, the use of many different models with possibly different responses to forcing and different amplitudes of natural variability means that natural variations cannot entirely be removed, and the forcing isolated, via this simple method. For these reasons, the approach used in this thesis utilizes the models to perform signal-to-noise (S/N) maximizing empirical orthogonal function (EOF) analysis (Allen and Smith 1997; Venzke et al. 1999; Chang et al. 2000; Ting et al. 2009) to determine the signal that the models have in common. This approach is preferable to using a multimodel mean not only because it eliminates contamination by noise resulting from the size of the sample, but also because it provides an optimized timeseries (signal) onto which the observations may be regressed. We begin by determining whether the observed 1960s to 1990s winter NAO and precipitation trends fall within the range of running thirty-year trends simulated by the IPCC AR4 CMIP3 models over the 20th Century. Using the same models we then employ the S/N maximizing EOF technique to estimate the externally forced signal and use regression to divide the observed winter trends in North Atlantic SLP and Mediterranean rainfall from 1960 to 1999 into internal and forced components.

The previous generation of GCMs from the CMIP3 is shown to be able to simulate the large-scale climatological features of Mediterranean region precipitation (see Figure 3.1). Increased spatial resolution in the newest generation, the CMIP5, in addition to other model advancements, potentially allows an improvement due to better representation of the complex topography of the region (Giorgi and Lionello, 2008). We examine the CMIP5 models to determine how well they perform in simulating Mediterranean precipitation climatology and trend spatially and in the seasonal cycle, and whether they represent modest improvement over CMIP3, possibly because of the increased horizontal resolution. Winter and summer Mediterranean precipitation trends since 1950 are then evaluated with respect to observations and the CMIP3 models. We

estimate the observed externally forced trend since 1950, as with the CMIP3 models before.

Climate models of the CMIP3 and CMIP5 project a robust drying of the Mediterranean region over the 21st Century, and a concomitant trend in North Atlantic SLP that projects strongly onto the positive phase of the NAO, and in the Northern Annular Mode due to radiative forcing (IPCC, 2007; Gillet et al., 2003; Giorgi and Lionello, 2008; Previdi and Liepert, 2007; Thompson et al., 2000). However, the dynamical mechanisms underlying the relationships between the greater Mediterranean moisture budget, and radiative forcing and NAO variability respectively, are not well understood, in particular the contributions to the total moisture divergence from the mean flow and the transients. The Mediterranean region is characterized by a climatological deficit (surplus) of precipitation minus evaporation (P-E) over water (land) that is balanced by a net atmospheric moisture divergence (convergence). Changes in the mean flow and eddies are known to be directly tied to anomalies in regional precipitation through the transport and convergence of atmospheric moisture (Hurrell, 1995). Seager et al. (2010, 2013) performed a breakdown of the moisture budget into these terms using the ERA Interim Reanalysis and a suite of CMIP5 models, further dividing the mean flow into terms related to mass divergence and moisture advection, and determined that the mass divergence was most important to the trend to increased atmospheric moisture divergence under global warming. This raises the question of whether the physical mechanisms of anthropogenic drying are the same, or different from, those of naturally-occurring, NAO-induced, drying. The prevailing consensus is that the poleward shift in the storm track and associated synoptic eddy activity during positive NAO phases is responsible for reduced precipitation over the Mediterranean and increased precipitation over northern Europe (Hurrell, 2003). However, the relative contributions of the mean and transients, and of the mass divergence and moisture advection, to the total NAO-induced variability has not been previously diagnosed. Trigo et al. (2000) showed a significant decrease in observed cyclone intensity but not frequency since 1960, and a decline in the strength of the most intense cyclones related to the poleward shift in the Atlantic storm track and positive NAO shift over this time. Another study showed an overall increase in observed evaporation from the Mediterranean Sea from 1958-2006,

primarily driven by SST warming (Mariotti, 2010). Another recent study found that the CMIP3 models were able to successfully simulate the locations of the two maxima of cyclone density in the Mediterranean, but that the models underestimate this density, likely due to limited spatial resolution (Ziv et al., 2013). Nonetheless it is worth examining whether coupled global climate models and reanalyses can be used to provide valuable insights into the dynamic and thermodynamic mechanisms associated with the Mediterranean moisture budget under the naturally-varying influence of the NAO. The moisture budget methodology has been successfully applied to the trend in the moisture budget under global warming (Seager et al., 2013), and we apply it here to the interannual natural variability.

This recent study using reanalyses and CMIP5 models has found that future Mediterranean drying is attributable predominantly to robust moisture divergence by the mean flow, due to an increase in low-level mass divergence, and that the transients actually can provide a moistening tendency (Seager et al., 2013). The models were shown to simulate the observed climatology in the moisture budget terms quite well, using reanalyses as ground truth, thus increasing confidence in these projections. That the transients act to oppose the trend in mean flow divergence is an interesting result. It has been shown that the transient component of the winter moisture budget over the Mediterranean exhibits a clear land-sea signature, with climatological convergence over land and divergence over water. To the extent that the transients change, they do more of what they do in the climatology, with water being extracted from the Mediterranean Sea and raining over land. In this thesis we seek distinguishing characteristics between the patterns of natural moisture budget change due to NAO variability and those of forced moisture budget change. We utilize moisture budget analysis to investigate the detailed mechanisms leading to NAO-induced moisture regional budget change, such as the role of the change in mean circulation versus that of the storm tracks for the six-month winter and summer half-years, using 15 CMIP5 models and the ERA Interim, and then compare with patterns of forced moisture budget change.

Last we shift our focus to a case study of Syria, as anthropogenic forcing and natural variability combined to produce the recent severe and persistent drought there prior to the Arab Spring uprising that occurred in early 2011. We begin by verifying that

the observed drought was the most severe and persistent Syrian drought in the instrumental record. Syrian water security was low prior to the onset of the drought, as the government had emphasized wheat production in the interest of national security and limited resources were used without regard for sustainability. The drought devastated the agriculture in Syria's "breadbasket region" and caused widespread crop failure, prompting a mass migration of farming families to urban peripheries, which resulted in food shortages, unemployment, and disruption of rural social structure. The addition of nearly 1.5 million drought refugees to the recent influx of Iraqi refugees greatly exacerbated conditions in the urban slums. We explore whether the severity and duration of the recent Syrian drought can be implicated as a cause of the current conflict, and determine the likelihood of occurrence of such an unusually severe observed drought without the contribution from the anthropogenic trend and whether it was made more likely by human interference in the climate system.

Some of the primary questions that we address in this thesis are:

1) How much has global warming contributed to observed winter Mediterranean drying since the mid-20th Century as compared to the contribution from the natural multidecadal variability of the NAO, and how is this relationship likely to change in the future?
2) How do the CMIP5 models perform in their simulation of Mediterranean precipitation climatology and trend over the latter half of the 20th Century compared to the previous generation, CMIP3, for all seasons?
3) How is the interannual natural variability of the NAO related to the greater Atlantic and Mediterranean moisture budget, and which terms within the budget are most important for causing Mediterranean drying during positive NAO phases?
4) How do the patterns of radiatively-forced and natural NAO-related moisture budget change compare? Can we determine a signature for forced moisture budget change that is distinct from the change associated with NAO variability?

5) Was the recent drought in Syria an important contributing factor in the uprising that led to civil war, and was the unusual severity and persistence of the drought influenced by anthropogenic climate change?

The organization of this thesis is as follows. In Chapter 2 we estimate the portion of the late 20th Century Mediterranean drying trend that was due to external forcing and conclude that over most of the region the multidecadal natural variability associated with the NAO was dominant, but that a radiatively-forced signal has begun to emerge. This work was published in Climate Dynamics as Kelley et al., 2012a. In Chapter 3 we assess the late 20th Century climatology and trend as simulated by the new generation of GCMs, the CMIP5, and find that while the new models show improvement over the previous generation, they simulate a very different seasonal cycle of precipitation trend than that observed to date. This work was published in Geophysical Research Letters as Kelley et al., 2012b. In Chapter 4 we explore the relationship between the interannually varying NAO and the Mediterranean moisture budget and show that under the NAO's influence, as with the trend, the mean flow divergence is the dominant contributor to the total moisture budget change, but that there are key differences between the patterns of forced and natural moisture budget change. This manuscript is in preparation. In Chapter 5 we examine the recent severe and persistent drought in Syria and conclude that the contribution from anthropogenic forcing made the drought worse, and that the resulting agricultural collapse and mass migration contributed in a significant way to the developing unrest, which culminated in the ongoing Syrian conflict. This manuscript is in preparation. Finally, in Chapter 6 we end with a brief summary of this thesis and some discussion of future directions.

Chapter 2

The relative contributions of radiative forcing and internal climate variability to the late 20th Century winter drying of the Mediterranean region

2.1 Introduction

The Mediterranean region experienced a downward trend in wintertime precipitation over the latter half of the 20th century (Hurrell, 1995; Hurrell et al., 2003). This observed winter drying trend, particularly from the 1960s to the 1990s (Fig. 2.1), was accompanied by a strong positive linear trend in the extended winter NAO. Because the linear trend in the winter NAO from the 1960s to the 1990s was the strongest thirty-year trend observed during the 20th Century, it led to considerable debate as to the mechanisms responsible. Did external radiative forcing in the form of rising CO_2 and global warming play an important role, as suggested by Shindell et al. (1999) and Feldstein (2002), or was the strong positive trend predominantly low frequency natural variability on multidecadal timescales (Schneider et al., 2003; Thompson, 2003)? The answer to this question has important implications for possible interdecadal predictability of the NAO and Mediterranean rainfall associated with external forcing. If this winter NAO trend was largely radiatively forced then drier conditions would be expected to continue as atmospheric CO_2 rises, consistent with model projections of drying in this region (IPCC, 2007). However, if it was dominated by natural variability then wetter conditions may return if the NAO swings to more negative values. To address this issue it is necessary to quantify the relative influence of anthropogenic, or human-induced, external forcing and natural low frequency variability on wintertime NAO and Mediterranean precipitation,

allowing for a better assessment of the model projections and how precipitation in the region could change in the future.

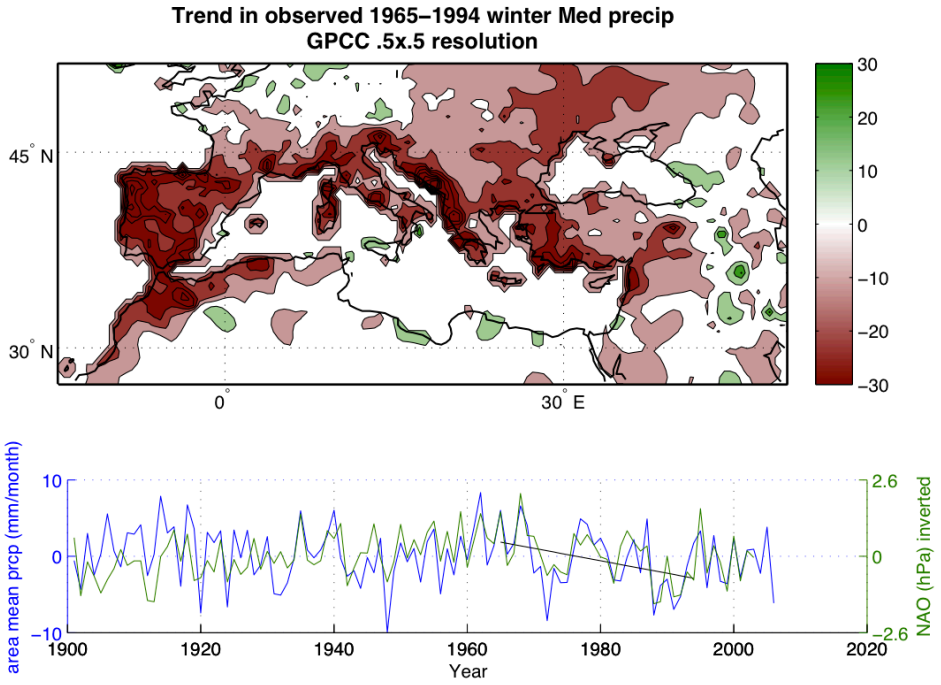

Figure 2.1: (Top) The change in observed winter Mediterranean precipitation from a linear best fit (mm/month per 30 yrs) from 1965-1994. (Bottom) Timeseries of the 20th Century area mean (27-52N, 15W-50E, land only) winter precipitation in blue and the NAO (inverted) in green, with a linear best fit line to the precipitation from 1965-94. Results are for the six-month (November-April) winter mean, using the GPCC .5 x.5 resolution and HadSLP2 5x5 resolution datasets.

As the leading mode of SLP variability in the North Atlantic (NA) sector, the winter NAO is the dominant influence on Mediterranean rainfall variability during extended winter (November to April) when, over much of the region, the majority of the annual precipitation falls (Hurrell et al., 2003; Dunkeloh and Jacobeit, 2003). The pattern of year-to-year Mediterranean rainfall variability associated with the NAO (e.g., Cullen and deMenocal, 2000) resembles the trend in Figure 2.1. The well-established negative correlation between winter half-year (Nov-Apr) precipitation in the Mediterranean region and the winter NAO is demonstrated in Figures 2.1 and 2.2 (bottom panels) as the

timeseries of the area mean (27-52N, 15W-50E) and the first PC of winter Mediterranean precipitation respectively, each plotted with the NAO timeseries (the first PC of NA SLP, here inverted).

Since 1950, as the number of observing stations has increased, the correlations between winter precipitation and the winter NAO are .77 (Fig. 2.1) and .78 (Fig. 2.2). From 1900 to the 1960s the winter NAO exhibited a negative linear trend, accompanied by a modest wetting trend in the Mediterranean. A strong positive NAO trend and robust drying in the Mediterranean followed from the mid-1960s to the '90s. After the late 1990s the NAO index abruptly dropped and then in winter 2009-10 reached its most negative value since 1950 as recorded by the Climate Prediction Center (CPC) NAO Index (not shown) (Barnston and Livezey, 1987), while winter Mediterranean precipitation increased. The first EOF pattern of winter Mediterranean precipitation is

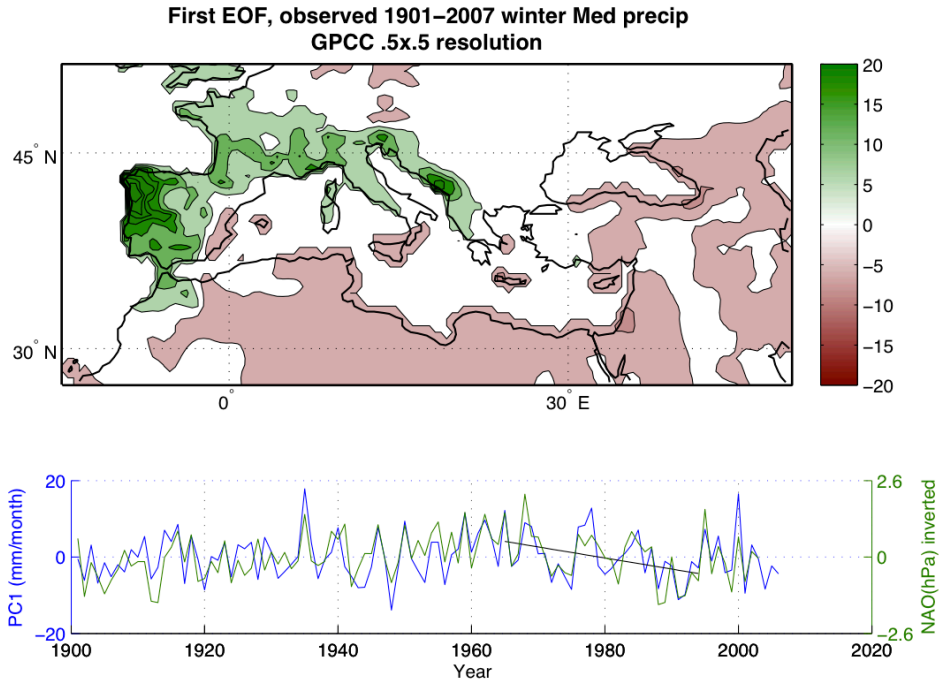

Figure 2.2: (Top) The first EOF of observed winter Mediterranean precipitation from 1901-2007. (Bottom) The corresponding first PC of observed winter precipitation from 1901-2007 in blue and the NAO in green, with the linear best fit to the precipitation from 1965-94. Results are for the November-April mean, using the GPCC .5 x.5 resolution and HadSLP2 5x5 resolution datasets.

also shown in Figure 2.2 (top) and corresponds with the first PC in the lower panel of the same figure. The first mode over this domain explains 21% of the total variance in winter precipitation from 1901-2007.

It has been previously reasoned that increasing concentrations of greenhouse gases (GHGs) will induce shifts towards the positive states of the annular modes (Thompson et al., 2000) and the NAO, effectively displacing much of the precipitation that would otherwise fall over southern Europe to northern Europe. However, multidecadal variability in the observed winter NAO and Mediterranean rainfall, clearly seen in the 20th Century record and including the recent NAO downturn, raises questions about how much of the observed variations were the result of anthropogenic forcing as opposed to arising from natural variability (Feldstein, 2002; Osborn, 2004). NAO-related atmospheric variability over different frequencies and timescales is primarily a result of the internal dynamics of the extratropical atmosphere (Thompson et al., 2003), and it has been argued that this internal atmospheric variability could have been responsible for the observed trends in the winter NAO index (Schneider et al., 2003). However, other studies have argued that the internal variability paradigm does not adequately explain the magnitude of the winter trend observed from the 1960s to the '90s (Thompson et al., 2000; Feldstein, 2002).

Using a Markov model constructed from daily atmospheric data Feldstein (2002) showed that such a strong trend was highly unlikely as a consequence of internal atmospheric variability alone, but that it could occur. Multi-century integrations using atmosphere-ocean coupled climate models have also shown that the late 20th Century positive NAO trend is outside the 95% confidence interval for internal variability alone (Osborn et al., 1999; Gillett et al., 2003; Osborn, 2004), again indicating that the observed trend is highly unusual but still possible. Osborn (2004) argues that the model simulations imply a small contribution from GHG forcing to the observed NAO trend from the 1960s to the 1990s, and that the observed record can potentially be explained as a combination of internally generated variability and a small GHG-induced positive trend. Osborn points to the more recent downturn (since the 1990s) in the NAO index as evidence of a reversal of the internally generated variation. There is also considerable uncertainty regarding the internal variability, however. Analysis using a 40-member

CCSM3 ensemble from 2005-2060 showed that internal atmospheric variability associated with the annular modes is the dominant source of uncertainty in the simulated climate response in the middle and high latitudes, accounting for at least half of the inter-model spread (Deser et al., 2011). Atmospheric interaction with the extratropical and tropical oceans has also been put forth as a possible explanation for the low frequency variability of the NAO (Kushnir et al., 2006). For example, it has been shown by forcing an AGCM with global SSTs and sea-ice distributions, that half of the amplitude in long-term wintertime NAO variability can be simulated with, in particular, tropical SST forcing dominated by warming in the Indo-Pacific (likely partly driven by rising GHGs), explaining some of the observed winter trend since 1950 (Hoerling et al., 2001; Hurrell et al., 2006). If in fact anthropogenic forcing has already begun to demonstrate a measurable influence over North Atlantic SLP and Mediterranean precipitation during winter then it is reasonable to expect that influence to increase during the current century relative to the natural variability. In summary, previous studies imply that external forcing could have been partially responsible for the winter NAO trend during this time, but to what extent and how the externally forced responses in both the NAO and in winter Mediterranean rainfall contribute to the total observed trend and its spatial variation remain largely unanswered.

To improve understanding of recent precipitation change in the Mediterranean region we first determine whether the observed 1960s to 1990s winter NAO and precipitation trends fall within the range of running thirty-year trends simulated by the IPCC AR4 CMIP3 models over the 20th Century. We then use a signal-to-noise maximizing EOF technique (see section 2.2 below) to obtain a model-based best estimate of the externally forced signal and use regression to divide up the observed winter trends in NA SLP and Mediterranean rainfall from 1960 to 1999 into internal and forced components. We conclude that the internal variability was dominant, with a small contribution from the external forcing, but that if the model simulated signal is realistic then the externally forced contribution to Mediterranean winter drying will increase over the 21st Century.

2.2 Data and methods

2.2.1 Observed data

We use the observed monthly sea level pressure from the Hadley Centre HadSLP2 dataset, which covers the period from January 1850 to December 2004 (Allan and Ansell, 2006). The monthly SLP has been regridded to 2.5º latitude by 2.5º longitude resolution from its original resolution (5º by 5º), consistent with the model data, and averaged over the extended winter season from November to April for the North Atlantic and Europe domain (75 ºW-50ºE 15º-75ºN). For observed precipitation we use the Global Precipitation Climatology Centre (GPCC) Full Data Product version 4 from the World Climate Research Programme (WCRP) Global Climate Observing System (GCOS), from January 1900 through December 2007 (Schneider et al., 2008). These data are available over land only. The resolution of the precipitation data is 0.5º latitude by 0.5º longitude, and we time average the data for the same extended winter season (November to April) for the Mediterranean region (15W-50E 27-52N), (see Figure 2.1).

2.2.2 Model simulations

For model data, we use 19 coupled CMIP3 models (Meehl et al., 2007) assessed within the IPCC AR4 (see Table 2.1), including all runs with available SLP and precipitation data over the 20th and 21st Centuries (46 total runs), with some models having single and others multiple runs. The 21st Century model projections are based on the so-called 'middle-of-the-road' A1B emissions scenario (Nakicenovic and Swart, 2000). For preindustrial runs, the same 19 models were used. All models are re-gridded to a common 2.5º latitude by 2.5º longitude resolution. Spatial domains and temporal averaging are the same as for the observed.

	Model	Country	Horizontal grid size
1	CGCM3.1 T47	Canada	96x48
2	CNRM CM3	France	128x64
3	CSIRO MK3.0	Australia	192x96
4	GFDL CM2.0	USA	144x90
5	GFDL CM2.1	USA	144x90
6	GISS AOM	USA	90x60
7	GISS-EH	USA	72x46
8	GISS-ER	USA	72x46
9	IAP FGOALS	China	128x60
10	INMCM3-0	Russia	72x45
11	IPSL CM4	France	96x72
12	MIROC3-2-hires	Japan	320x160
13	MIROC3-2-medres	Japan	128x64
14	MPI ECHAM5	Germany	192x96
15	MRI CGCM2.3.2a	Japan	128x64
16	NCAR CCSM3.0	USA	256x128
17	NCAR PCM1	USA	128X64
18	UKMO HADCM3	UK	96x73
19	UKMO HADGEM1	UK	192x145

Table 2.1: CMIP3 models used in this study, their country of origin and the dimensions of their horizontal grids.

2.2.3 Methods

There are two primary methods that are traditionally used to define the NAO. The first is indexing using normalized pressure differences between pairs of stations representing the northern and southern SLP nodes. The second definition, and the one adopted in this study, is based on empirical orthogonal function (EOF) analysis using area weighted SLP over the North Atlantic domain (75 ºW-50ºE 15º-75ºN). The first principal component (PC1) and empirical orthogonal function (EOF1) of SLP represent the temporal and spatial variation of the NAO. The two methods are highly correlated (Hurrell et al., 2003). Similarly, the model NAOs were determined by EOF analysis for each individual model run. The pattern correlations between each model simulated NAO and the observed NAO pattern were calculated, for validation purposes.

We computed running 30-year trends for the NAO and Mediterranean precipitation indices for both models and observations. For Mediterranean precipitation indices the first principal component over the domain (15W-50E 27-52N) was used rather than the timeseries of the spatial mean due to the large spatial variation within the domain. In our running trend analysis we use a time step of five years, with trends calculated as linear least squares fits to the first PCs, resulting in 15 thirty-year trends over one hundred years for the observed and 690 (15 x 46 runs) trends for the models. For this part of the analysis we used 46 runs in the 20th Century, consistent with the number of runs available in the 21st Century. Trend magnitude, or total change in the linear trend, is simply represented by the difference between the last value and the first value in the linear best fit. Statistical significance of regression coefficients was performed using a student's t-test, assuming a Gaussian distribution. Multidecadal variabilities of the observed and modeled NAO are further compared by applying a low pass Butterworth filter with a 9-year cutoff to the SLP and representing the NAO as the PC of the first EOF of these SLP fields.

After testing whether the 20th Century model-simulated thirty-year trends are able to span the range of observed trends we use signal-to-noise (S/N) maximizing EOF analysis (Allen and Smith, 1997; Venzke et al., 1999; Chang et al., 2000; Ting et al., 2009) applied to NA SLP and Mediterranean precipitation in boreal winter. There are two primary reasons for utilizing this approach rather than simply using a multimodel mean: first, it provides an optimized timeseries (signal) onto which the observations may be regressed, and secondly the available sample size of models and the use of many different models with possibly different responses to forcing means that natural variations cannot be removed, and the forcing isolated, simply by averaging across the ensemble. This technique should help eliminate contamination by noise resulting from the size of the sample. In order to retain only the decadal and longer timescale variations in the NA SLP and Mediterranean precipitation we employ a 9-year low pass Butterworth filter prior to application of the S/N maximizing EOF.

The terminology of "signal-to-noise (S/N) maximizing EOF analysis" refers to a method of identifying the "common" response to external forcing from an ensemble of forced GCM experiments. Here we follow the formulation proposed by Venzke et al.

(1999) and Chang et al. (2000), using the method to distinguish between the climate response to prescribed external forcing common to all ensemble members, hereafter referred to as "the signal", and internal variability, which is temporally uncorrelated between ensemble members. We use a multimodel ensemble, constructed using one realization from each of the 19 CMIP3 models for the 20th Century. As in Venzke et al. (1999) we assume that the total covariance matrix is a sum of two linearly independent matrices, one for the forced signal and the other for internal variability or "climate noise." When, as we expect, there is spatial correlation in the climate noise, the EOFs of the total covariance matrix will constitute a mix between the patterns of the signal and those of the noise. To untangle the mix and remove the signature of the noise a "pre-whitening" procedure is applied to the covariance matrix, which amounts to projecting the variability on the leading EOFs of the noise covariance matrix. Under the linear independence assumption, this operation diagonalizes the noise component of the covariance matrix and the resulting matrix is not affected by the spatial structure of the latter (adding a diagonal matrix to another symmetric matrix does not affect the EOFs of the former, see Venzke et al., 1999 for details). In our particular application of the procedure, we used the last 100 year preindustrial integrations of 19 available multi-model ensemble members to estimate the climate noise EOFs for the pre-whitening procedure. For each model the 100-year mean is subtracted first and all the preindustrial model anomalies are then pooled to calculate the noise EOFs. In this way, model biases in representing the variability are included in the noise.

After we obtain the model-derived best estimate of the forced signal (PC1 of the S/N EOF) we regress the observed 20th Century data fields of SLP (x,y,t) and precipitation (x,y,t) onto it as:

$$\alpha(x,y) = corr(x,y)\frac{\sigma(variable(t))}{\sigma(PC1(t))} \tag{2.1}$$

where *corr(x,y)* is the time correlation and σ is the standard deviation, thus obtaining spatial patterns of the forced regression coefficients, *α(x,y)*. We can then reconstruct the externally forced portion of *SLP*(x,y,t)* [or *precip*(x,y,t)*] in time and space as follows:

$$SLP^*(x,y,t) = \alpha(x,y) * PC1(t) \tag{2.2}$$

The reconstructed externally forced field is then subtracted from the total field to get the residual internal component:

$$SLP^{resid}(x,y,t) = SLP(x,y,t) - SLP^{*}(x,y,t) \tag{2.3}$$

The total, externally and internally forced SLP (and precipitation) trends from 1960-2000 can then be computed as the linear trends of *SLP, SLP* and SLP^{resid}*, respectively.

2.3 Modeled and observed trends in winter NA SLP and Mediterranean precipitation

2.3.1 20th Century SLP trends

To determine whether the observed NAO trend from 1965 to 1995 is outside the range of what the 19 IPCC AR4 models simulate, and to assess the overall capability of the multimodel ensemble to produce NAO trends of magnitude comparable to those observed in the 20th Century, we begin by examining running thirty-year trends of each model's NAO (first mode of SLP variability). A distribution of modeled trends is then created for each trend period, beginning with 1900-30 and advancing in five-year increments to the final trend, 1970-2000. Figure 2.3(a) (top) shows the time evolution and spread of the modeled thirty-year NAO trends. Each boxplot contains 46 model-produced trends for the respective period and includes the quartiles, medians, means, whiskers and outliers. Whiskers extend from each box to the maximum trend values that fall within 1.5 times the interquartile range, and the outliers are represented as red crosses. The observed thirty-year trends are also shown in each box, as black asterisks. All of the observed trends, ranging from -1 to 1.7 hPa/30yrs, are within the total spread of the simulated trends, which span -2 to +2.5 hPa/30yrs. The strongest observed trend (from 1965-95) is the only observed trend outside the respective whisker interval of modeled trends of the same time period but falls within the full 20th Century range of most negative and most positive model simulated trends.

The time evolution of the observed thirty-year trends reflects the multidecadal variability of the NAO with downward trends in the early part of the 20th Century and upward trends afterwards. The mean of the modeled trends for each period (indicated

with a blue cross) has markedly smaller trends than the observed NAO trends. This should be expected if the observed and modeled trends arise from internal variability because the model mean is an average across models with differing out-of-phase variability. To the extent that the model mean or median trends can be taken as estimates of the radiatively forced NAO trend, and the spreads as the range of natural variability, the forced trends are small at all times indicating that the observed trend from 1965 to 1995 is mostly a result of natural variability rather than external forcing.

However, because the forced signal and the response to given forcings are not necessarily the same in each model, a multimodel ensemble mean is not necessarily a precise characterization of the externally forced portion of NAO trends. Therefore, removing the ensemble mean from each run does not necessarily represent the intrinsic climate variability of that run, motivating the signal-to-noise maximizing EOF approach used below.

2.3.2 20th Century precipitation trends

We also apply the running trend analysis to the first mode of Mediterranean winter precipitation, shown in Figure 2.3(b) (bottom). In the observations and in the model simulations the largest thirty-year precipitation trends are on the order of +/-9 mm/month/30yrs. Twice, from 1940-70 and from 1965-1995, the observed trends were outside the whisker interval of the simulations for that particular time period. However, as with the NAO trends, all of the observed 30-year trends in the first PC of Mediterranean precipitation are within the overall 20th Century distribution (i.e. within the range of most negative and most positive values) of modeled 30-year trends during the entire century. Hence, the individual simulations can produce multidecadal variability that resembles the observations, although most of the observed thirty year trends of the winter NAO and precipitation shown are outside the outside the 25th and 75th percentiles of the time-corresponding modeled trend distributions.

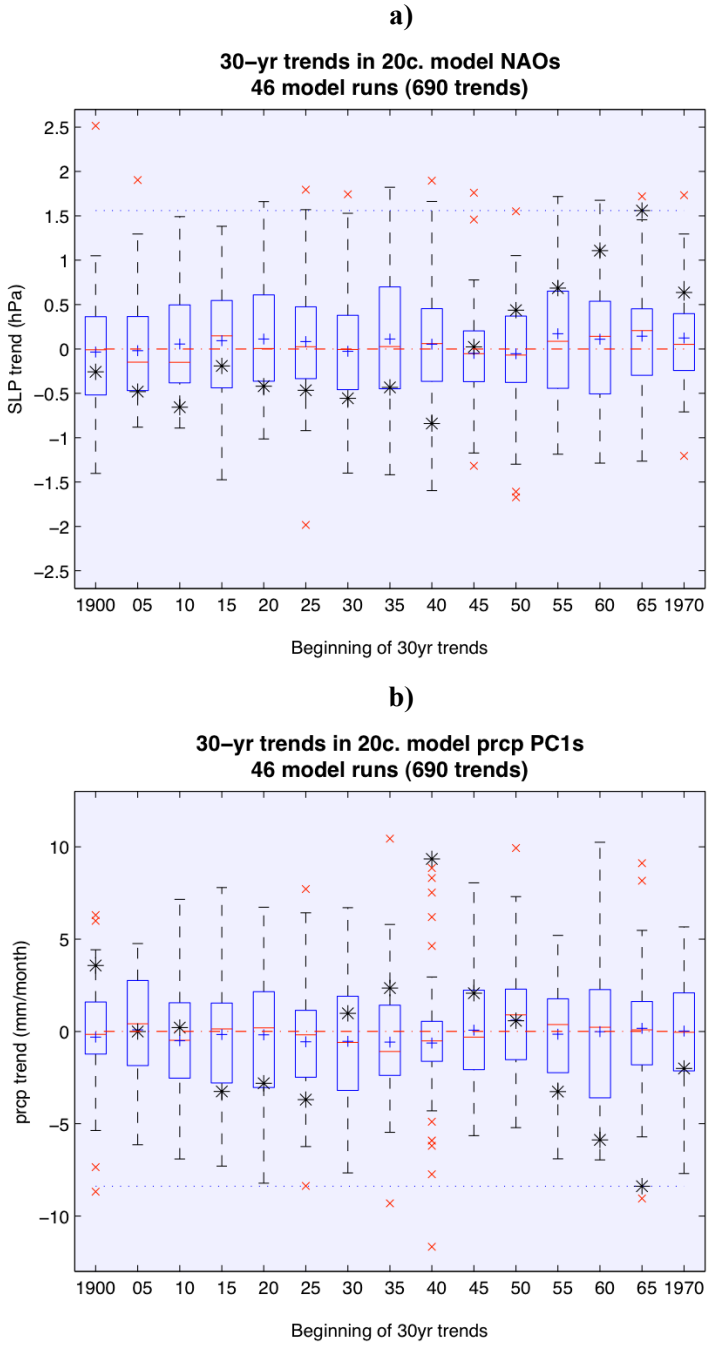

Figure 2.3: Boxplots of running thirty-year trends in the NAO (top) and Mediterranean precipitation (bottom) (first PC) from 1900-2000, in 5-year time step increments, using the first PC of 46 available runs from 19 CMIP3 models. Each box has lines at the lower quartile, median, and upper quartile values. Whiskers extend from each end of each box to the maximum values within 1.5 times the interquartile range. Blue crosses represent the means of each distribution, and red x's indicate outliers, or values outside the whiskers. HadSLP2 and GPCC observed trends are shown as black asterisks. Units are hPa per thirty years and mm/month per thirty years, using the November-April mean.

2.3.3 Temporal behavior of 20th Century observed and modeled SLP and precipitation

In order to compare observed and model simulated variability at all timescales ten years or longer, we apply a 9-year low pass filter to the observed and model-simulated runs for the 20th Century and then calculate the NAO and precipitation timeseries from the first modes. It can be seen from six of the coupled models (Figure 2.4) that the differences between the most positive and most negative values in the modeled low-frequency NAO and precipitation timeseries over the century are similar to the observed. The decadal to interdecadal variability in the six models shown is representative of all 19 models (not shown). Additionally, the fraction of total variance of total winter SLP and precipitation variability explained by the first modes for the observations are near the center of the spreads of the variance explained by the first mode for all 19 models. Based on visual examination of the spatial patterns (not shown) of the first modes, the models as a whole represent the observed NAO pattern fairly well, with some differences in the location of the dipoles with respect to the observed NAO. The area-weighted spatial correlations between each model's NAO pattern and the observed NAO pattern range from .78 to .98. There are also differences, however, in the low frequency variability between the observed and modeled NAOs and first modes of precipitation. The observed NAO during the 20th Century is dominated by low frequency variability on the order of thirty to sixty-year half-oscillations, but the longest half-oscillations in the modeled NAOs are closer to ten to fifteen years. That the observed winter NAO is dominated in the 20th Century by longer timescales (~30-60 year variability) than the model simulations (~20 year variability) is consistent with the observed thirty-year trends being outside the 25th and 75th percentiles, in the extremes of the modeled trend distributions. The difference between the observed and modeled low frequency variability in the first mode of precipitation however is less distinct. Despite the differences in low frequency variability compared to the 20th Century observations, the models do a credible job of simulating the variability of the winter NAO and can create thirty-year NAO trends of comparable magnitude to those observed during the 20th Century, although not as often.

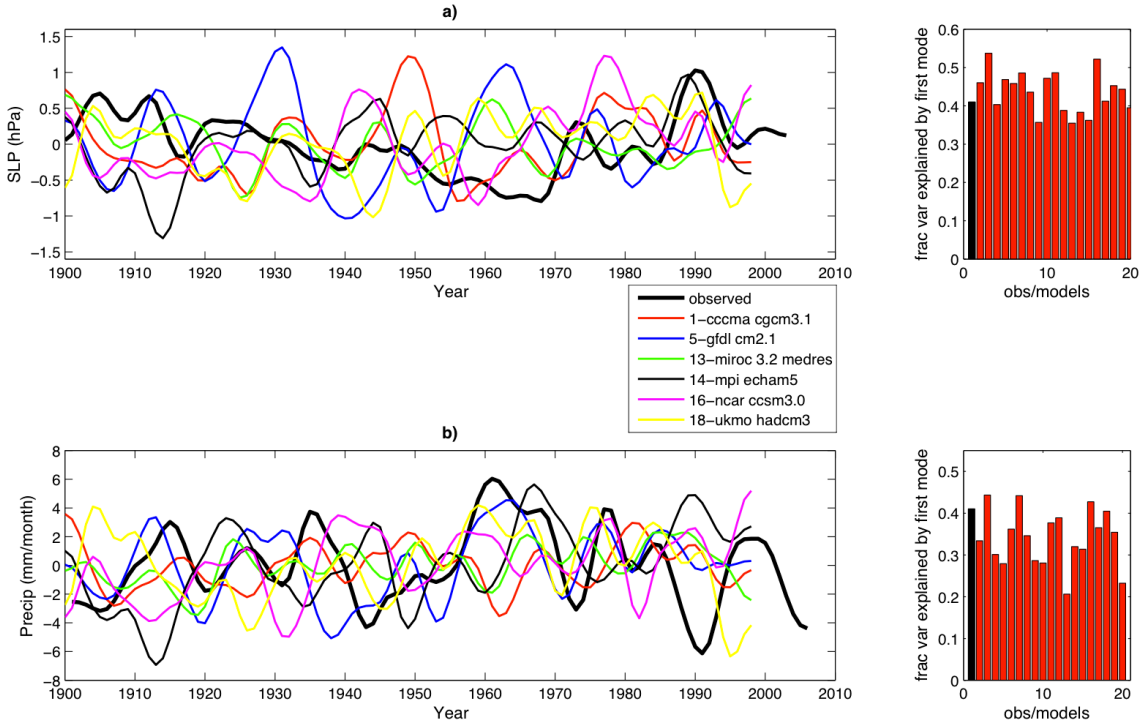

Figure 2.4: Timeseries of 20th century observed and model simulated NAOs, calculated as the first modes of SLP (top) and Mediterranean precipitation (bottom) derived from 9-year low pass filtering, in hPa and mm/month. Six coupled models are shown at left. The panel on the right displays the fraction of total variance explained by the first mode for the observations and the 19 CMIP3 models, using the November to April mean.

2.3.4 Comparing observed and modeled SLP and precipitation trends from the preindustrial era through the 21st Century.

In Figure 2.5 we show histograms of all model simulated thirty-year winter NAO and Mediterranean precipitation (first mode) trends, for preindustrial, 20th Century and 21st Century runs, as well as for a 600-year tree-ring NAO reconstruction. The means, standard deviations, skewness, and chi-squared goodness of fit statistics of each histogram are shown. A value of zero for the chi-squared statistic indicates that the null hypothesis (no difference from a Gaussian distribution) cannot be rejected, here using a 90% confidence interval. For the NAO, the mean and median of the thirty-year model simulated trends during the 20th Century (left column, second panel from top) are .06 and .02 (hPa/30yrs), with a standard deviation of .67, and the distribution is skewed slightly right. The chi-squared statistic indicates a rejection of the null hypothesis, indicating that

the data are not a random sample from a normal distribution at this confidence level. As in Figure 2.3 it can be seen that the observed winter NAO trend from 1965-95 is within the distribution, although the number of positive trends simulated by the models that exceed this trend is small. Based on the first mode of winter precipitation, the modeled thirty-year trend distribution has a mean and median of -.18 and -.16 (mm/month/30yrs), and a standard deviation of 3.3. Unlike for the NAO distribution, the chi-squared statistic indicates a normal distribution for the 20th Century modeled precipitation based on the confidence interval. The observed trend from 1965-95 is shown, and the number of model-simulated trends exceeding this value is also small, although greater than for the NAO case.

Because it is possible that different models will have different responses to even the same forcings and also there are differences in how the models are forced, we therefore turned to the preindustrial runs of the models as an alternate means of determining the NAO trends resulting from each model's internal variability alone. Preindustrial runs also provide the benefit of a longer period with which to characterize multidecadal internal variability in the models. The top panels in Figure 2.5 (a)(e) show that the modeled distributions of these thirty-year trends, using a larger sample size, are essentially Gaussian. The bottom panel of Figure 2.5 (d) shows NAO trends calculated from a 600-year winter (Dec-Mar) NAO index reconstruction (1400-2001) using tree-ring records (Cook et al. 2002) that span the transition from the preindustrial to the present and are used for comparison with the model-simulated trends. Before calculating the trends using this reconstruction, it was necessary to rescale the mean and standard deviation of the timeseries to match the mean and standard deviation calculated from the observed winter (Nov-Apr) NAO (first mode of SLP) from 1980-2000. Applying the 9-year low pass filter to the winter NAO tree-ring reconstruction reveals that some one hundred year periods (not shown) more closely resemble the low frequency temporal variability of the 20th Century observed winter NAO timeseries, exhibiting variability in the thirty to sixty-year range, while others are more similar to the variability of the model simulated NAOs during the 20th Century with shorter timescales. This indicates that the presence of thirty to sixty-year half-oscillations during the observed 20th Century winter

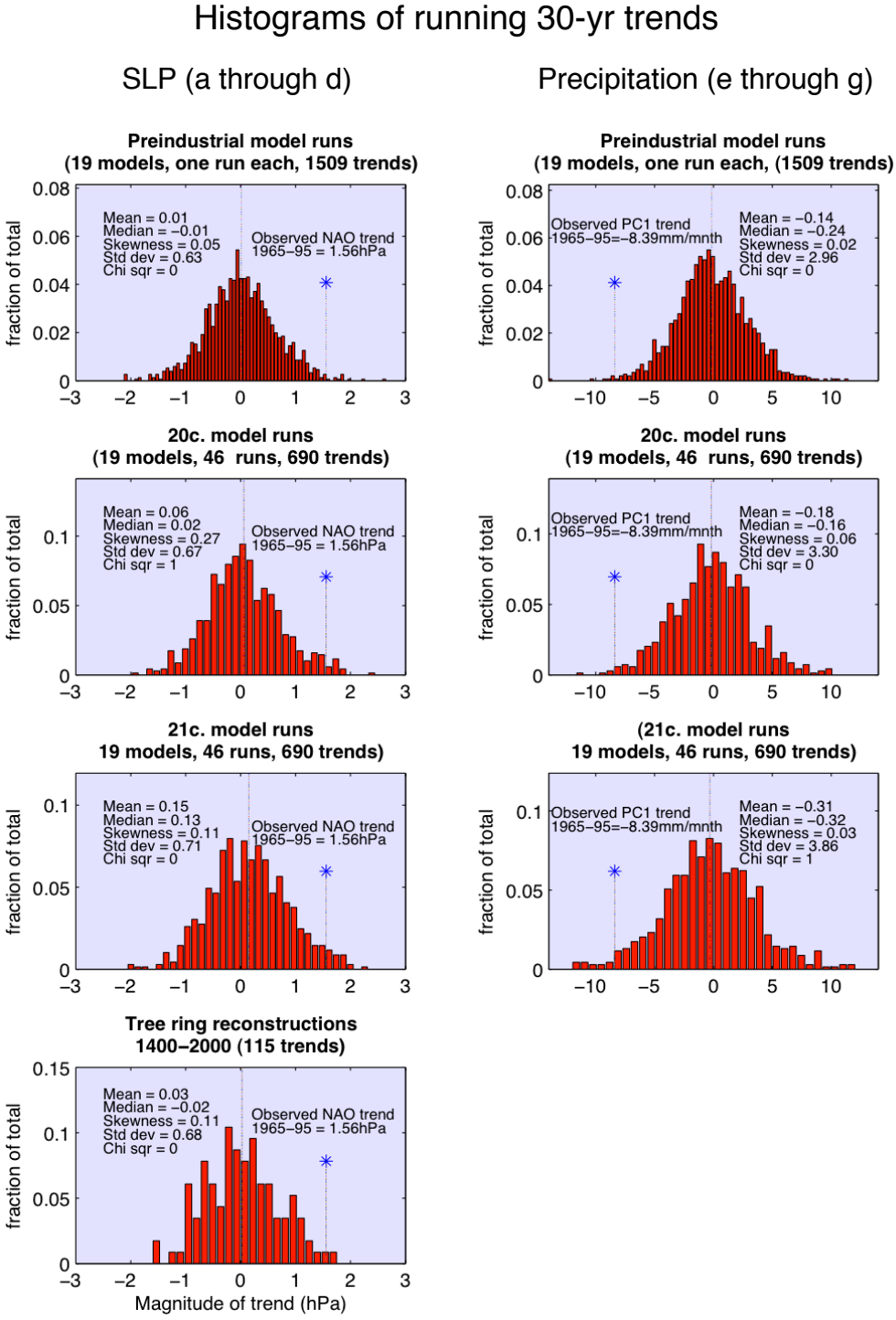

Figure 2.5: Histograms of running thirty-year trends in the NAO (left) and Mediterranean precipitation first mode (right), in five-year time step increments. From top to bottom: 19 preindustrial runs (of varying length for each model); 46 runs during the 20th Century; 46 runs during the 21st Century; and a 600yr tree ring NAO reconstruction from 1400-2000 (left). Results are for the November-April mean. The trend units are in hPa and mm/month, per thirty years.

NAO may be atypical compared to several of the previous centuries. Even though the distribution is based on a smaller sample size, the mean (.03), skewness (.11) and standard deviation (.68) shown in Figure 5(d) are consistent with the range of statistics for the larger samples of the preindustrial, 20th and 21st Century histograms in Figure 5(a)(b)(c). Trends of magnitude greater than the observed trend from 1965-95 although rare have occurred over the last six hundred years according to this NAO reconstruction.

It can be seen (Fig. 2.5) that as the external forcing increases with time the mean of the modeled NAO trend distribution (left side) increases, from the preindustrial through the 21st Century, indicating a tendency toward an increasing number of positive thirty-year NAO trends. This positive shift in the mean trend of the distribution is accompanied by a small increase in the standard deviation of the trend distribution, indicating a widening of the distribution or an increase in the number of strong positive and negative thirty-year trends as the external forcing increases. The opposite shift in means can be seen in the Mediterranean precipitation trends (right side), but like the NAO case there is an increase in the standard deviation of the trends. In this case however the increase is much stronger, particularly from the 20th to the 21st Century, leading to stronger thirty-year precipitation trends both positive and negative. The z-score for the pooled standard error of the preindustrial and 20th Century NAO trends is 1.26, indicating that the shift in the means is well below (inside) the 90% confidence interval threshold. This is not the case when comparing the preindustrial to the 21st Century, however, as the z-score is 3.67, demonstrating a highly significant shift in the mean thirty year NAO trend. For the precipitation, the corresponding z-scores are .47 and 1.91 respectively, again indicating significance of the mean shift at the 90% level for the 21st Century, although less so than for the NAO. The magnitude of the observed NAO and precipitation trends from 1965-95 (1.56hPa and -8.39mm per month per 30 yrs) is shown in each panel, and it can be seen that the models are more likely to produce trends that exceed the observed trend when radiative forcing is included, during the 20th Century and 21st Century, but that even in the preindustrial distribution the strong observed trend is not entirely outside the range of model simulated thirty-year NAO trends. Unlike the 20th Century, the chi-squared statistic for the 21st Century histograms

indicates a normal distribution for the NAO trends, but a rejection of the null hypothesis for the precipitation trends based on a 90% confidence interval.

In all, the capability of the models to produce NAO and precipitation trends with a reasonable magnitude lends confidence in their suitability for creating a best estimate of the externally forced low frequency variability in both NA SLP and Mediterranean rainfall through the use of signal-to-noise EOF maximization.

2.4 Externally forced variability using signal-to-noise maximization EOF

To determine more quantitatively the NAO and Mediterranean rainfall trends due to external forcing versus internal climate variability we use the signal-to-noise maximizing EOF method (Chang et al., 2000; Ting et al., 2009 and see section 2.2). In this section the signal-to-noise EOF is applied to NA SLP (75W-50E 15-75N) and Mediterranean precipitation (15W-50E 27-52N) using one run of each of the 19 CMIP3 coupled models to calculate the multimodel ensemble mean, and using the last century from the preindustrial runs of the same models for the noise covariance matrix. Figure 2.6 shows the leading modes of the model-derived externally forced responses of NA SLP and Mediterranean precipitation calculated from the 20th Century (left) and from the 20th and 21st Centuries combined (right). For the two centuries combined, the first mode in each case explains approximately 74% (top) and 85% (bottom) of the total variance respectively (of SLP and precipitation). The timeseries associated with the SLP and precipitation responses to the external forcing (the "signals") mirror each other well, showing an initial change several decades prior to the end of the 20th Century and continuing in a steady fashion with a positive NAO trend, and Mediterranean drying through the end of the 21st Century. The spatial structures are also consistent, with reduced rainfall under increasing SLP. Although there are some differences between the first EOFs and the canonical observed NAO pattern, the structures are very NAO-like.

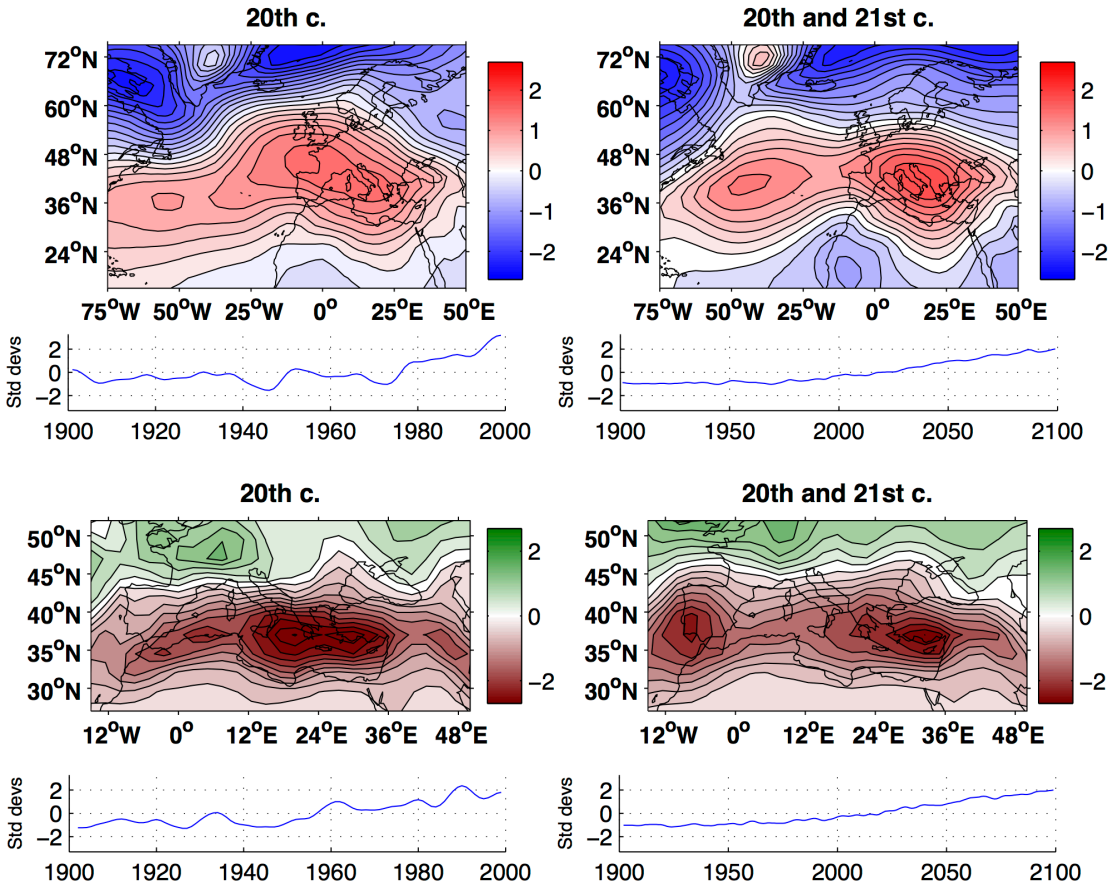

Figure 2.6: First modes of the signal-to-noise maximizing EOF of (top) North Atlantic SLP and (bottom) Mediterranean precipitation (inverted) for the 20th (left) and 20-21st centuries (right) using the preindustrial, 20th and 21st Century runs from 19 CMIP3 models. A 9-year Butterworth low pass filter was applied prior to maximization. Results are for the November-April mean. Units are in standard deviations of the pattern and of the timeseries, respectively.

Taking the model-derived signals (timeseries) to be our best estimate of the externally forced responses we regress the observed NA SLP and Mediterranean precipitation for the extended boreal winter onto the 20th Century time series shown in Figure 2.6 (left). The total SLP (precipitation) anomalies are then separated into two parts, one associated with the external forcing (Eq. 2.2, above) and another with internal variability (Eq. 2.3), which again includes any intermodel differences in response to forcing. The trends over the last forty years of the 20th Century (in order to fully capture the beginning and end of the strongest 30-year trend) are then calculated for the three

sub-components (total, external, residual). This provides us with a best estimate of the forced trend based on combining models and observations. The three trends for SLP are shown in Figure 2.7, along with the multimodel mean trend for the same period. It can be seen that the magnitude of the total trend (top left) is only slightly larger than the residual trend (bottom left), which appears to be roughly three times larger than the externally forced trend (top right). We can quantify the portion of the total trend for which the external forcing is responsible by taking the ratio of the root mean square (calculated over the domain) of the two trend patterns, externally forced and total, and the result is 32.6%. The stippling in Figure 2.7 indicates the statistically significant regression coefficients (outside a 90% confidence interval). The two areas in Figure 2.7(b) (top right) where externally forced trends are consistently significant are over the Labrador Sea and Mediterranean Basin respectively. Both the forced and residual SLP trend patterns resemble a positive NAO over the NA and Europe, in the sense of lower SLP in subpolar regions and increased SLP in the subtropics. However, it is a curious feature that over the Labrador Sea the external and internal trends oppose each other, with the internal trend dominating. Directly over the Mediterranean region the externally forced and residual SLP trends appear comparable in magnitude, which would seem to indicate that the external trend in SLP was in fact relevant.

Although it is much smaller than the residual trend, the overall magnitude of the externally forced NA SLP trend is slightly larger than the magnitude of the multimodel mean trend (Fig. 2.7(c), bottom right). Notice that multimodel trends do not take into account any of the observational information and are purely model-produced, whereas the forced trend in Figure 2.7(b) (top right) is estimated using information from both observations and models. Both estimates contain substantial errors, but looking at both provides a range of possible amplitudes for the externally forced observed trends. A simple multimodel mean not only includes some noise contamination when the sample size is sub-optimal, but could also average out some intermodel differences in external forcing and response. Alternatively, regressing observed data onto a model-derived signal to obtain the externally forced part of the observed trend implies that the observed signal and model-derived signal are similar, which is not necessarily the case.

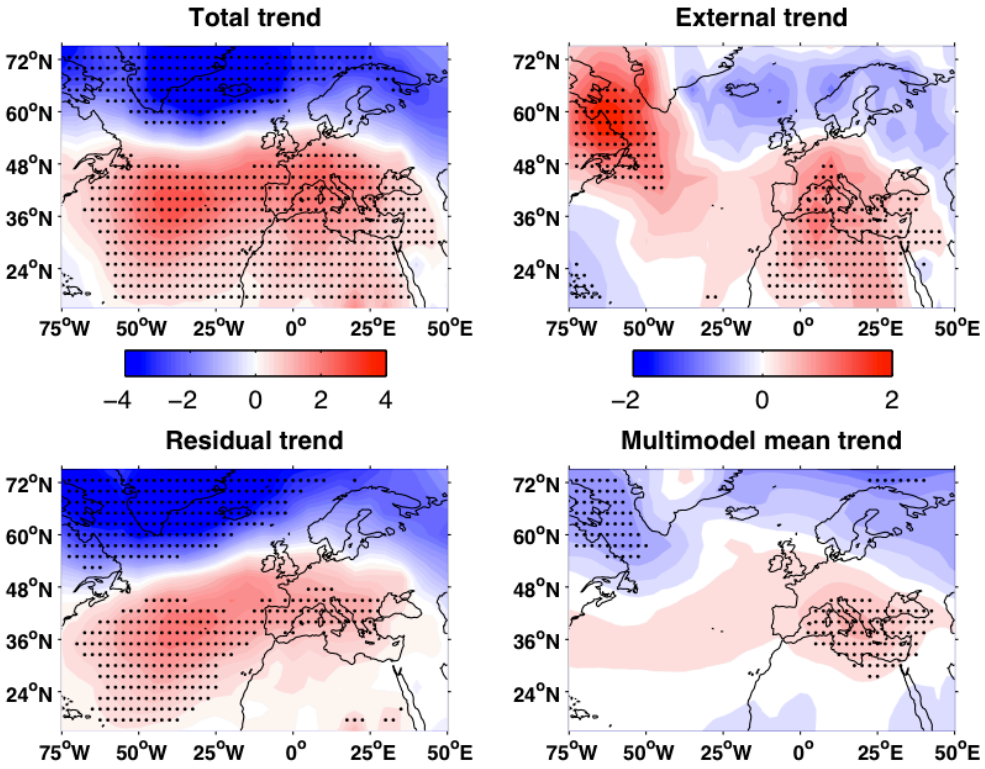

Figure 2.7: North Atlantic SLP 1960-2000 observed trend attribution, clockwise from top left: a) total trend, b) externally forced trend, c) multimodel mean trend, d) residual trend. Color scales apply to top and bottom panels. Trends are the change based on a linear best fit, with units of hPa per forty years. Results are for the November-April mean.

In Figure 2.8 we show the same attribution as in Figure 2.7 but now for the winter precipitation trend over the Mediterranean region. The overall rainfall trend pattern attributable to external forcing is much weaker than the residual trend arising from internal variability over most of the region. The ratio of the root mean squared externally forced and total trend patterns in this case is only 20.8%, indicating only a modest fraction of the total drying trend was externally forced. Nearly all of the strong drying observed over Ionia, the African coast north of the Atlas Mountains and over most of the Alps and Italy is due to the residual trend, with little contribution from the external forcing. There is considerable disagreement in sign between the two patterns over northern Europe and the Eastern Mediterranean. In the latter region there is strong, statistically significant drying in the externally forced pattern but statistically significant

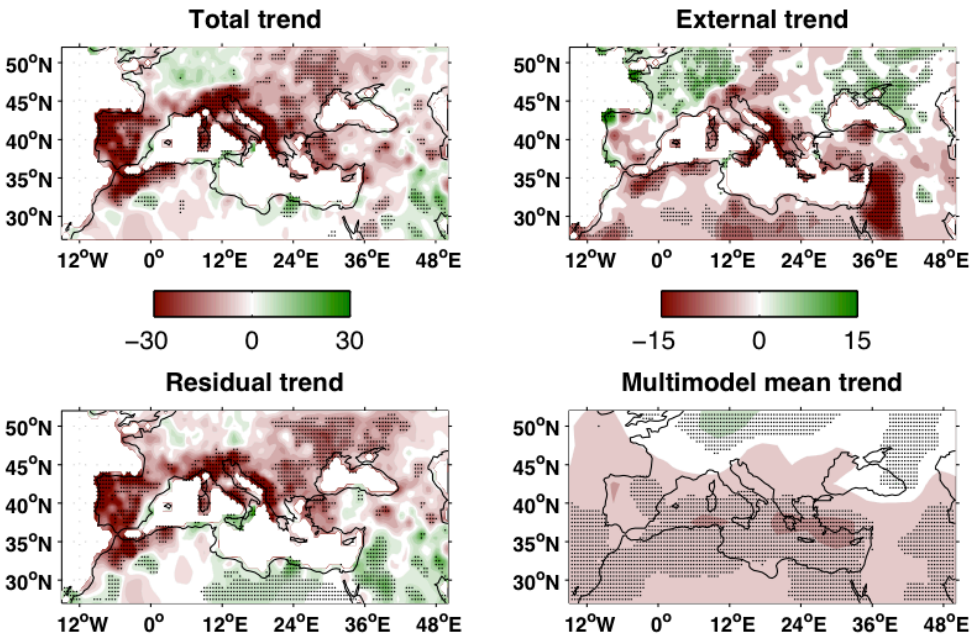

Figure 2.8: Mediterranean precipitation 1960-00 observed trend attribution, clockwise from top left: a) total trend, b) externally forced trend, c) multimodel mean trend, d) residual trend. Color scales apply to top and bottom panels. Trends are the change based on a linear best fit, with units of mm/month per forty years. Results are for the November-April mean.

wetting in the residual. The only sub-region over which the externally forced drying approaches the magnitude of residual drying is along the eastern Adriatic coastline, predominantly over Montenegro and Albania. Also, over much of northern Africa the residual trend is positive, while the externally forced trend is negative. As with the SLP, the difference between the externally forced trend using observations and the multimodel mean trend represents a range of possible amplitude for the observed trend resulting from external forcing.

To address the question of when the anthropogenically forced precipitation trend may approach the amplitude of the internal multi-decadal trend over the Mediterranean, we estimated the externally forced trend over the 21st Century by extrapolating the estimated forced trend in the 20th Century into the 21st Century via linear regression, using the 21st Century signal time series together with the 20th Century regression coefficient as follows:

$$Pr^*(x,y,t) = \alpha(x,y)\, PC1(t) \quad (2.4)$$

Where α (x,y) is the regression coefficient based on the 20th Century observations at each grid point, and PC1 is the S/N EOF time series for the 21st Century. We then computed the 21st Century linear trend in Pr*. The resulting pattern is shown in Figure 2.9, along with the multimodel mean precipitation trend for the 21st Century. The two patterns are substantially similar, but there are notable differences, particularly over the prominent topographical features surrounding the basin (a discrepancy that can be explained by the model's smooth topography) and in the Eastern Mediterranean. As with the 20th Century (Figure 2.8, top and bottom right) the multimodel mean trend pattern as a whole is weaker than the externally forced portion of the observed trend. The two patterns in Figure 2.9 can be used to represent an estimated range of externally forced 21st Century drying. The extrapolated 21st Century externally forced drying over much of the Mediterranean region is as strong or stronger than the total drying trend observed from 1960-2000, with the notable exception of the Iberian Peninsula where the external drying contribution is less, indicating that the future forced drying trend could, by the end of this century, approach the magnitude of the late 20th Century observed drying due to natural variability.

2.5 Conclusions

Using 46 runs from 19 IPCC AR4 model simulations of the 20th Century we are able to show that the model simulations are capable of producing thirty-year NAO and Mediterranean precipitation trends of magnitude comparable to those observed in the late 20th Century. The observed North Atlantic SLP and Mediterranean winter precipitation trends from 1965 to 1995 are within the overall estimated distributions of those simulated during the 20th Century by the models yet are outside the range defined by the lower and upper quartiles. However there is no systematic relation between the timing of the observed and model-simulated trends, which is consistent with both arising predominantly from internal variability. The models are able to produce trends of the magnitude of the observed trend from 1965-1995 as unusual events. The tree ring NAO

reconstruction also indicates that the observed winter NAO trends during the 20th Century are unusual in the context of the last 600 years.

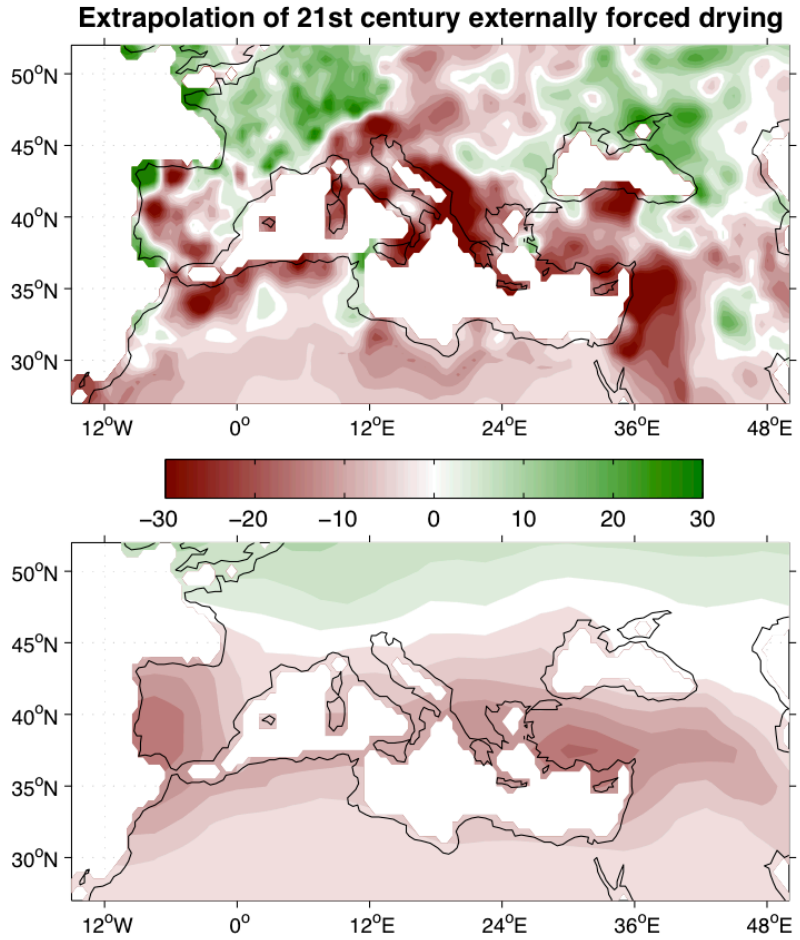

Figure 2.9: Top: Mediterranean precipitation externally forced trend extrapolation for the 21st century, based on regression coefficients from the 20th century. Locations for which extrapolated drying exceeded the 20th century climatology are shown as the climatology. Bottom: Multimodel mean trend for the 21st century. Units are mm/month per hundred years. Results are for the November-April mean.

The apparent ability of the models to simulate multidecadal NAO and Mediterranean precipitation trends, with the caveat that one hundred years is not a very long record for characterizing multidecadal variability, allows us to use preindustrial and 20th Century model simulations and signal-to-noise EOF maximization to determine

relative contributions of natural variability and radiative forcing to 20th Century SLP and precipitation trends. The externally forced responses to SLP and precipitation are consistent and indicate strong positive NAO and drying trends that began in the late 20th Century and continue through the current century, becoming increasingly clear amidst the natural variability as the 21st Century progresses. However, regressing the observed variability onto the timeseries of the forced response shows that the externally forced component represents only a modest fraction of the total NAO trend and Mediterranean rainfall trends for 1960-99, and that the magnitude of the residual trend (taken to be internal variability) was several times larger. The magnitude of the spatial patterns of the NA SLP trend attributed to the external forcing and the multimodel mean trend in NA SLP are similar, implying that the signal-to-noise based estimate is realistic. The accumulation of evidence therefore suggests that the external radiative forcing and the internal variability combined from the 1960s to the '90s to produce a strongly positive SLP trend and robust drying in the Mediterranean, but that the multidecadal natural variability dominated the contribution from the external forcing. These results are true only to the extent that the individual models and the multimodel mean are able to provide a realistic estimation of the forced signal. According to our best estimate of the external radiatively forced responses we should expect their contribution to trends to grow relative to the internal variability through the 21st Century. Based on the linear increase in the signal projected by this model-based estimate under the A1B emissions scenario, the forced precipitation change could begin to approach the magnitude of observed multidecadal natural variability by the end of the 21st Century establishing the level of aridity seen in the late 20th Century as the new climate. However if the strength of the natural variability observed in the 20th Century (which could also change in the future) persists, then the path towards this drier climate might not be smooth but involve drier and wetter periods of varying length around a steadily drying mean climate.

Chapter 3

Mediterranean precipitation climatology, seasonal cycle, and trend as simulated by CMIP5

3.1 Introduction

As a subtropical region, the Mediterranean region is expected to dry as a consequence of rising concentrations of greenhouse gases (GHG) (IPCC, 2007). Even in the absence of any future changes in interannual variability, the long-term drying of the Mediterranean will lead to an increase in the likelihood of severe dry years, which would have important consequences for water resource in many Mediterranean countries, especially those already experiencing water insecurity. In Chapter 2 we concluded, using the CMIP3 models and observations, that a decrease in precipitation due to increasing radiative forcing has begun to emerge during recent decades, amid the often large natural interannual and multidecadal precipitation variability. Now we assess the new CMIP models.

The previous generation of climate models from the CMIP3 was able to simulate the large-scale climatological features of Mediterranean region precipitation (see Fig. 3.1). In the newest generation of global climate models, the CMIP5, in addition to other model advancements, increased spatial resolution potentially allows improved representation of the climatological pattern and amplitude associated with the complex physiography and orography of the region (Giorgi and Lionello, 2008). With regard to the trend, the Mediterranean experienced a decline in precipitation since 1950 (Hurrell et al., 2003), which we have shown in Chapter 2 to be the result of a combination of dominant low frequency multidecadal variability and emerging response to external

forcing via increasing greenhouse gases (Osborn, 2004; Mariotti and Dell'Aquila, 2012; Hoerling et al., 2012). The greater Mediterranean drying was not uniform however as there were some southern and eastern subregions that experienced a wetting trend during the second half of the 20th Century (Jacobeit et al., 2007). This chapter intends to address how well the CMIP5 models simulate the observed Mediterranean precipitation climatology, seasonal cycle and trends, and to what extent we can trust the multimodel mean trends as representing the externally forced trends.

3.2 Data and methods

3.2.1 Data

We use two high resolution (.5 degree by .5 degree) gridded datasets of observed precipitation over land, from the Climate Research Unit (CRU) version 3.1 (New et al., 1999, 2000; NCAS BADC, 2008) and the Global Precipitation Climatology Centre (GPCC) Full Data Product version 5 (Schneider et al., 2008) and compare with CMIP3 (Meehl et al., 2007) and CMIP5 (Taylor et al., 2012) global climate models.

We use all available models from the CMIP3 and CMIP5 to create the multimodel mean (Table 3.1). In doing so we avoid any subjective bias associated with model selections. We use one run per model in forming the multimodel mean to avoid bias toward any model. In the box plot, however, all model runs are included.

	Horizontal resolution	# historical runs used	
MODEL	**(lon x lat)**		**Modeling center**
bcc-csm1-1	2.81x2.81	3	Beijing Climate Center
CanESM2	2.81x2.81	5	Canadian Centre for Climate Modeling and Analysis
CCSM4	1.25x.94	6	National Center for Atmospheric Research
CNRM-CM5	1.41x1.41	8	Centre National de Recherches Meteorologiques
CSIRO-Mk3-6-0	1.88x1.88	10	Commonwealth Scientific and Industrial Research Organisation
GFDL-CM3	2.5x2	3	Geophysical Fluid Dynamics Laboratory
GFDL-ESM2G	2.5x2	3	Geophysical Fluid Dynamics Laboratory
GFDL-ESM2M	2x2.5	1	Geophysical Fluid Dynamics Laboratory
GISS-E2-H	2.5x2	5/5 (two phys)	Goddard Institute for Space Studies
GISS-E2-R	2.5x2	6/5/5 (three phys)	Goddard Institute for Space Studies
HadCM3	3.75x2.5	10	Met Office Hadley Centre
HadGEM2-CC	1.88x1.25	1	Met Office Hadley Centre
HadGEM2-ES	1.88x1.25	4	Met Office Hadley Centre
inmcm4	2x1.5	1	Institute for Numerical Mathematics
IPSL-CM5A-LR	3.75x1.89	5	Institut Pierre-Simon Laplace
IPSL-CM5A-MR	2.5x1.27	1	Institut Pierre-Simon Laplace
MIROC-ESM	2.81x2.81	3	Model for Interdisciplinary Research on Climate, Univ. of Tokyo
MIROC-ESM-CHEM	2.81x2.81	1	Model for Interdisciplinary Research on Climate, Univ. of Tokyo
MIROC-4h	.56x.56	3	Model for Interdisciplinary Research on Climate, Univ. of Tokyo
MIROC-5	1.41x1.41	4	Model for Interdisciplinary Research on Climate, Univ. of Tokyo
MPI-ESM-LR	1.88x1.88	3	Max Planck Institut
MRI-CGCM3	1.13x1.13	3/2 (two phys)	Meteorological Research Institute, Japan
NorESM1-M	2.5x1.89	3	Norwegian Climate Centre

Table 3.1: CMIP5 models used in this study, horizontal resolution, number of runs and modeling groups.

3.2.2 Methods

In order to make spatial intercomparisons possible, all datasets and model outputs were first linearly interpolated to a common .5º x .5º horizontal grid for the greater-Mediterranean region (10W - 50E, 20 - 60N). Due to the sparseness of observed station data prior to 1950 we perform all of the analysis with post 1950 data, with the exception of determining the external trend (detailed below). Trends are calculated via a linear least-squares fit to the time series at each grid point. For better comparison with observations, only precipitation over land is considered in this chapter.

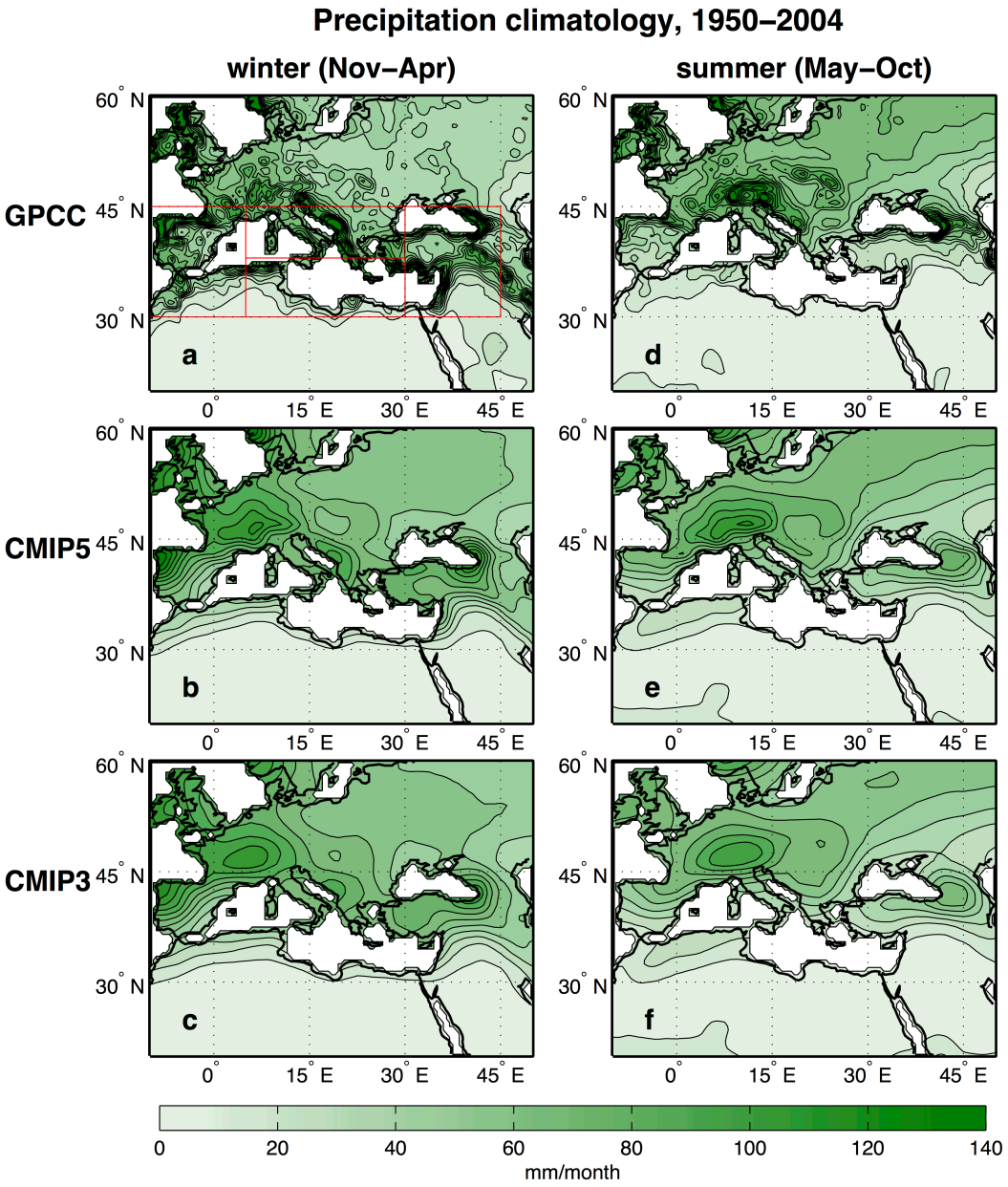

Figure 3.1: Left, winter half (Nov-Apr) and right, summer half (May-Oct) precipitation climatology, 1950-2004, from the GPCC (top), CMIP5 multimodel mean (center) and CMIP3 multimodel mean (bottom). The red lines in (a) outline the region used in Figure 3.2.

As in Chapter 2, we employ a model-based S/N maximizing EOF analysis (Allen and Smith, 1997; Venzke et al., 1999; Chang et al., 2000; Ting et al., 2009) to obtain the externally forced precipitation signal. The S/N maximizing EOF is first applied to a CMIP5 multi-model ensemble (one run each) for 1900 to 2004 and uses the

corresponding models' preindustrial experiments to represent the noise covariance. The technique uses the noise pattern to remove any intermodel differences, structural and temporal, as well as internal variability of the coupled systems that remain in the multimodel mean, providing a maximized "signal". The gridded GPCC observed precipitation is then projected onto the S/N first principal component (PC1, or signal timeseries) for the entire period (1900-2004). The externally forced trend from 1950-2004 was then calculated from the reconstructed precipitation at each grid point. More details of the method can be found in the supplementary material.

3.3 Precipitation Climatology

The six month cold and warm season averaged (Nov-Apr and May-Oct, respectively), observed GPCC climatologies from 1950 to 2004 are shown in Figure 3.1 (top panels). In the vicinity of the Mediterranean Sea, the majority of annual precipitation amounts fall during the six month cold season, whereas over much of the rest of Europe, a substantial contribution comes from the summer half. The corresponding precipitation climatology for CMIP5 and CMIP3 multimodel means are shown in the middle and bottom panels of Figure 3.1. The coastal precipitation maximum in the winter half year is captured to some extent by the models, but at a much reduced amplitude. There are some improvements from CMIP3 to CMIP5 however, possibly due in part to the slightly enhanced spatial resolution in the recent generation models. As a result, the spatial pattern correlation (Pearson correlation) between the observed and modeled fields increases slightly from CMIP3 (0.83) to CMIP5 (0.86). For the summer, the agreement is better between models and observations with spatial pattern correlations of 0.95 for CMIP5 and 0.94 for CMIP3. The better agreement between models and observations in summer is mainly due to drier conditions along the Mediterranean coasts compared to winter. As a comparison, the two gridded data sets, CRU and GPCC, are correlated at 0.94 for winter and 0.97 for summer (Fig. 3.2). The Taylor diagram (Taylor, 2001) in Figure 3.2 compares more closely the individual models' simulations of the precipitation climatologies in winter and summer.

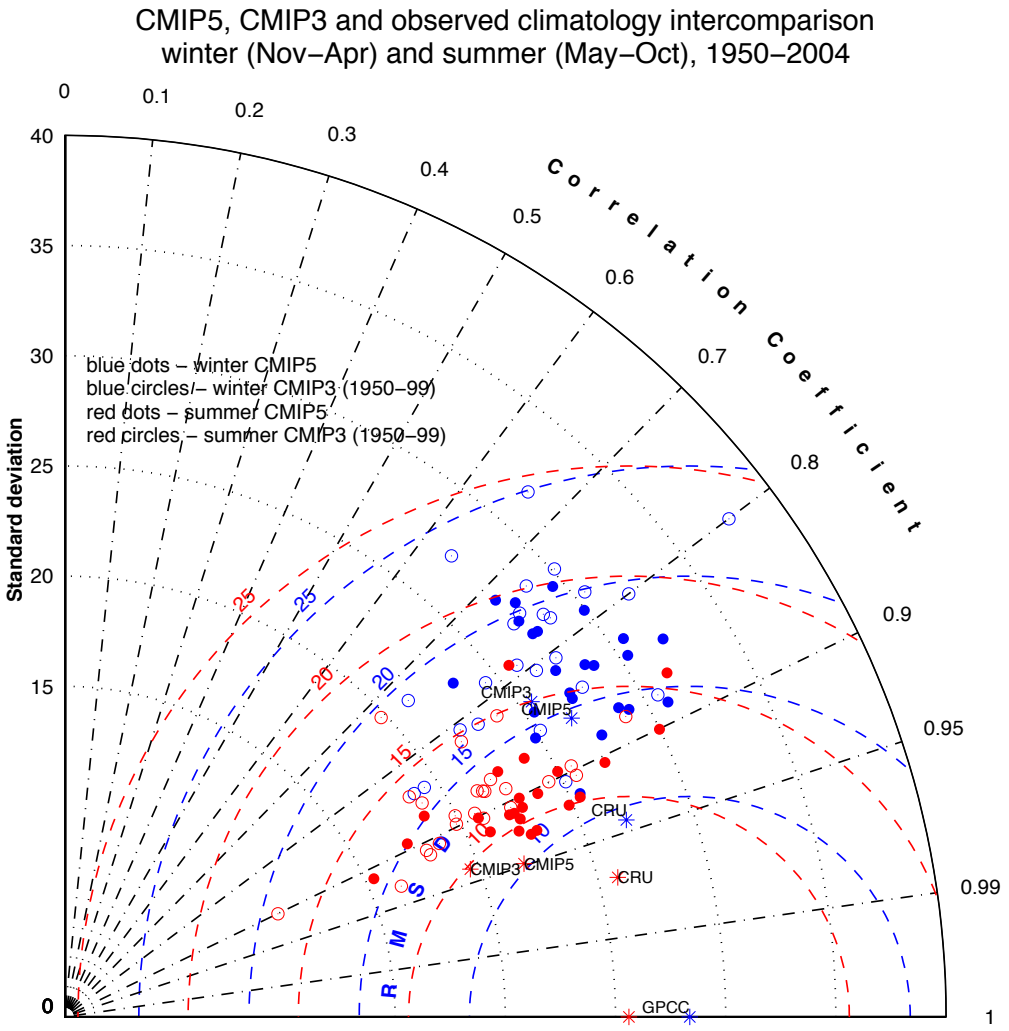

Figure 3.2: Winter (Nov-Apr) and summer (May-Oct) Mediterranean (-10 to 50, 20 to 60) precipitation climatology intercomparison, 1950-2004, in a Taylor Diagram. GPCC gridded precipitation is used as a reference state. Blue dots are for the six-month winter (Nov-Apr) and red for summer (May-Oct). Open circles are for CMIP3 and solid for CMIP5 models. The asterisks are for observed and multi-model mean precipitation, as indicated on the plot.

To quantify the model spread and the seasonal cycle of the CMIP5 model simulated climatological rainfall, we show in Figure 3.3 (left panels) the box and whiskers diagram for four selected regions, the entire Mediterranean region, the western, northern, and eastern Mediterranean (areas outlined in Fig.1a), for the four three-month

seasons and the annual mean. The box edges indicate the 25% and 75% range of the model simulated climatological rainfall while the horizontal bar and red dot inside the box indicate the median and mean model rainfall, respectively, the two horizontal lines outside the box (whiskers) indicate the range of .35% and 99.65%, or +/-2.7 standard deviations for a normal distribution, and the asterisks show the GPCC observed rainfall. A total of 109 model runs are used from 23 available CMIP5 models (see supplementary table A1) in Figure 3.3. In the four regions considered, the observed rainfall shows a clear seasonal cycle with maximum rainfall in the winter and minimum in summer, a characteristic of the Mediterranean climate. It is also clear that the transition seasons often contribute substantially to the annual rainfall total. The CMIP5 models simulate the seasonal cycle reasonably well, but the majority of the models underestimate the winter maximum and overestimate the summer minimum, thus underestimating the amplitude of the seasonal cycle. Compared to CMIP3 (not shown), the CMIP5 model climatologies are wetter in each season and annually, representing improvement relative to the observed with the notable exception of summer, in which case CMIP5 overestimates the summer rainfall more than CMIP3. The CMIP5 models show a larger spread in summer compared to other seasons, despite a higher spatial pattern correlation between multimodel means and observations in summer. It is unclear why the intermodel agreement is less during summer. One possibility is that summer precipitation is due less to the large scale circulation but rather is caused by convective processes and therefore is more sensitive to each model's physical parameterization scheme. Overall, the climatological rainfall over the Mediterranean region is well simulated by the CMIP5 models. We next examine the rainfall trends simulated in these models.

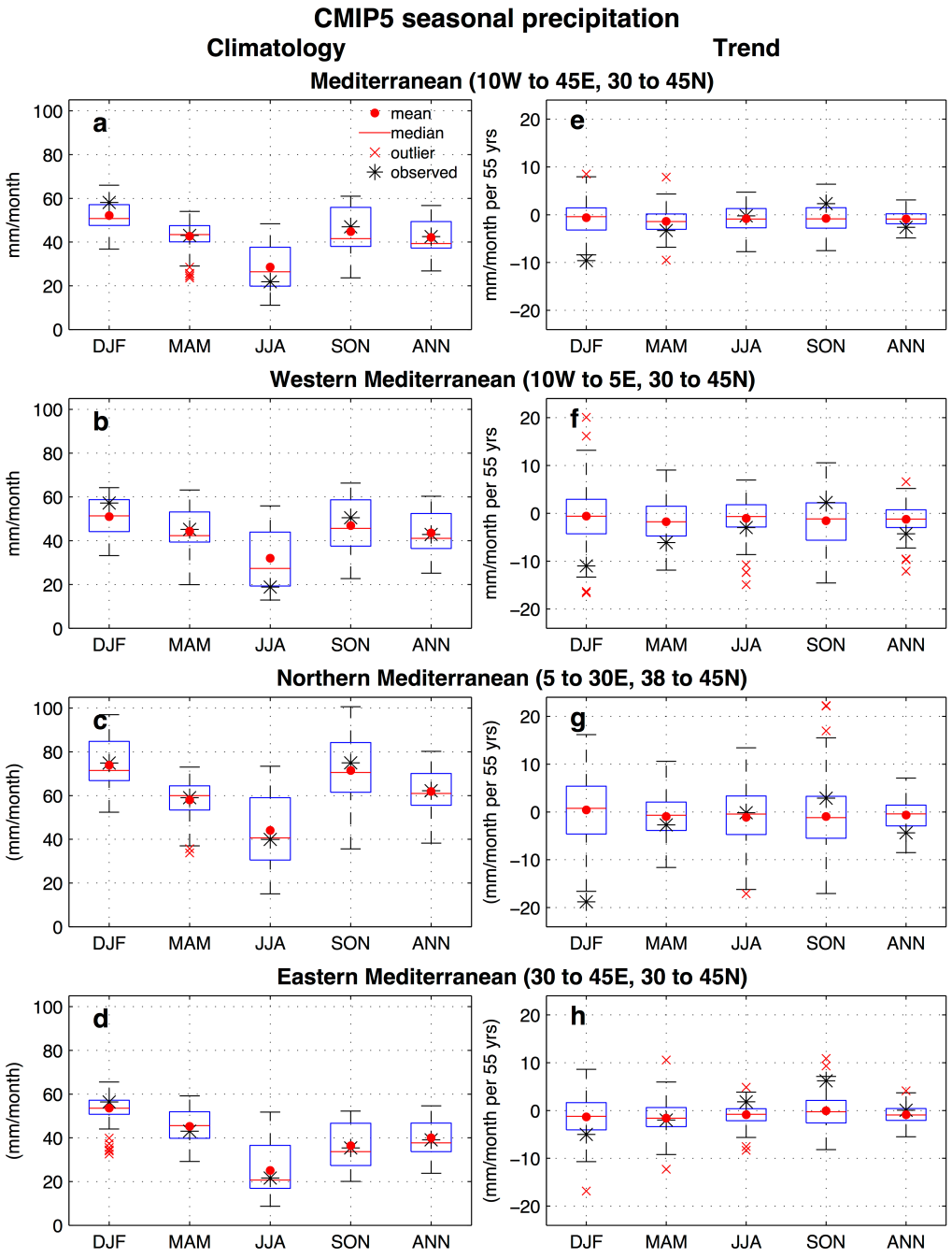

Figure 3.3: Precipitation climatology (left) and trends (right) for 1950 to 2004 plotted as box and whisker diagrams using 109 historical runs from 23 CMIP5 models. The 25th and 75th percentiles of the model distributions are shown by the edges of the boxes, and the whiskers as the range of .35% and 99.65% or +/-2.7 standard deviations for a normal distribution. Figure legend is as shown in panel a). Results are shown for the entire (a,e), western (b,f), northern (c,g) and eastern (d,h) Mediterranean region.

3.4 Precipitation Trends

The rainfall trends for the period from 1950 to 2004 in the CMIP5 models as compared to observations are summarized in the right panels of Figure 3.3. For the entire Mediterranean region (top right), the mean and median of all models show a modest drying throughout the seasonal cycle with the largest drying trend in spring. But the

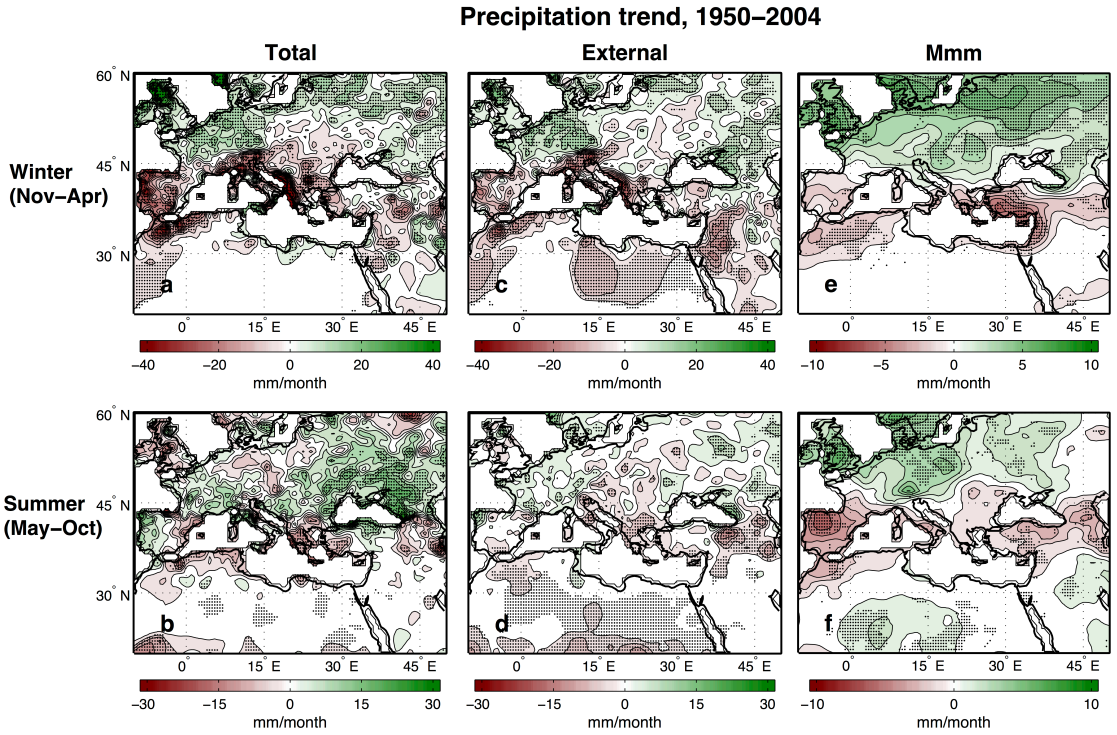

Figure 3.4: Winter half (top) and summer half (bottom) GPCC precipitation total (left panels) and external (center panels) trend and CMIP5 multimodel mean (one run from each model) trend (right panels) for the 55 year period from 1950 to 2004. Significance based on a 90% confidence interval is shown for the total and external trends. For the MMM, the hatching represents locations where more than 75% (17/23) of models agree on the sign of the trend.

observed trend shows a large seasonal cycle, ranging from a substantial drying in winter to a wetting trend in autumn. The winter observed rainfall trend for the 55 year period is significant (hereafter indicates a 90% confidence interval) and larger than 99.65% of the model trends, with an almost 10 mm/month reduction, or about 17% of the total winter season rainfall. For the rest of the seasonal cycle the difference between the observed

trend and the model mean trend is smaller, although autumn season precipitation shows a wetting trend (not significant) outside of the middle half of the model predictions. The model underestimation of the observed winter drying comes mainly from the northern and western Mediterranean regions, where the winter observed trends were significant, and less so from the eastern Mediterranean. The largest discrepancies between the observations and models occur in the regions and seasons with strong observed trends. The difference between the models and observations in the autumn trend is dominated by the eastern Mediterranean region, where the observed trend was significant.

In Chapter 2 we examined the observed winter precipitation trends for the period 1960 to 2000 and determined the contribution to the total trend from the externally forced (estimated based on CMIP3 simulations) and the natural component (residual). We concluded that the externally forced trend is distinctive in its spatial pattern compared to the pattern of internal climate variability. The discrepancies between modeled and observed winter trends in Figure 3.3 may indicate that the observed drying was dominated by multidecadal internal variability, such as that seen in the NAO, rather than external radiative forcing. As shown in Chapter 2 and in previous studies (Giorgi and Lionello, 2008), the individual models' multidecadal internal variability may have differing frequency from the 20th Century observations thus producing different internal multidecadal trend. To further examine the externally forced and the total observed trend, we show the total and externally forced (discussed more below) observed trend for 1950-2004 in Figure 3.4 for winter and summer half years. The winter total observed trend (Fig. 3.4(a)) shows a significant drying over the western and northern Mediterranean, consistent with Figure 3.3, coupled with significant wetting trend in northern Europe. This pattern resembles the precipitation anomalies associated with the NAO (Hoerling et al., 2012), thus suggesting the natural variability as a likely cause. The summer observed trend (Figure 3.4(b)) is weaker, and has a significant wetting trend around and north of the Black Sea. We follow the technique in Chapter 2 and estimate the externally forced precipitation trend due to radiative forcing using the signal to noise maximizing EOF PC1 obtained from the CMIP5 multimodel ensemble for the period 1900 to 2004 (see supplementary material for details). The estimated GPCC externally forced trend for the winter and summer half years, constructed based on the S/N PC1

(Fig. 3.5 bottom left), are shown in Figure 3.4(c) and 3.4(d). The externally forced trend in Figure 3.4c is much reduced compared to the total trend over the western and northern Mediterranean coasts, but slightly larger in the eastern coasts. This result is consistent with Chapter 2, which focused on a period that is dominated by a positive NAO trend (1960-2000) and thus the total precipitation trend is more dominated by natural variability than indicated in Figure 3.4(a) and 3.4(c). The close resemblance between the observed total and external trends in Figure 3.4(c), however, suggests that the method

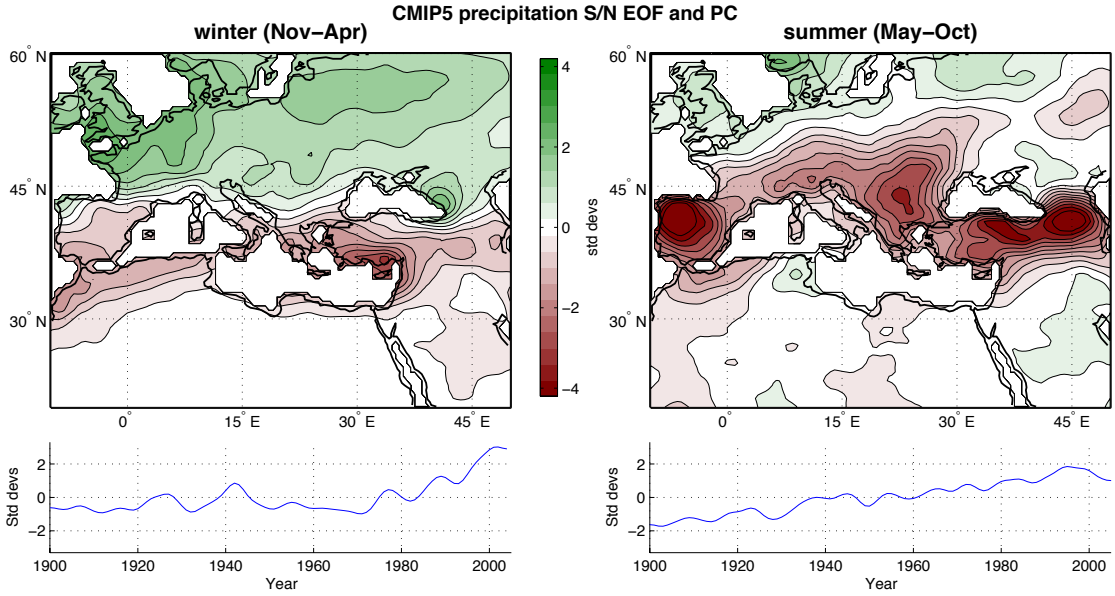

Figure 3.5: Signal-to-noise maximizing EOF spatial pattern (top) and PC1 timeseries (bottom) for GPCC six-month winter (Nov-Apr) and summer (May-Oct) precipitation over the greater Mediterranean region as shown in Fig. 3.1.

of estimating the external trend may not be able to remove entirely the trend associated with the NAO-related multidecadal precipitation variability. Over the eastern Mediterranean, the strong externally forced drying there indicates a more likely external cause. The summer observed external trend, while showing a consistent pattern of drying along most of the Mediterranean coasts, exhibits a much weaker amplitude throughout the region than its winter counterpart. The most significant observed drying in summer occurs south and east of the Black Sea, in Turkey.

The CMIP5 multimodel mean trend pattern (Fig. 3.4(e)(f)) shows a much weaker

drying throughout the Mediterranean region (notice the reduced color scale) compared to the observations, consistent with Figure 3.3. There is a general agreement between the observed and modeled winter trends in that both have maxima on the western and eastern Mediterranean coasts. However, the maximum over the northern coasts is largely missing from the multimodel means. For the summer half year, while the amplitude of the multimodel mean trend is smaller than observed, the difference in amplitude between multimodel mean trend and observed trend is not nearly as large as in winter. There is some correspondence between model and observations in summer drying over Turkey with the exception of eastern Turkey which experienced an observed wetting trend. Over Spain, the multimodel mean has a stronger drying trend in summer compared to observations whereas Portugal shows observed wetting.

It is interesting that the best agreement between CMIP5 multimodel mean trends and the observed trends in both half years is in the eastern Mediterranean region (Fig. 3.4). This is also true in Figure 3.3, where the eastern Mediterranean observed trend is closer to the model mean than any of the other regions. This indicates that the eastern Mediterranean may have the most significant externally forced drying trend. The greenhouse forcing of the eastern Mediterranean drying is also implicated in Hoerling et al. (2012), where they show that a global uniform warming, and a differential warming, either meridional (tropics versus midlatitudes) or zonal (Indian Ocean versus Pacific), of sea surface temperature (SST) can lead to strong eastern Mediterranean drying. Hoerling et al. (2012) suggest that the regional drying is accomplished primarily through a teleconnection linking global SST warming to increases in subtropical atmospheric high pressure, which in turn reduces cyclogenesis in the eastern Mediterranean basin. Trigo et al. (2010) also explain the recent drought in the Fertile Crescent, the most intense since the 1940s, with dominant high pressure that inhibited synoptic activity over the eastern Mediterranean Sea and favored dry air advection to the region from the northeast. The atmospheric response to the Hoerling et al. (2012) Indian Ocean differential warming experiment has a zonally symmetric expression resembling an expanding Hadley Cell and poleward migration of the storm tracks. Because the eastern Mediterranean is also a region of great water stress, for example in Turkey, Syria and Iraq, and because the future drying due to greenhouse warming will inevitably further deteriorate water availability, it

is of vital importance to understand the mechanisms which govern the precipitation change there.

3.5 Summary

Using the newest global climate models from the CMIP5, we showed that the Mediterranean precipitation climatology was generally well simulated in both spatial pattern and seasonal cycle. All models simulated the winter maximum and summer minimum in precipitation but the model mean and median slightly underestimated the amplitude of the seasonal cycle. There was a modest improvement of the CMIP5 climatology over CMIP3, possibly because of improved horizontal resolution.

In contrast, the Mediterranean precipitation trends of the last half century in the CMIP5 multimodel means and the observations differed significantly, particularly in winter and over the northern Mediterranean region. The CMIP5 multimodel mean trend indicated a modest drying throughout the seasonal cycle, with the strongest drying in the March, April and May spring season. The observed trend, on the other hand, showed a predominantly winter drying. It is not entirely clear what caused this discrepancy, although there was an indication that the strong observed winter drying might have been due to multidecadal natural variability, as shown in Chapter 2. Our estimate of the externally forced trend in observations also showed a predominant winter drying over the region. There was a reasonable agreement in the spatial patterns of the CMIP5 multimodel mean trend and the observed trend over the eastern Mediterranean region, moreso in winter than summer.

The modest agreement in spatial patterns between modeled and the observed external trends leads us to further conclude that the radiatively forced portion of the precipitation trend has only begun to emerge relative to natural variability on multidecadal timescales, but that its influence is likely to grow in the future as the forcing increases. Future decreases in Mediterranean region precipitation brought on by global warming, even in the absence of any changes to the internal variability, will have important consequences, reinforcing the need for further research and better understanding of the mechanisms driving the region's hydroclimate. The CMIP5 model ensembles will likely prove a useful tool to this effect.

Chapter 4

Change in moisture budget associated with the North Atlantic Oscillation

4.1 Introduction

In Chapters 2 and 3 we showed that the total reduction in observed rainfall in the greater Mediterranean in recent decades was dominated by the large multidecadal variability of the NAO, but that the contribution to this drying from anthropogenic forcing has begun to emerge and is most readily apparent over the eastern Mediterranean where the influence of the NAO is weakest. Much of the model-projected future reduction in Mediterranean rainfall has been previously attributed to a poleward shift in the storm tracks and jet stream that project onto the positive phase of the NAO (Wu et al. 2012, 2013; Simpson et al., 2013; Chang et al. 2012; Previdi and Liepert 2007; Yin 2005), and to an expanding Hadley Cell (Lu et al. 2007). In addition to large-scale dynamic and thermodynamic contributions to Mediterranean drying (Seager et al. 2010; Held and Soden 2006), regional and local processes are also thought to be important, specifically related to decreases in the frequency of winter storms (Ziv et al. 2013; Zappa et al. 2013; Trigo et al. 2000; Lionello and Giorgi 2007).

A recent study (Seager et al. 2013), using a CMIP5 multi-model ensemble, examined the moisture budget associated with future drying and found that the increase in mean mass divergence is actually the dominant contributor to the overall trend in Mediterranean drying. These results indicated that for the current winter climatology the mean flow diverges moisture from the Mediterranean region and the transient eddies converge moisture. It was found that, under global warming, the mean flow divergence increased by more than the transient eddy moisture flux convergence did leading to

drying. Whether this balance, with mean flow changes dominant, holds true or not for the NAO-related changes in the moisture budget of the region is not known.

To examine the relationship between natural variability of the NAO and the greater Mediterranean region moisture budget, we here examine a suite of 15 CMIP5 models as well as the ERA Interim reanalysis to address the following questions. First, what is the relative importance of the mean versus transient contributions to the total moisture budget changes associated with the NAO? Second, what are the dominant mechanisms for the mean flow contribution to the NAO-related moisture budget variability changes i.e. changes in mean mass divergence and moisture advection? And finally, how do NAO-related moisture budget changes relate to changes in the storm track and other atmospheric circulation features such as the vertical velocity field? A prime motivation is to determine the similarities and differences between mechanisms of natural variability and radiatively-forced change as part of a larger effort to determine the causes of ongoing hydroclimate change

We first introduce the data and methods in the next section, and then perform a detailed comparison of the CMIP5 model-simulated and observed (using the ERA-I reanalysis) relationships between the NAO and the greater Atlantic and Mediterranean moisture budget from 1979-2004 in sections 4.3 and 4.4. In section 4.5 we examine the relationship between the NAO and the large-scale atmospheric circulation. In section 4.6 we examine the forced moisture budget from 1950-2050, for comparison with the natural changes associated with the NAO, followed by the conclusions and summary in section 4.7.

4.2 Data and methods

In this chapter we compare the same 15 CMIP5 models used in Seager et al. (2013), one run each (see Table 4.1), to the ERA Interim Reanalysis, using the CMIP5 "historical" experiments. The ERA-I represents a step forward in its representation of the hydrologic cycle over its predecessor, the ERA-40, making it suitable for our purpose (Dee et al. 2011). The period of comparison is from 1979 to 2005, and we examine the six-month winter and summer seasons as defined by November-April and May-October, respectively. The models and reanalysis were linearly interpolated to a common 2° by 2°

horizontal resolution. In order to characterize the interannual natural, or unforced, variability of the NAO we began by removing the first principal component (PC) of the

MODEL	Horiz. Res. (lon x lat)	Modeling center
bcc-csm1-1	2.81x2.81	Beijing Climate Center
CanESM2	1.88x1.88	Canadian Centre for Climate Modeling and Analysis
CCSM4	1.25x.94	National Center for Atmospheric Research
CNRM-CM5	1.41x1.41	Centre National de Recherches Meteorologiques
CSIRO-Mk3-6-0	1.88x1.88	Commonwealth Scientific and Industrial Research Organisation
GFDL-CM3	2.5x2	Geophysical Fluid Dynamics Laboratory
GFDL-ESM2G	2x2.5	Geophysical Fluid Dynamics Laboratory
GFDL-ESM2M	2x2.5	Geophysical Fluid Dynamics Laboratory
HadGEM2-CC	1.88x1.25	Met Office Hadley Centre
inmcm4	1.5x2	Institute for Numerical Mathematics
IPSL-CM5A-LR	3.75x1.88	Institut Pierre-Simon Laplace
IPSL-CM5A-MR	2.5x1.25	Institut Pierre-Simon Laplace
MPI-ESM-LR	1.88x1.88	Max Planck Institut
MPI-ESM-MR	1.88x1.88	Max Planck Institut
NorESM1-M	2.5x1.89	Norwegian Climate Centre

Table 4.1: CMIP5 models used in this study. For each model the first available run was used, with the exception of the CCSM4, for which run 6 (r6i1p1) was used. For the HadGEM2-CC there was no available 500hPa vertical velocity data available and it was excluded from that calculation.

model ensemble mean, representing the common model forcing, from each model at each gridpoint, essentially performing a nonlinear detrending. After removing each model's mean we pooled the models in time and used empirical orthogonal function (EOF) analysis to determine the unforced model ensemble NAO, represented by the first mode of sea-level pressure (SLP). The moisture budget analysis performed here then follows that in Seager and Henderson (2013), which provides a thorough explanation of the analysis and numerical methods used. The steady state moisture budget in pressure coordinates is given by:

$$P-E=-\frac{1}{g\rho_w}\nabla\cdot\int_0^{p_s}\boldsymbol{u}q\,dp \tag{4.1}$$

where P represents precipitation, E is evaporation, g the gravitational constant, ρ_w the density of water, p atmospheric pressure (equal to p_s at the surface) and $\boldsymbol{u}$ the vector horizontal velocity. The vertical integration is actually done as a sum over pressure levels, and therefore Equation 4.1 can be rewritten as:

$$P-E=-\frac{1}{g\rho_w}\nabla\cdot\sum_{k=1}^{K}\boldsymbol{u}_k q_k dp_k \tag{4.2}$$

where K represents the total vertical pressure levels. After taking the time mean on both sides of Equation 4.2, we get the following:

$$\overline{\overline{P}}-\overline{\overline{E}}=-\frac{1}{g\rho_w}\nabla\cdot\sum_{k=1}^{K}\overline{\left(\overline{\boldsymbol{u}}_k\,\overline{q}_k+\overline{\boldsymbol{u}'_k q'_k}\right)\overline{dp}_k} \tag{4.3}$$

where overbars represent monthly means, primes daily departures from monthly means, and double overbars climatological monthly means. The two terms on the right side of Equation 4.3 represent convergence by the mean flow and by submonthly transient eddies, respectively. The mean flow contribution is further subdivided into two terms as:

$$\overline{\overline{P}}-\overline{\overline{E}}=-\frac{1}{g\rho_w}\left[\sum_{k=1}^{K}\overline{\left(\overline{\boldsymbol{u}}_k\cdot\nabla\overline{q}_k+\overline{q}_k\nabla\cdot\overline{\boldsymbol{u}}_k\right)\overline{dp}_k}+\nabla\cdot\sum_{k=1}^{K}\overline{\overline{\boldsymbol{u}'_k q'_k}\;\overline{dp}_k}\right]-\frac{1}{g\rho_w}\overline{\overline{q_s\boldsymbol{u}_s}\cdot\nabla p_s} \tag{4.4}$$

where the first two terms are related to mean flow moisture advection and the mass divergence, respectively. Here we moved the divergence operator inside the summation, which results in a surface term, as shown in the last term in Equation 4.4. This surface term is generally small and mainly associated with orographic features, and is neglected in this study. Please refer to Seager and Henderson (2013) for sources of errors associated with these calculations.

In this chapter we are concerned with winter and summer and six-month means are taken before the multi-year climatological averages. The moisture budget terms are regressed onto the NAO timeseries to obtain the moisture budget associated with the NAO. The significance of the regression coefficients is determined using an alpha threshold of 0.1. Transient terms are calculated based on daily deviations from the monthly mean values for the CMIP5 model analysis and the ERA-Interim analysis.

Last we regress the same moisture budget terms onto the forced response from 1950 to 2050, using the rcp85 representative concentration pathway for the 21st Century portion. The nonlinear forced response is determined as above by taking the EOF of the multimodel mean, and by then applying a Butterworth 20 year low pass filter to PC1.

4.3 The winter and summer NAO in ERA-I and CMIP5 models

The winter NAO spatial patterns and timeseries for ERA Interim and the CMIP5 models are shown in Figure 4.1 (top panels). In both ERA-I and the CMIP5 models, the NAO is defined as the first EOF of the sea level pressure over the period 1979 to 2005. The models were pooled in time, resulting in a time series that is a multiple of 26 years by 15 models in length and that represents the models' common NAO pattern. Here the spatial pattern is shown as the SLP regressed onto the PC1 timeseries. In this, and all subsequent figures, the regression pattern is shown with color shading, stippled for significance (α=.1), and the white contours represent the climatology. In both models and observations, the positive NAO is characterized by a dipole pattern that is a northward shift of the climatological SLP patterns. The southern center of the dipole NAO pattern (color shadings) has large amplitude over the Mediterranean, resulting in a large influence on the climate of the region. The models and observations agree remarkably well in both the NAO and the climatological SLP patterns, with the models exhibiting a slight tendency toward a more zonal orientation of the greater north Atlantic SLP than in the observations, as demonstrated in previous studies (Woollings 2010), as well as a slight high pressure bias in the subtropical north Atlantic that extends over northern Africa. The total variance explained by the NAO (first mode) is larger for the ERA-I (52%) than for the pooled models (43%). The model-simulated subtropical center of the NAO is centered eastward of the ERA-I, over the northern coast of Spain and the Pyrenees Mountains. The large-scale circulation associated with a positive NAO is dominated by northerly winds over the Mediterranean region, advecting colder and drier air, and westerly wind anomalies over Central Europe and easterly anomalies over much of the Sahara. The precipitation and evaporation regressions onto the NAO are shown in panels c through f of Figure 4.1. The precipitation anomalies associated with the positive phase of the NAO in both models and observations show very good agreement and are

characterized by a dipole with broad subtropical drying and increased precipitation over much of northern Europe. Table 4.2 shows that the observed and modeled NAO-induced precipitation change patterns are highly correlated spatially (R=.79 over the entire domain, .83 over the Mediterranean).

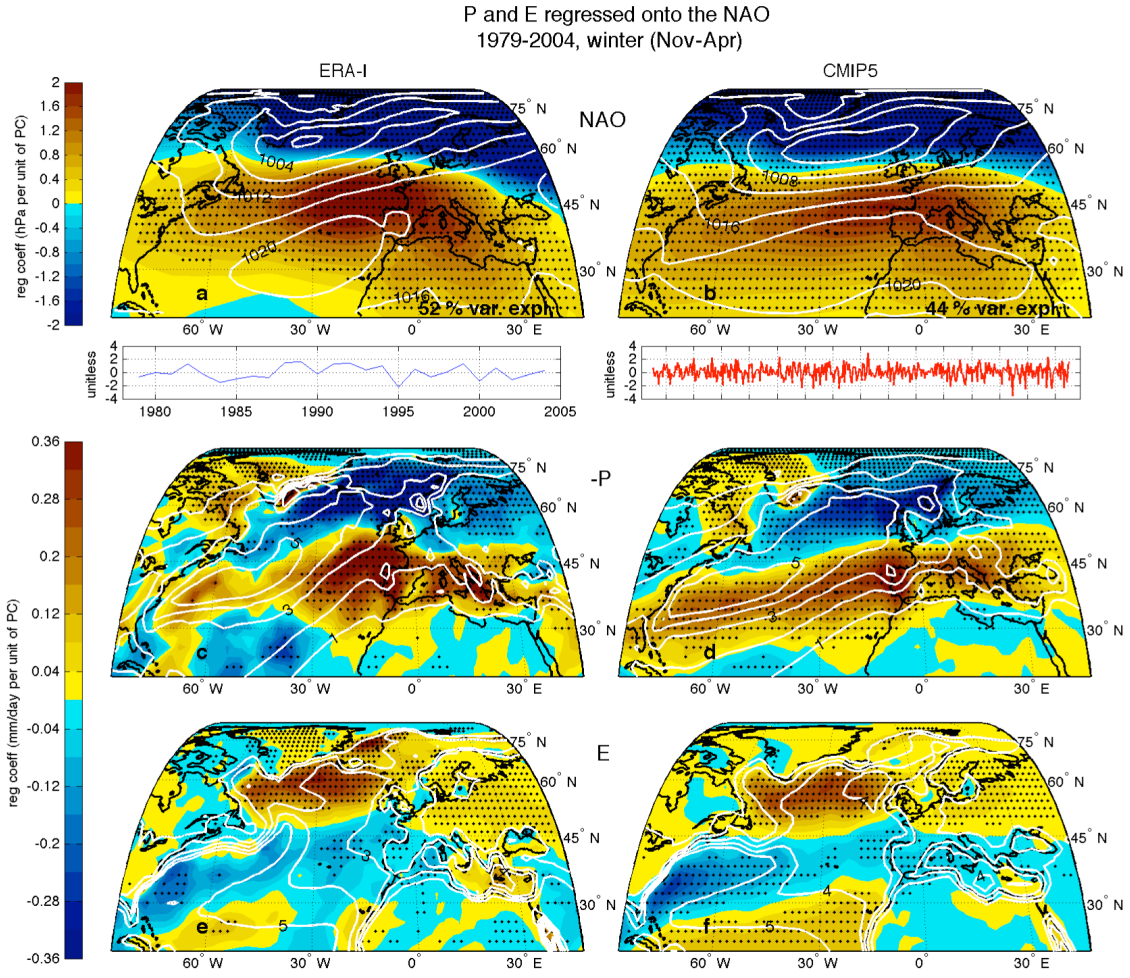

Figure 4.1: Regression of observed (ERA-I reanalysis) and CMIP5 pooled model (a,b) sea-level pressure, (c,d) precipitation and (e,f) temperature, onto the NAO timeseries from 1979-2004 for six month winter (Nov-Apr). Regression coefficients are color shaded, hatching indicates significance (p<.1) and white contours display the climatology.

Regression correlation, ERA with CMIP5				
	WINTER		SUMMER	
	Atl	Med	Atl	Med
PmE	0.70	0.74	0.56	0.54
P	0.79	0.83	0.60	0.62
E	0.75	0.57	**0.21**	**0.25**
mean flow	0.74	0.73	0.44	**0.27**
transients	0.62	0.57	**0.18**	**0.05**
mass div	0.62	0.55	0.42	**0.25**
moist adv	0.77	0.63	0.33	**0.30**

Table 4.2: Correlations between moisture budget NAO regression patterns of the ERA-Interim and the CMIP5 models, 1979-2004, six-month winter (Nov-Apr) and summer (May-Oct).

In the observed case the drying is more pronounced off the coast of Portugal and less so in the subtropical western north Atlantic than in the models. In both cases the pattern of drying is fairly consistent over the Mediterranean region. Similar to the SLP pattern, the precipitation anomalies associated with a positive NAO reflect the northward shift of the climatological rainfall pattern (contours). In terms of evaporation, the observations and models also agree well (R=.74), particularly in showing consistent anomalous evaporation poleward of 45°N, over the Atlantic and Europe associated with a positive NAO and increased precipitation in the same region. Over the Mediterranean, there is less agreement (R=.54), although both show reduced evaporation over Iberia and increased evaporation over the eastern Mediterranean Sea.

Similar to the winter, the summer NAO (top panels in Fig. 4.2) is characterized by a north-south dipole with low-pressure anomalies to the north and high-pressure anomalies to the south during a positive phase, indicative of a northward-shifted climatological pattern. The models show a climatological high-pressure bias over much of the domain, although the locations of the subtropical high and subpolar low are essentially the same as observed. As with winter, the observed summer NAO represents more of the total SLP variance (43%) than for the models (33%). The observations show an NAO pattern that is separated into two subtropical nodes, one over the western north Atlantic and another over Europe and the Mediterranean. This is not obvious for the models, which indicate a much more zonally symmetric pattern over the entire

subtropical domain that is centered over the eastern north Atlantic at approximately 20°W longitude. In both cases there is broad incidence of easterly wind anomalies over the greater Mediterranean. The subpolar center of the NAO during summer is located over southern Greenland, resulting in a northwest-southeast dipole orientation and increased southwesterly flow from Canada to Scandinavia during a positive NAO. This NAO pattern brings about decreased precipitation (panels c,d) over all of Europe and increased precipitation over much of the Mediterranean Sea in both observations and in models. There is little to no agreement between models and observations with respect to the pattern of the relationship between the NAO and evaporation over the greater Mediterranean (R=.21), although the influence is weak in both cases.

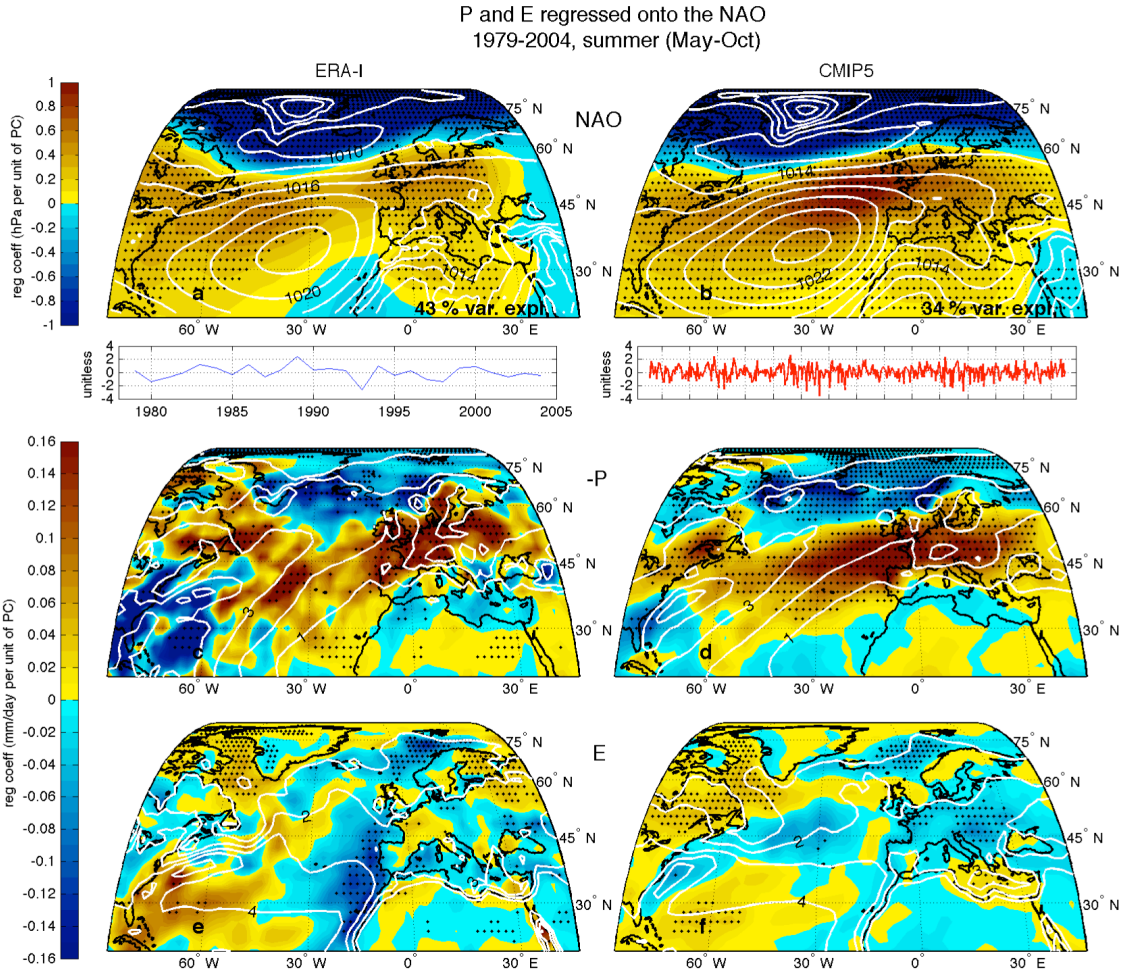

Figure 4.2: As in Figure 4.1, but for summer (May-Oct).

4.4 Moisture budget associated with the NAO

To examine the causes of the hydroclimate changes associated with the NAO, in this section we examine the detailed moisture budget. The winter and summer regressions of the CMIP5 ensemble and the ERA-I moisture budget from 1979-2004 onto the NAO are shown in Figures 4.3 and 4.4. The P-E term in the moisture budget is balanced by the total moisture flux convergence (Eq. 4.1), and the latter can be divided into mean and transient moisture convergence components (Figs. 4.3 and 4.4 (c)(d)(e)(f)) (Eq. 4.3). Panels g through j further show the mean moisture divergence term separated into contributions associated with mean mass divergence and with the mean moisture advection (Eq. 4.4).

Figures 4.3 and 4.4 also show the climatologies of the moisture budget terms for the models and ERA-I and we begin by comparing them. The pattern correlations for these are given in Table 4.3. In both seasons the climatology of the net influx of water at

Climatology correlation, ERA with CMIP5				
	WINTER		SUMMER	
	Atl	Med	Atl	Med
PmE	0.96	0.93	0.93	0.87
P	0.97	0.91	0.96	0.93
E	0.98	0.95	0.98	0.89
mean flow	0.87	**0.62**	0.86	0.75
transients	0.92	0.89	0.90	0.85
mass div	0.83	**0.60**	0.87	0.80
moist adv	0.85	0.79	0.87	0.86

Table 4.3: Correlations between moisture budget climatology patterns of the ERA-Interim and the CMIP5 models, 1979-2004, six-month winter (Nov-Apr) and summer (May-Oct).

the surface (white contours, top panels in Figs. 4.3, 4.4) agrees very well between models and ERA-I, with correlations R=.96/.93 for the greater Atlantic domain during winter/summer, and R=.93/.87 for the Mediterranean region alone. The Mediterranean climatology patterns are shown in greater detail in Figure 4.5. Table 4.3 indicates that for

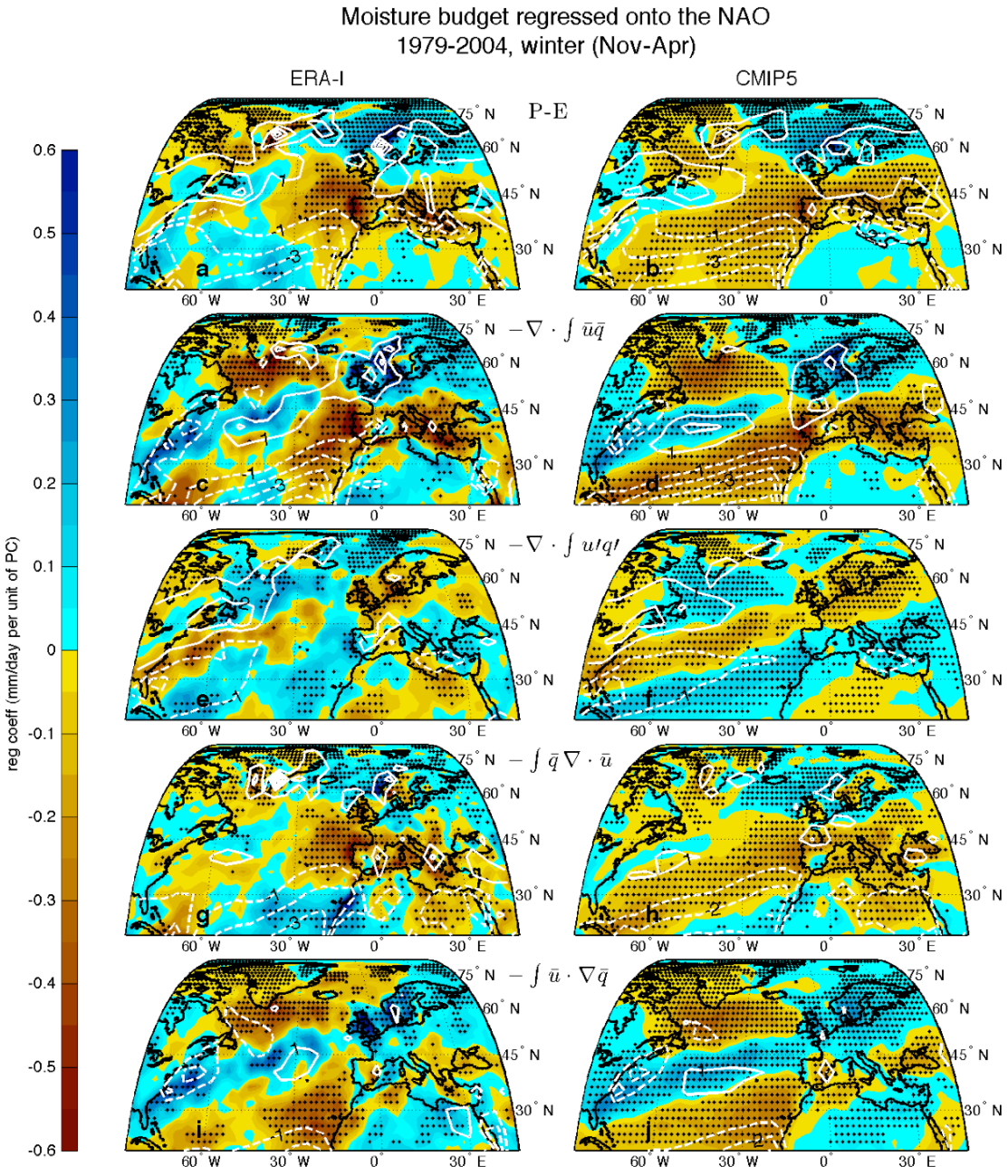

Figure 4.3: Regression of observed (ERA-I reanalysis) and CMIP5 pooled model moisture budget terms, (a,b) precipitation minus evaporation (P-E), (c,d) mean flow moisture divergence, (e,f) transient moisture divergence, (g,h) mass divergence, and (i,j) moisture advection, onto the NAO timeseries from 1979-2004 for six month winter (Nov-Apr). Regression coefficients are color shaded, hatching indicates significance ($p<.1$) and white contours display the climatologies for each term.

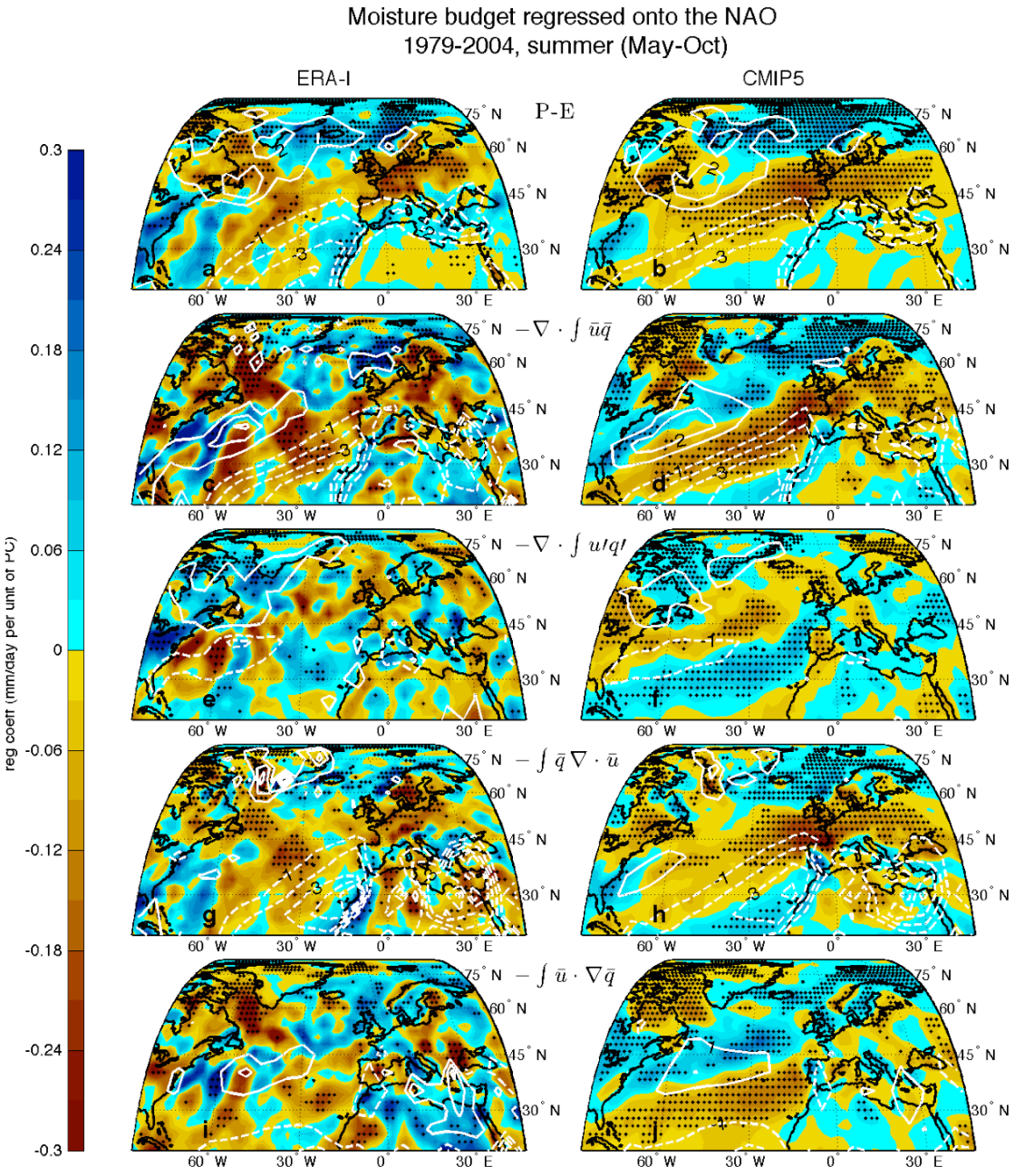

Figure 4.4: As in Figure 4.3, but for summer (May-Oct).

this region the relationship between the observed and modeled winter mean and mass divergence terms are less highly correlated (R=.62/.6) than the other terms during both seasons, which are correlated above R=.75. Observations and models indicate a broad P-E deficit over the subtropical north Atlantic, extending over the Mediterranean Sea, Black Sea and Red Sea, a smaller deficit over north Africa, and a general surplus of P-E in the midlatitudes and over most of Europe during winter. With respect to the greater Mediterranean region (Fig. 4.5(a)) the winter pattern can be described as positive P-E over land and negative P-E over water, with the exception of north Africa which is nearly zero. The mean flow exhibits moisture convergence over northern Europe and divergence over north Africa, much of the Mediterranean Sea and along the coast of Spain, France and Italy (Fig. 4.3 contours, and Fig. 4.5(c)). The transient pattern during winter is nearly identical to the total P-E pattern, providing moisture convergence over land and strong divergence over the Mediterranean Sea (Fig. 4.5(e)). The mean and transients combine to produce divergence over water, whereas over land the mean flow produces moisture convergence north of the Pyrenees and Alps and divergence south, along the coast.

During summer (Figs. 4.4, 4.5 and Table 4.3), the modeled climatology patterns once again show strong resemblance to the large-scale patterns of the observations, although the modeled patterns are more coherent, likely due to the reduced sample size in the ERA-I case as compared with the use of 15 models. In climatology, the pattern of subtropical P-E deficit and midlatitude P-E surplus is much less zonally symmetric over the subtropical Atlantic than in winter. During winter over the Mediterranean the transient climatology exhibits a clear land-sea contrast, but this is not the case for summer (Fig. 4.5(f)) when the eddies are reduced and the mean flow dominates the overall pattern of P-E deficit (Fig. 4.5(b)) over the greater Mediterranean. The models are shown to simulate the observed climatologies of the moisture budget in both seasons quite well, providing confidence in our ability to use them to examine the relationship with the NAO.

The observed regressions of P-E onto the NAO during winter agree well with the CMIP5 modeled terms over the Atlantic and the Mediterranean (Fig. 4.3), with correlations of R=.7 and .74, respectively (Table 4.2). The observed patterns do have a

	WINTER					SUMMER			
	ATLANTIC DOMAIN								
	(-86:46 lon, 20:88 lat)								
	climatology correlation with PmE		NAO regression correlation with PmE			climatology correlation with PmE		NAO regression correlation with PmE	
	ERA-I	CMIP5	ERA-I	CMIP5		ERA-I	CMIP5	ERA-I	CMIP5
PmE	1.00	1.00	1.00	1.00		1.00	1.00	1.00	1.00
P	0.03	0.09	**0.88**	**0.82**		0.24	0.21	**0.89**	**0.95**
E	**-0.72**	**-0.68**	-0.01	0.05		**-0.57**	**-0.67**	-0.27	-0.06
mean flow	**-0.63**	**-0.70**	**-0.67**	**-0.72**		**-0.74**	**-0.82**	**-0.51**	**-0.65**
transients	**-0.69**	**-0.67**	0.10	0.22		-0.21	-0.28	-0.05	**-0.02**
mass div	**-0.64**	**-0.70**	**-0.53**	**-0.58**		**-0.69**	**-0.77**	**-0.48**	-0.59
moist adv	-0.27	-0.35	-0.12	-0.29		-0.16	-0.32	-0.08	-0.01

	MEDITERRANEAN ONLY								
	(-10:40 lon, 30:45 lat)								
	climatology correlation with PmE		NAO regression correlation with PmE			climatology correlation with PmE		NAO regression correlation with PmE	
	ERA-I	CMIP5	ERA-I	CMIP5		ERA-I	CMIP5	ERA-I	CMIP5
PmE	1.00	1.00	1.00	1.00		1.00	1.00	1.00	1.00
P	0.28	0.40	**0.95**	**0.98**		0.17	0.20	**0.79**	**0.93**
E	**-0.78**	**-0.73**	-0.10	0.41		**-0.80**	**-0.82**	-0.40	0.29
mean flow	-0.22	-0.47	**-0.80**	**-0.85**		**-0.50**	**-0.65**	-0.16	**-0.60**
transients	**-0.84**	**-0.82**	0.41	0.33		0.03	0.07	-0.19	**0.13**
mass div	-0.17	-0.33	**-0.47**	**-0.34**		**-0.45**	**-0.63**	-0.06	-0.27
moist adv	-0.15	-0.13	-0.01	-0.02		0.22	0.38	0.02	0.20

Table 4.4: Correlations of moisture budget climatology and NAO regression patterns for the ERA-Interim and the CMIP5 models, 1979-2004, six-month winter (Nov-Apr) and summer (May-Oct).

stronger relationship with the NAO than is the case for the models (based on the root-mean squares [RMS] of the Atlantic and Mediterranean domains, Fig. 4.6)). In first comparing the winter P-E (Fig. 4.3(a)) and precipitation (Fig. 4.1 (c)(d)) regressions, we can see that the two patterns are largely the same, confirming the dominance in winter of precipitation variability (see Table 4.2). This is not the case for the climatology, in which negative P-E in the subtropics arises from strong evaporation (Fig. 4.3(a)(b) and Fig. 4.1(e)(f), and this can be seen in the spatial correlations (Tables 4.3, 4.4). There are three centers of action in the larger Atlantic domain where the observed and modeled NAO and the total moisture budget are most strongly related (Fig. 4.3(a)(b)). The greater

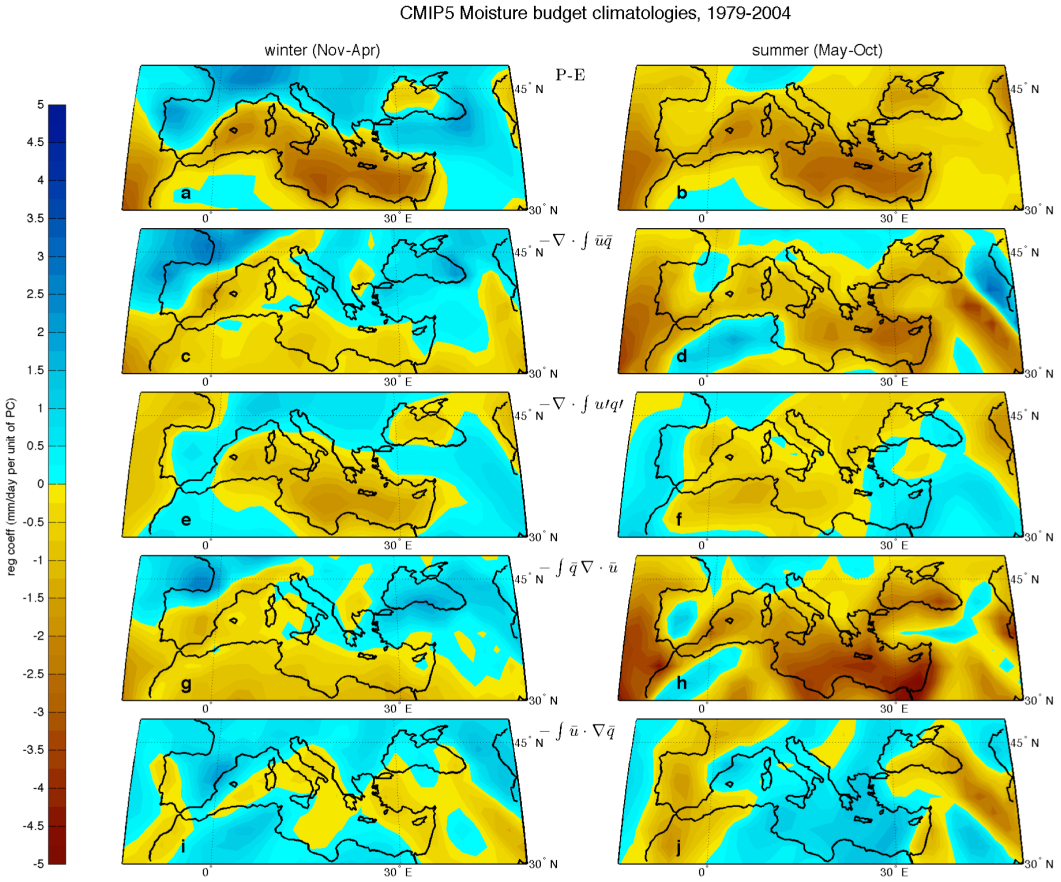

Figure 4.5: CMIP5 Mediterranean moisture budget climatologies, 1979-2004, for six-month winter (Nov-Apr) and summer (May-Oct).

Mediterranean region has an anomalous water deficit during positive NAO winters. This negative P-E center is most pronounced over Portugal, extending off its coast to the west and eastward across southern Europe, and in the models southwestward across the north Atlantic. The second center is of positive P-E over the coast of Norway, stretching from Iceland across Scandinavia. In addition to the broad subtropical Mediterranean drying, there is also a pronounced negative P-E anomaly that stretches from Greenland across the Labrador Sea to Canada.

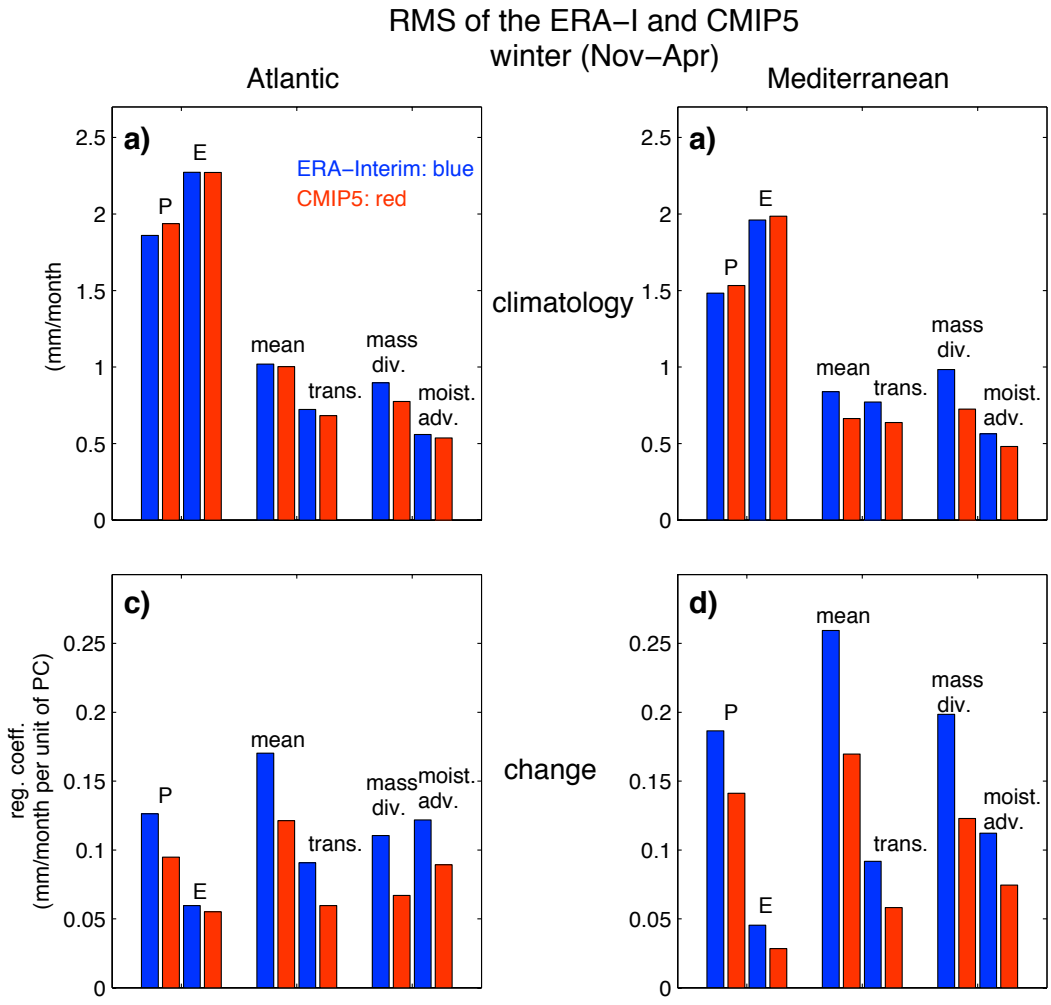

Figure 4.6: RMS of moisture budget climatologies and NAO-associated change over the greater Atlantic and Mediterranean domains, for winter (Nov-Apr).

During summer, the NAO-related P-E change in the observations and in the models (Fig. 4.4(a)(b)) are less related than during winter (Table 4.2). As with winter, precipitation (Fig. 4.2(c)(d) is largely responsible for the P-E change (Fig. 4.4(a)(b) rather than evaporation (Fig. 4.2(e)(f) (which is more important for the climatology). The broad subtropical band of negative P-E anomalies, shifted poleward from the winter case, now covers nearly all of Europe (Fig. 4.4(a)(b)). Over much of the Mediterranean Sea, the P-E anomaly is actually slightly positive for a positive NAO while the models tend to have

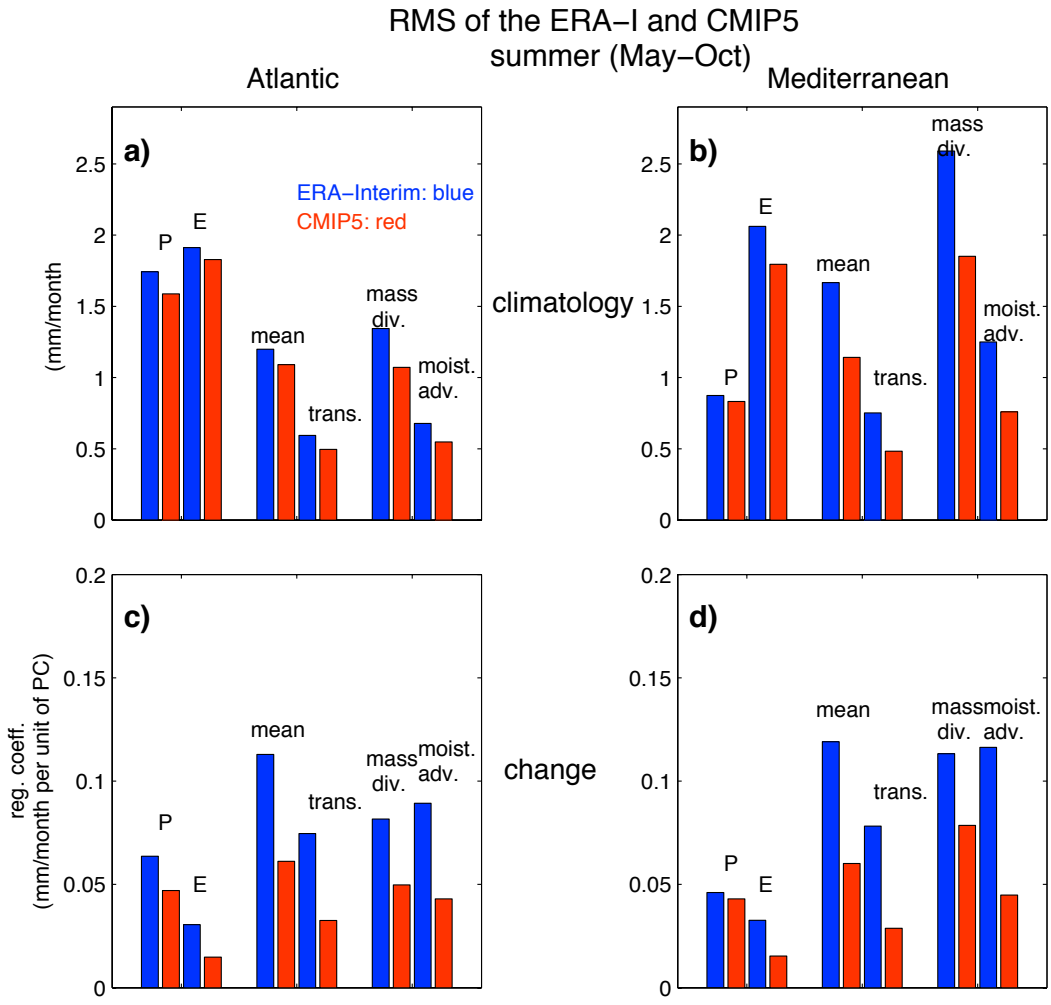

Figure 4.7: As in Figure 4.6, but for six-month summer (May-Oct).

a negative P-E anomaly. This negative P-E anomaly in the models also extends into southeastern Europe but not in observations though neither changes here are statistically significant. Previous studies have shown that CMIP3 models exhibit considerable disagreement with observations in their simulation of the summer NAO and its relationship to Mediterranean precipitation (Blade et al., 2012). This holds true for the CMIP5 models as well and the NAO-related moisture budget anomalies are not highly correlated with observations (Tables 4.2, 4.4). Much of this disagreement appears to be

related to differences in the patterns of evaporation anomaly, not only for the Mediterranean but for the greater Atlantic domain as well (Fig. 4.2(e)(f)).

Next we examine the contributions from the mean moisture convergence and the transient eddies to the NAO-associated P-E anomaly. Nearly all NAO-induced total P-E deficit over the greater Mediterranean region during winter is due to the monthly mean moisture divergence (shading in Fig. 4.3(c)(d) while the transient eddies (Fig. 4.3(e)(f)) actually provide a moisture convergence anomaly. The RMS values (Fig 4.6) for the mean contribution are nearly three times as large as for the transients. Over the Mediterranean Sea the transients' dependence on the NAO is small, but off the western Iberian coast and over the eastern Mediterranean Sea basin it is statistically significant (α=.1). For the climatology (or NAO-neutral conditions) both the transients and the mean flow dry the Mediterranean Sea itself so the fact that they oppose each other during NAO variability, is noteworthy. During positive NAO winters the mean circulation shifts well poleward providing a positive mean flow moisture convergence anomaly over northwestern Europe with the transient eddies once more offsetting and contributing a drying tendency. Hence, rather than the moisture convergence by storm systems dominating the NAO-related moisture budget variability, both the observations and the models demonstrate that the NAO impacts Mediterranean and Europe hydroclimate through shifts in the mean flow moisture divergence with the transient eddies opposing these changes. However, it is known that the effect of the transients can extend beyond the wave moisture flux, acting to drive some of the anomalous mean circulation, by accelerating the upper-level jet for instance.

In summer, as with winter, the mean and transients combine to produce climatological divergence over the Mediterranean Sea, but in this season the mean contribution is more dominant than in winter, particularly over the eastern Mediterranean (Fig. 4.4(c)(d)(e)(f)). For a positive NAO the models indicate drying over the Mediterranean Sea in the mean but wetting from the transients. This is not the case for the observations, in which the patterns are less coherent and the contributions from the mean and the transients are more equal (Fig. 4.4, Table 4.4).

Last we examine the mass divergence and moisture advection contributions to the mean flow moisture divergence (Eq. 4.4). For the Mediterranean winter half year, the

moisture divergence related to mass divergence under a positive NAO (Fig. 4.3(g)(h)) resembles the total mean flow moisture divergence and the total P-E spatial patterns. This makes clear that the mass divergence term is most responsible for the total mean flow moisture divergence. Over the North Atlantic and northern Europe, the total mean flow moisture budget pattern resembles the contribution from moisture advection (Fig. 4.3(i)(j)) more than that from the mass divergence. The spatial correlation between the moisture advection and total P-E patterns for the entire Atlantic domain (including the Mediterranean) is not robust, but is stronger in the models (R=.3) than in the observations (R=.12). In summer (Fig. 4.4) the moisture budget term related to mass divergence is dominant over central and northern Europe, and over the greater Atlantic (Table 4.4), while over the Mediterranean the moisture advection term contributes more equally to the total mean flow moisture divergence.

In comparing the patterns of the transients to the mass divergence and moisture advection patterns (see Table 4.5), we see that in climatology each of the correlations is weak, for the Atlantic and for the Mediterranean, but during a positive NAO the transient pattern is highly-correlated (R=.77/.81) with the moisture advection over the greater Atlantic. This is less so over the Mediterranean, at R=.49/.21 for the models and observations, respectively. During summer the observed versus modeled relationship with the NAO exhibits much more uncertainty (Blade et al., 2012), and should therefore be treated with cautious regard.

correlation with transients									
		Atlantic				**Mediterranean**			
		climatology		**regression**		**climatology**		**regression**	
		ERA-I	CMIP5	ERA-I	CMIP5	ERA-I	CMIP5	ERA-I	CMIP5
WINTER	**mass div**	0.19	0.22	-0.07	-0.21	-0.01	0.00	-0.10	-0.05
	moist adv	-0.21	-0.26	**-0.77**	**-0.81**	0.14	0.23	**-0.49**	-0.21
SUMMER	**mass div**	-0.09	-0.03	-0.11	-0.14	-0.25	**-0.32**	0.01	**-0.49**
	moist adv	**-0.35**	**-0.32**	**-0.72**	**-0.76**	**-0.43**	-0.24	**-0.58**	-0.45

Table 4.5: Correlations between transients and mass divergence and moisture advection patterns, climatology and NAO regression, for the ERA-Interim and the CMIP5 models, 1979-2004, six-month winter (Nov-Apr) and summer (May-Oct).

4.5 Links between large-scale circulation and NAO variability in the CMIP5 models

To further explore the relationship between the NAO and the mean and transient contributions to the moisture budget in the CMIP5 models we next examine the seasonal mean storm track (850hPa $\mathbf{v}'^2$), 500hPa vertical velocity ($\boldsymbol{\omega}$), and low-level (850hPa) specific humidity (**q**), air temperature (**T**) and zonal (**u**) and meridional (**v**) components of the horizontal wind vector (Fig. 4.8). The climatological mean values are shown in white contours (black arrows for the horizontal wind vector) and the NAO-related anomalies as color shading. In both winter and summer, the storm track associated with a positive NAO is shifted northward of its climatological position. Over the Mediterranean region, there is a marked decrease in storm activity during a positive NAO in both seasons. It would be expected to see increased transient eddy moisture flux convergence (divergence) poleward (equatorward) of the maximum $\mathbf{v}'^2$ anomaly. Comparing Figure 4.8(a) with Figure 4.3(f) this is in general the case with the transient anomaly drying much of Europe equatorward of the maximum storm track anomaly and moistening poleward of there. During summer (Fig. 4.8(b)) the pattern is weakened and shifted poleward. During this season however, the relationship between transient moisture convergence (Fig. 4.4(f)) and $\mathbf{v}'^2$ over Europe and the Mediterranean is much less coherent than over the Atlantic.

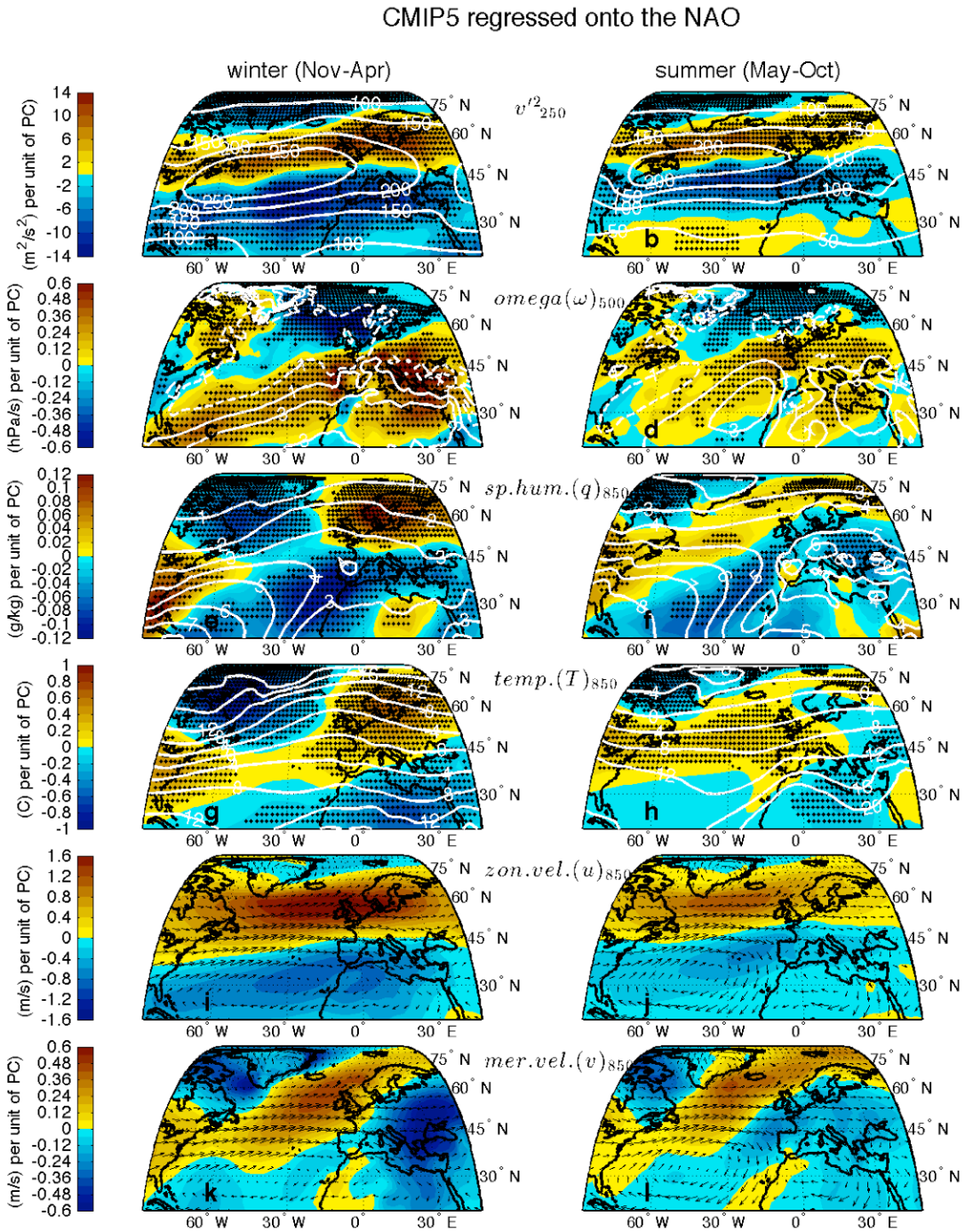

Figure 4.8: CMIP5 pooled model regression of (a,b) 250hPa vector meridional velocity variance (**v**'^{2}), (c,d) 500hPa vertical velocity (**ω**), (e,f) 850hPa specific humidity (**q**), (g,h) 850hPa air temperature (**T**), and 850hPa zonal (**u**) and meridional (**v**) components of the horizontal wind vector, onto the NAO from 1979-2004, for six-month winter (Nov-Apr) and summer (May-Oct). Regression coefficients are color shaded, hatching indicates significance ($p<.1$) and white contours display the climatology.

For both seasons and across the Atlantic Ocean and over Europe and the Mediterranean the NAO-induced winter 500hPa vertical velocity pattern (Fig. 4.8(c)) closely resembles the pattern of the moisture budget term involving the mass divergence (Fig. 4.3(h)). In winter there is broad subsidence stretching from the western tropical Atlantic to the greater Mediterranean and Europe with ascent over northwest Europe. In summer the same patterns of subsidence and ascent occur but are shifted northward relative to winter. For winter near-surface (850hPa) moisture under a positive NAO (Fig. 4.8(e)) there is decreased humidity over the greater Mediterranean and increased humidity over northern Europe. Figure 4.8(g) shows the change in winter temperature, warm over most of Europe and the eastern Mediterranean and cool over North Africa and the eastern Mediterranean. The low-level (850hPa) zonal and meridional wind components demonstrate a robust increase over the subpolar north Atlantic, resulting in enhanced southwesterly flow toward northern Europe, much stronger during winter, which is responsible for the warming and increased humidity. The winter meridional field also shows a northerly anomaly over eastern Europe, bringing colder, drier air towards the eastern Mediterranean during a positive NAO.

4.6 Forced moisture budget

Last we examine the differences in pattern between the moisture budget change due to the forced change (see Data and Methods) and the change due to the naturally varying NAO (Figs. 4.1, 4.2, 4.3, 4.4). Here we have regressed onto a nonlinear forced SLP response from 1950-2050 to determine the moisture budget forced change, or trend. The resulting patterns are qualitatively the same as those of Seager et al. (2013), which were determined by taking the difference between two periods 2021-2040 and 1979-2005, which implies that the change is quasi-linear. The forced change in the NAO, precipitation and evaporation is shown in Figure 4.9. The forced NAO pattern (Fig. 4.9(a)) is distinctly different than that of the natural NAO (Fig. 4.1(b) during winter. The forced increase in SLP extends over most of the North Atlantic domain, including Greenland, and covers the greater Mediterranean. The natural NAO pattern is much more zonally symmetric, and includes North America. This shows that the models' trend

toward a positive NAO under global warming is not an amplification of the canonical NAO pattern but rather has a separate and distinct signature of SLP change. For precipitation change (Fig. 4.9(c)) we see a similar broad subtropical band of drying in the forced case as under a positive NAO (Fig. 4.1(d)), but the forced band of drying is located slightly equatorward of the natural case and this difference is particularly evident over the eastern Mediterranean. Over the northern North Atlantic the forced and natural change patterns are quite different, as the forced case shows a robust increase in precipitation over North America, extending into the North Atlantic, a more modest increase over northern Europe, and strong drying south of Greenland. With respect to evaporation, we see similar subtropical drying over the North Atlantic in the forced (Fig. 4.9(e)) and natural (Fig. 4.1(f)) patterns, and wetting on its poleward flank. Over much of Europe the patterns are nearly the same, with decreased evaporation over Iberia, and increased evaporation over the remainder of Europe. There is a marked difference over the Mediterranean Sea however, which shows strong evaporation under forcing rather than modestly reduced evaporation there under a positive NAO. Further comparison between forced (Fig. 4.10) and natural (Fig. 4.3) moisture budget change patterns during winter also indicates similar forced and natural subtropical drying signatures. The chief difference, as with the precipitation change, is that the forced band of drying is located equatorward of the natural case and this difference is largest for the transients (Figs. 4.1(f), 4.10(e)). This distinction is pronounced over the Mediterranean, where the transients produce drying under forcing but wetting under a positive NAO. It is also noted that this forced transients pattern has opposite sign over land than that in Seager et al. (2013). This could be due to the nonlinear regression used here, or to the difference in length of time. Over the northern North Atlantic the forced and natural moisture budget changes show very little resemblance. Over northern Europe the agreement is better with the exception of the moisture advection change (Figs. 4.3(j), 4.10(i)), which is clearly wetter under a positive NAO but drier under forcing.

During summer (Figs. 4.2, 4.9), the differences between the forced and natural NAO, precipitation and evaporation changes are much more pronounced. As with winter however, the patterns of change in the other moisture terms indicate a similar equatorward orientation under the forcing.

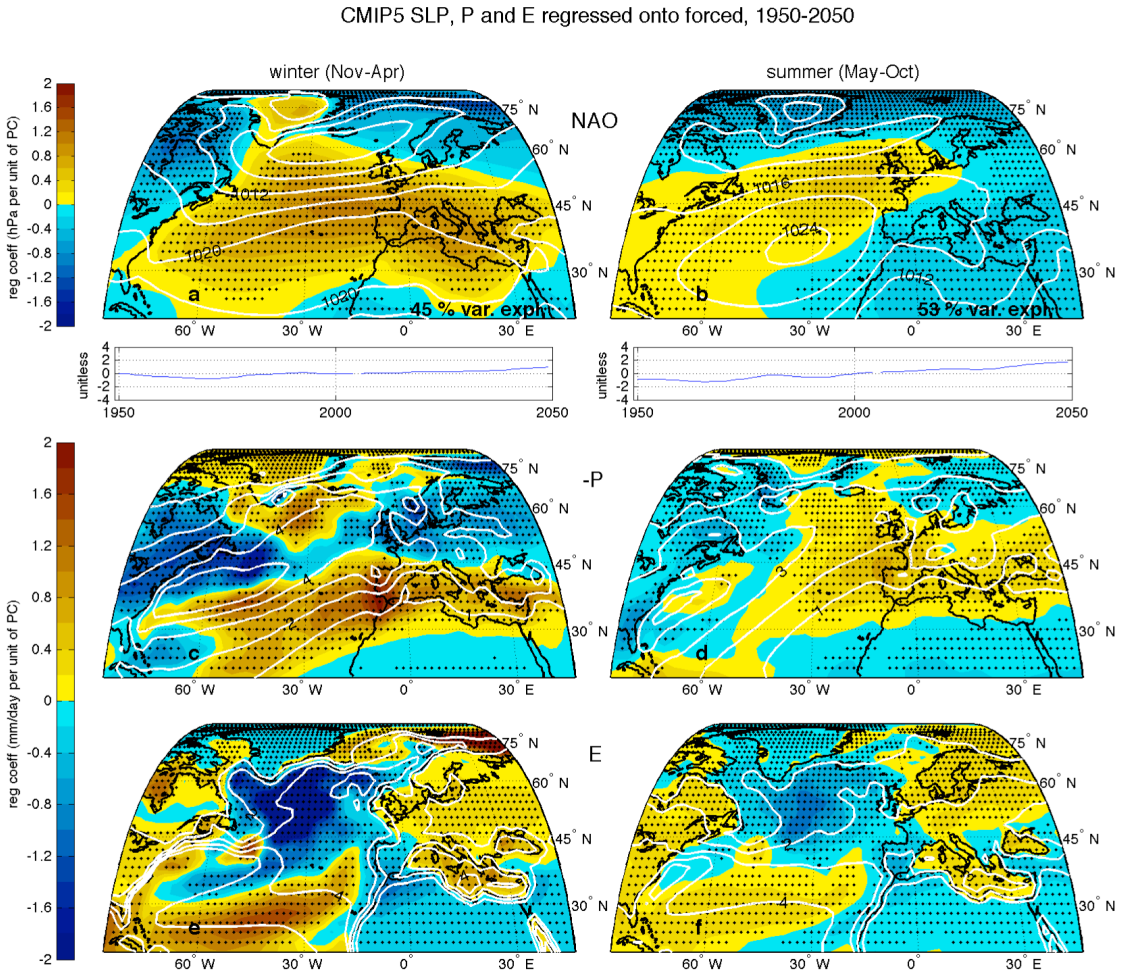

Figure 4.9: Regression of CMIP5 model (a,b) sea-level pressure, (c,d) precipitation and (e,f) temperature, onto the NAO forced timeseries (see Data and Methods) from 1950-2050 for six month winter (Nov-Apr) and summer (May-Oct). Regression coefficients are color shaded, hatching indicates significance ($p<.1$) and white contours display the climatology.

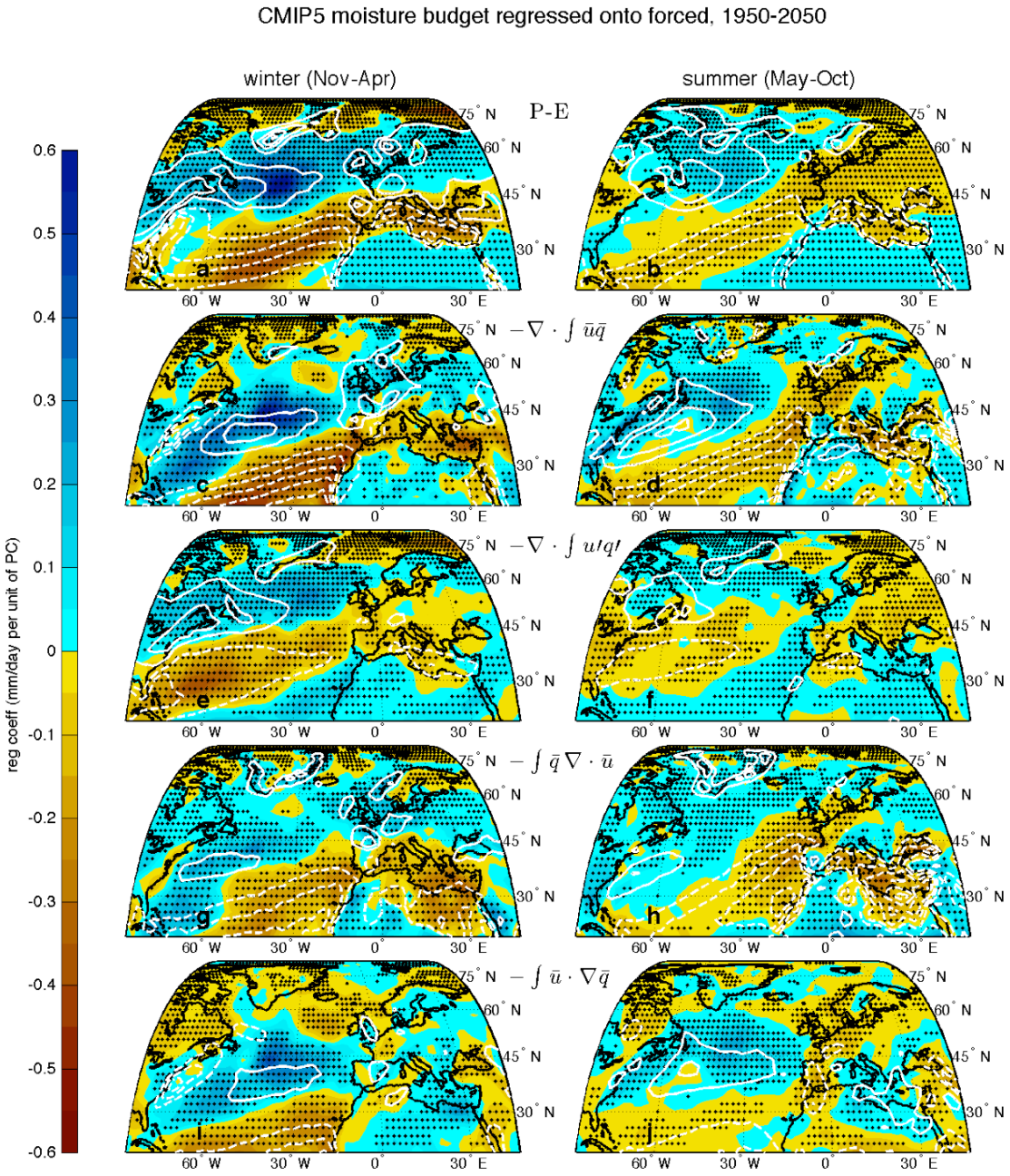

Figure 4.10: Regression of CMIP5 pooled model moisture budget terms, (a,b) precipitation minus evaporation (P-E), (c,d) mean flow moisture divergence, (e,f) transient moisture divergence, (g,h) mass divergence, and (i,j) moisture advection, onto the NAO forced timeseries (see Data and Methods) from 1950-2050 for six month winter (Nov-Apr) and summer (May-Oct). Regression coefficients are color shaded, hatching indicates significance ($p<.1$) and white contours display the climatologies for each term.

4.7 Conclusions and summary

It has been previously shown that anthropogenic forcing will decrease precipitation during winter and increase evaporation during summer, thereby increasing the climatological annual P-E deficit over the Mediterranean Sea and reducing the P-E surplus over surrounding land areas. This drying is due largely to increased moisture divergence by the monthly mean flow and is related to a shift towards increased low level mass divergence (Seager et al. 2013). Here, in contrast to climate change, we have examined the natural interannual variability of the NAO and its relationship with the respective moisture budget terms, comparing an ensemble of 15 CMIP5 models to the ERA-I reanalysis. We find that the same terms that dominate the overall P-E climate change also dominate the year-to-year NAO variability. During the winter season, when the Mediterranean region receives most of its rainfall, the total NAO-induced moisture divergence over the North Atlantic is largely accounted for by the mean flow moisture divergence and is opposed by the transient eddy moisture convergence. It is difficult to calculate how much the transient wave fluxes may influence the anomalous mean circulation itself, and we make no attempt to do so here.

Overall the CMIP5 models perform quite well in their large-scale simulation of the observed relationship between the NAO and the atmospheric moisture budget, although the agreement is less during summer. Over the Mediterranean region there are some sub-regional inconsistencies with respect to the ERA-I reanalysis that could be due to the small sample size of 26 years, or to topographic and orographic features that are not fully resolved by the global climate models with their limited spatial resolution. What does appear clear however, is that during a positive NAO, the resulting poleward shift in both the mean flow and in the transient eddies combines to bring about robust drying of the Mediterranean region, and that the drying is due to the shift in the mean flow while the transients provide a modest, offsetting, anomalous moisture convergence. The importance of the mean flow moisture divergence is reflected in the pattern of large-scale subsidence associated with the NAO, with, for a positive NAO, widespread subsidence anomalies across the Mediterranean region and much of Europe and ascent

over northwest Europe. The anomalies in the transient moisture flux convergence dry on the equatorward flank of the maximum storm track anomaly and moisten on the poleward side as expected. For a positive winter NAO this means the transients dry most of Europe. The anomalous moistening by transients over the Mediterranean region during a positive NAO occurs despite weaker eddies here and may be related to a weaker meridional moisture gradient that causes a reduction in moisture transport into Europe from the Mediterranean Sea. However this last relation needs more research to verify.

Last, we compare the moisture budget changes associated with NAO variability to the changes under global warming (here determined by regression onto nonlinear forced NAO response, shown to reproduce qualitatively the same trend patterns as in Seager et al., 2013) over the Mediterranean during winter, to facilitate discrimination between the patterns of climate change and climate variability. We find there are key differences, which include:

1) A decrease in winter precipitation over the eastern Mediterranean that is located poleward in the NAO case but under climate change is centered more on the Mediterranean Sea.
2) Enhanced evaporation over the Mediterranean Sea, Italy and eastern Europe under climate change, but a modest reduction of evaporation there during a positive NAO.
3) The total change in P-E in both cases is dominated by the precipitation change. Therefore, as in 1), the pattern of drying under natural variability is shifted poleward of the climate change pattern, which is more strongly tied to the Mediterranean Sea. Most of this total subtropical P-E change is due to the mean flow contribution, under natural variability and under forcing.
4) The largest difference between what occurs naturally versus under climate change lies with the transients. Under climate change the wintertime transients were shown to provide divergence over nearly all of Europe and the Mediterranean. Under a positive NAO the shift in the storms actually opposed the mean, causing convergence over the Mediterranean and divergence over northern Europe.

Chapter 5

Climate change and political instability in Syria

5.1 Introduction

In Chapter 3 we showed that anthropogenic drying is more pronounced in the eastern Mediterranean, where there is less multidecadal natural variability. This leads us to investigate the recent drought in Syria. Syria lies at the heart of the Fertile Crescent where agriculture and animal herding began some 12,000 years ago (Salamini et al., 2002). The breadbasket region in the northeast produces over two-thirds of the country's cotton and wheat (Massoud, 2010). One-third of the cultivated land is irrigated and thus dependent on increasingly limited groundwater supplies, while the remainder is rain-fed, leaving farmers dependent on year-to-year rainfall (Erian, 2011). Nearly all of Syrian rainfall occurs during the six-month winter season, November through April, along the country's Mediterranean Sea coast and in the northeast (Fig. 5.1), and has large interannual variability (Fig. 5.2(a)).

The five-year period of below-normal rainfall that began in the winter of 2004/5 (Fig. 5.2(a)) had dramatic consequences for the entire country, particularly the northeast. The last three years of this drought were especially severe, representing the worst three-year drought of the instrumental record (Trigo et al., 2010). Even before the drought, government policies intended to increase agricultural production had endangered Syria's water security by fostering the use of limited land and water resources without regard for sustainability (Rodriguez et al., 2010). These policies resulted in severe groundwater depletion and disincentives to modify inefficient irrigation techniques. The drought produced massive crop failures as the two-thirds of the cultivated land solely dependent

on rainfall suffered from "zero or near zero" production, and small-scale livestock herders (less than 100 animals) lost nearly all of their herds (FAO et al., 2008).

Estimates of the number of people internally displaced by the drought run as high

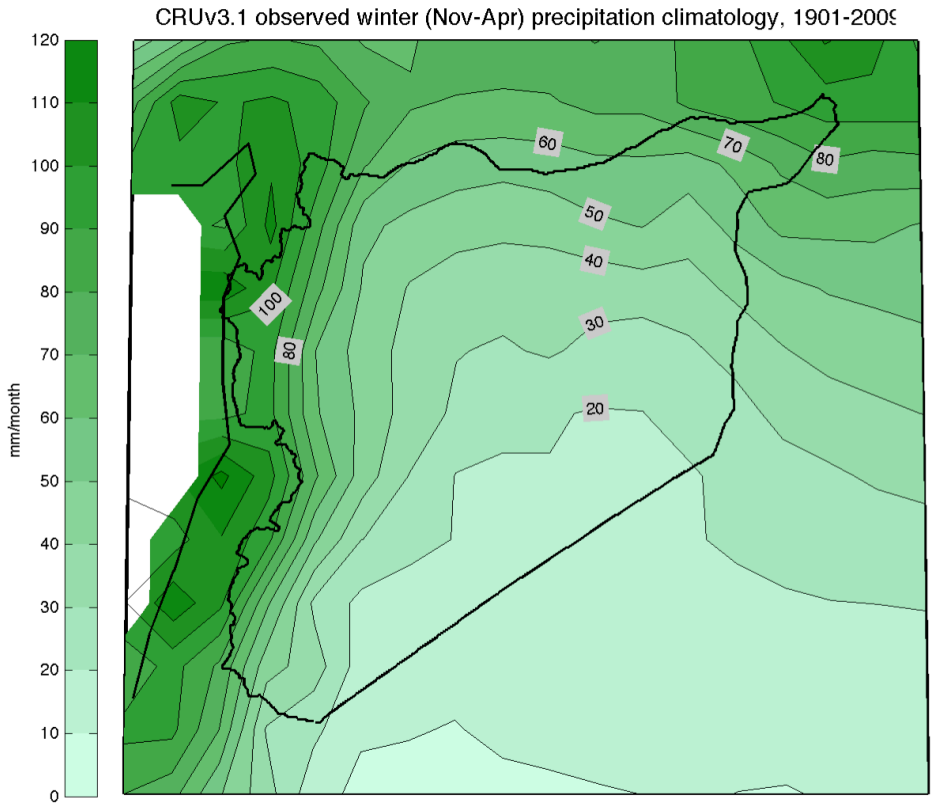

Figure 5.1: Observed winter (Nov-Apr) precipitation climatology, 1901-2009, University of East Anglia (UEA) Climate Research Unit (CRU) version 3.1 data.

as 1.5 million (Massoud, 2010; IRIN, 2009; Shadid, 2011; Solh, 2010). Most migrated to the peripheries of Syria's cities, which were already burdened by strong population growth (~2.5%) and the influx of an estimated 1.2 to 1.5 million Iraqi refugees between 2003 and 2007 (al-Khalidi et al., 2007). There is considerable anecdotal evidence that the added strain on the limited resources in and around these urban areas was an important factor in the civil unrest that began in March 2011 (Hinnesbusch, 2012; Friedman, 2013).

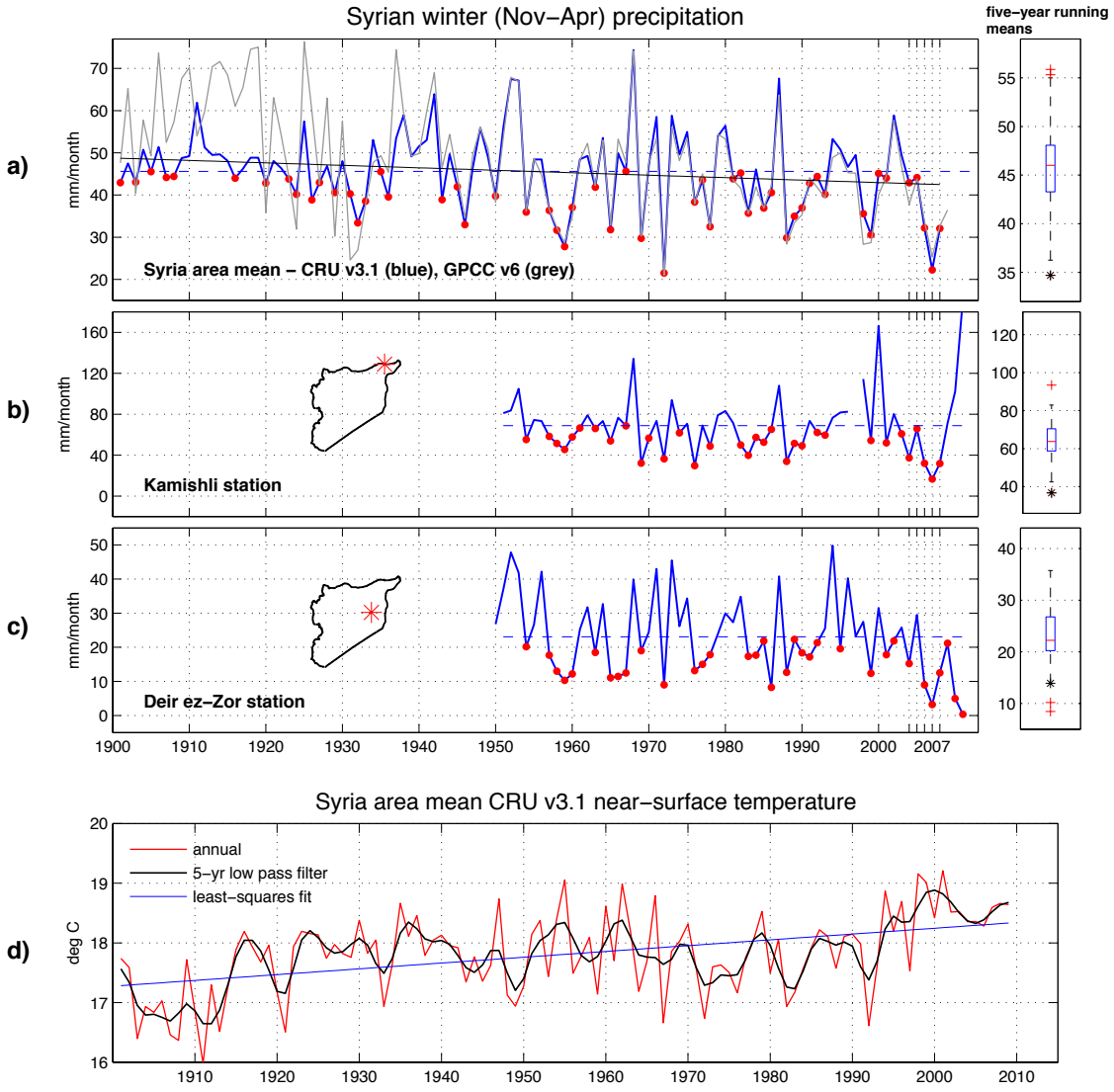

Figure 5.2: a) Six-month winter (November-April mean) Syria area mean precipitation, using CRU3.1 and GPCCv6 gridded data at .5x.5 resolution, with linear least-squares fit and time mean (dashed line) for the CRU. b) Six-month winter Kamishli and c) Deir ez-Zor precipitation station records from the GHCN. Red dots indicate years below the time mean for the lengths of the respective records. Boxplots are of running five-year means, with black asterisks representing the recent five-year drought (2004/05 – 08/09), box lines at the quartiles, whiskers extending to the maximum values within 1.5 times the interquartile range and red crosses indicating outliers. d) Annual CRU3.1 near-surface temperature for the Syria mean, with 5-year Butterworth low-pass filter and least-squares fit.

The unusual severity and persistence of the recent drought in the context of the historical climate record inevitably raises the question of whether anthropogenic climate change was an important contributing factor. It is a generic property of a time series consisting of an oscillatory part and a downward trend that the minimum is most likely to occur toward the end of the time period when the negative influence of the trend is greatest, at a time when the oscillation is also in a negative phase. Observations indicate that Syria experienced a drying trend over the entire 20th Century, and that the recent drought occurred during a negative phase of a (presumably) natural oscillatory pattern (Fig. 5.2(a)). Projections of the future made with global climate models overwhelmingly agree that the Eastern Mediterranean (EM) region will become drier as a consequence of rising greenhouse gases (IPCC, 2007; Giorgi and Lionello, 2008). In Chapter 3 we showed that in the EM human-induced drying is already distinguishable from natural variability. Our review of past studies and the new analysis presented here lead to the conclusion that the unusual severity and duration of the recent drought are likely attributable to human influence on the climate system.

5.2 Government policies

Government agricultural policy is prominent among the many factors besides drought that affected the course of events in Syria. During his rule from 1971-2000, President Hafez al-Assad promoted food self-sufficiency in the interest of national security. The government initiated policies of land redistribution and irrigation projects, policies intended to garner the support of rural constituents (Hinnebusch, 2012). Despite persistent water scarcity and frequent droughts, the production of strategic crops such as barley, wheat and water-intensive cotton were encouraged (Barnes, 2009). With the subsequent rapid growth of food production Syria achieved wheat self- sufficiency in the mid-1990s (Barnes, 2009; USDA).

Generous government subsidies for diesel fuel greatly devalued the price of water and animal feed, quickening the expansion of livestock herds, agriculture and water-intensive crops beyond the limited land and water capacities (Salman and Mualla, 2008). Farms unreachable by irrigation canals linked to river tributaries relied on pumped groundwater, which accounted for 60% of all irrigation water sources (Rodriguez et al.,

2010). The subsidies dissuaded farmers from updating inefficient, outdated irrigation techniques, resulting in the over-consumption and severe depletion of groundwater (de Chatel, 2010). Though the Syrian regime enacted a law in 2005 that required a government license to dig wells for groundwater access, the legislation was not enforced (de Chatel, 2010). Groundwater extraction remains largely unregulated and greatly exploited; thousands of illegal wells were dug after the law's inception (de Chatel, 2010). The drying of the Khabur River in the northeast of Syria around 2000 has been attributed to the overuse of groundwater (Massoud, 2010; de Chatel, 2010).

In 2000 power passed from Hafez al-Assad to his son Bashar. His government was less willing and less able to address the consequences of the drought for rural communities.

5.3 The societal impacts of the drought

The prolonged drought, which lasted from the 2004/5 growing season until 2010, devastated the region. Syria's wheat production failed in 2008, falling far short of self-sufficiency and for the first time in over a decade Syria was forced to import large quantities of wheat (FAS/USDA). The devastating impact on vegetation, especially in the northeastern wheat-growing region, is clearly evident in satellite imagery (Fig. 5.3).

In 2003, agriculture accounted for 25% of Syrian GDP. In 2008, three years after the start of the drought, the agricultural share of GDP fell to 17%. Atieh El Hindi, the director of the Syrian National Agricultural Policy Center (NAPC), writes that between 2007 and 2008, drought was a main factor, in addition to a rise in international food prices, in the unprecedented rise in Syrian food prices; in this single year, wheat, rice and feed prices increased over 100% (Nehme, 2008). In February of 2010, the United Nations news agency IRIN reported that the price of livestock feed had increased by three-fourths, given the drastic cut in barley yields, leading to 80% mortality for livestock on medium-sized farms (IRIN, 2010). Nearly half of Syrian herders own fewer than 100

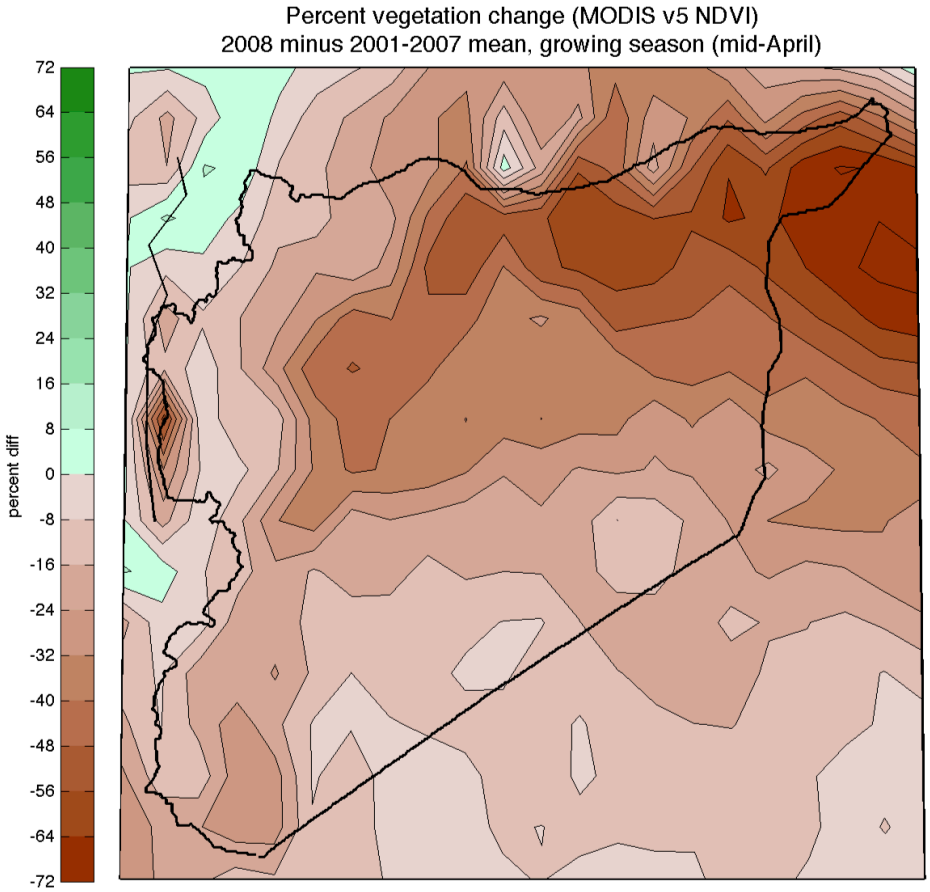

Figure 5.3: Percent change in the high resolution MODIS Normalized Difference Vegetation Index (NDVI) version 5, comparing 2008 and the mean of the previous seven years, for mid-April. The data were smoothed (area-averaged) to a coarser .25-degree by .25-degree grid prior to taking the difference.

animals, and during the drought nearly all such herds were obliterated (FAO et al. 2008). There was a drastic increase in nutrition-related diseases among children in the northeast provinces (OCHA, 2008) and in parts of the region enrollment in schools dropped by as much as 80% as many families left the region (De Schutter, 2010). The heavy reliance of rural Syria on year-to-year agricultural production left it ill suited to outlast a prolonged drought.

The most significant consequence was the internal migration of an estimated 1.5 million people to the peripheries of urban centers during the drought years (Massoud, 2010; IRIN, 2009; Shadid, 2011; Solh, 2010). For context, the total urban population of Syria in 2002 was 8.9 million and in 2010 it was 13.8 million, the increase made up of

roughly equal numbers due to natural increase, Iraqi refugees, and drought refugees (Fig. 5.4). Unlike past migrations when male household members moved to cities on a seasonal basis to generate income, entire families now abandoned some 70% of villages in the rural northeast and migrated on a more permanent basis (Khawaja, 2002; al-Khalidi, 2007).

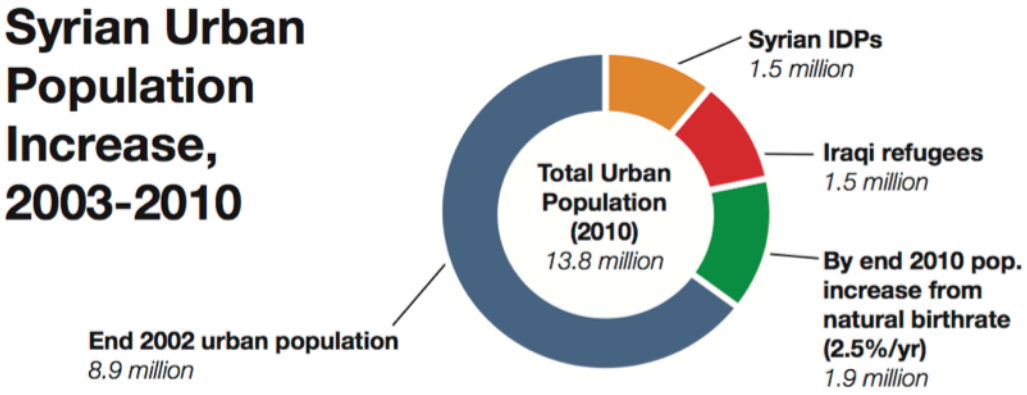

Figure 5.4: Pie chart of estimated population increase from 2002-2010 with contributions from Iraqi refugees, Syrian internally displaced persons (IDP) and population growth.

The rapidly growing urban peripheries of Syria, marked by illegal settlements, overcrowding and poor infrastructure, now make up half of the urban population (Khadour, 2009). There has been a sharp increase in crime where the new rural migrants settled, having been uprooted from "tight-knit farming communities" (IRIN, 2009b). The internal migration due to drought increased the strain on the cities' resources, already stressed by the 1.2–1.5 million Iraqi refugees who migrated to Syria's urban centers between 2003 and 2007. The Iraqi migration alone is estimated to have increased water consumption by 21%, and the price of housing in Damascus by 300% (al-Khalidid, 2007). The Iraqi migration continued despite the newly imposed visa restrictions in 2007, and the number of Iraqis entering Syria consistently surpassed those returning to Iraq (UNHCR, 2010). By 2010, internal migrants and Iraqi refugees made up an estimated

20% of Syria's urban population (Fig. 5.4).

The urban peripheries to which the majority migrated remained neglected by the Assad regime and became the heart of the developing unrest (Hinnebusch, 2012). At the same time, the regime implemented policies of "economic liberalization" by cutting fuel and food subsidies, further increasing the prices of staple goods (Hinnebusch, 2012). A considerable body of work indicates that the direct and indirect effects of drought can expose a regime's vulnerabilities, and that rapid demographic change encourages instability (Albala-Bertrand, 1993; Werrell and Femia, 2013). In the case of Syria, instability was exacerbated by the poorly planned economic policies of the elder Assad's regime and by the slow and ineffective response of the current Assad regime to the drought-induced demographic shift. In this context, the drought contributed to the mounting grievances that led to the uprising in March 2011 in Dara'a. Protests spread across the country, initiating the ongoing civil war. Whether it was a necessary factor behind the current conflict is impossible to know, but the drought was a visible and likely substantial contributing factor. Figure 5.5 presents a timeline summarizing the events that preceded the Syrian uprising.

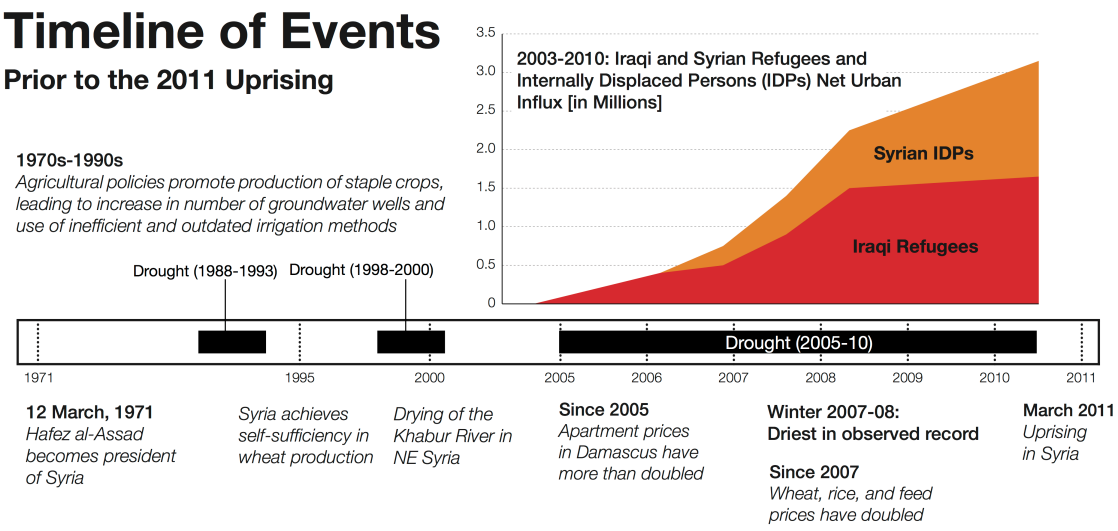

Figure 5.5: Timeline of events leading up to the civil uprising that began in March of 2011.

5.4 The meteorological drought in the context of the 20th Century

The timeseries shown in Figure 5.2, constructed using the CRU and GPCC gridded precipitation data sets and the GHCN station precipitation data (see Data and Methods, below) clearly show that the recent drought years were unusually harsh, reaching an extreme in the three consecutive winters from 2006/7 to 2008/9. The persistence of this five-year drought (2004/5 winter to 2010) also stands out (Fig. 5.2) in the Syria area mean rainfall (Fig. 5.2(a)) as well as in the only two GHCN stations located in northeastern Syria, Kamishli (Fig. 5.2(b)) near the Turkish border and Deir ez-Zor (Fig. 5.2(c)) on the Euphrates River. For the two northeastern stations the 2007/8 winter was easily the driest on record. For Syria as a whole, 1972/73 was also exceptionally dry but that drought did not persist, lasting only a single year. At Kamishli and Deir ez-Zor, the recent drought contained the driest five consecutive years on record. Distributions of running five-year means of six-month winter precipitation are shown in box and whiskers diagrams in Figure 5.2 at right. In each case the recent five-year drought (2004/5-2008/9) was in the tail of the distribution ($p<.01$). At Deir ez-Zor drought extended through the winters of 2010/11 and 2011/12 but Kamishli received well above normal rainfall in these last two winters. According to the CRU index, episodes in the early 1930s, and the late 1950s, 1980s and 1990s may be considered analogs to the recent drought, indicating that multiyear droughts do occur naturally in Syria. However, the late 1990s episode never fully recovered before collapsing into the recent severe drought again. Thus Syria has been in moderate to severe drought since 1998.

As noted above, the impact of the recent drought was aggravated by depleted groundwater reserves. Moreover, streamflow was down in the Euphrates and Tigris, whose numerous tributaries have supplied much of the water to Syria's breadbasket region. The Euphrates and Tigris are fed by orographic precipitation in the mountainous regions of eastern Turkey, and their low flow at this time (see Fig. 5.6 for precipitation timeseries) was presumably due to natural variability, related to a positive phase of the NAO (Cullen and deMenocal, 2000).

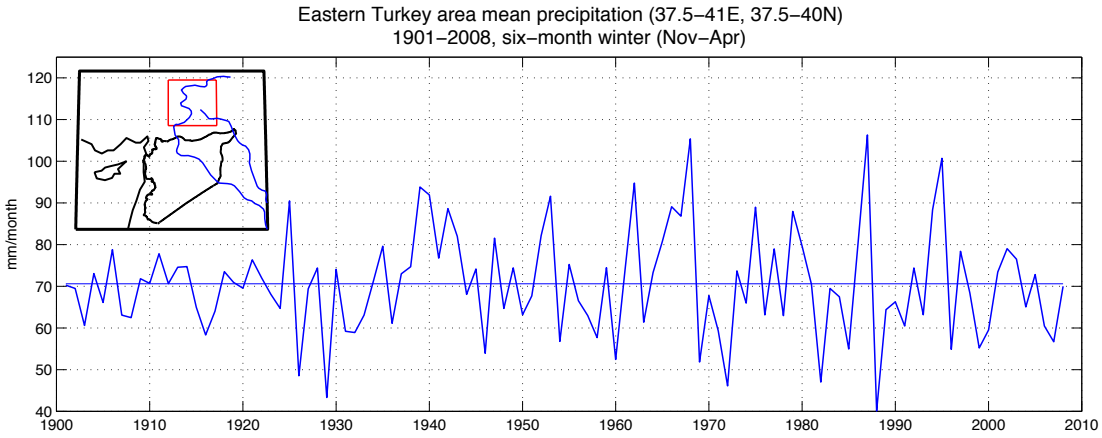

Figure 5.6: Observed area-mean winter (Nov-Apr) precipitation, 1901-2008, of the Euphrates and Tigris Rivers' headwater region, CRU 3.1 data.

Figure 5.2(a) shows an obvious downward trend in rainfall since 1900. A linear least-squares fit to the CRU Syrian area mean time series indicates that Syria as a whole experienced a significant ($p<0.05$) winter drying trend, a 13% reduction in rainfall over this period. The GPCC timeseries (in grey) yields a much larger (37%) reduction. This difference is primarily due to the lack of agreement during the first 50 years, when data were quite sparse; the two data sets agree that the reduction from 1951 to 2008 was 17 to 20%. Even the conservative estimate of a 13% (~6mm/month) change due to the long-term trend is nearly as large as the standard deviation of the timeseries (~9mm/month). Examination of GHCN stations in the greater Fertile Crescent domain (see Data and Methods for station selection criteria), after determining the change due to a least squares fit for each timeseries respectively, reveals that 17 of the 25 stations exhibit long term drying (Fig. 5.7 and Fig. 5.8). Although there is uncertainty associated with the duration and temporal coverage of these stations, here we are primarily interested in whether we can discern a pattern of consistent long term drying for this region and the preponderance of stations suggests this to be the case. Although only six of the stations indicate linear trends that are statistically significant ($p<.1$), five of these six show a reduction in rainfall (Fig. 5.7 and Fig. 5.8), two of which are in Syria (Deir Ezzor and Aleppo). The only station of the 25 that shows a significant wetting trend is Sivas, Turkey in the extreme northwest of the domain (Fig. 5.7). That three quarters of the stations exhibit no

significant trend, either drying or wetting, should be expected if in fact anthropogenic forcing has only begun to assert itself.

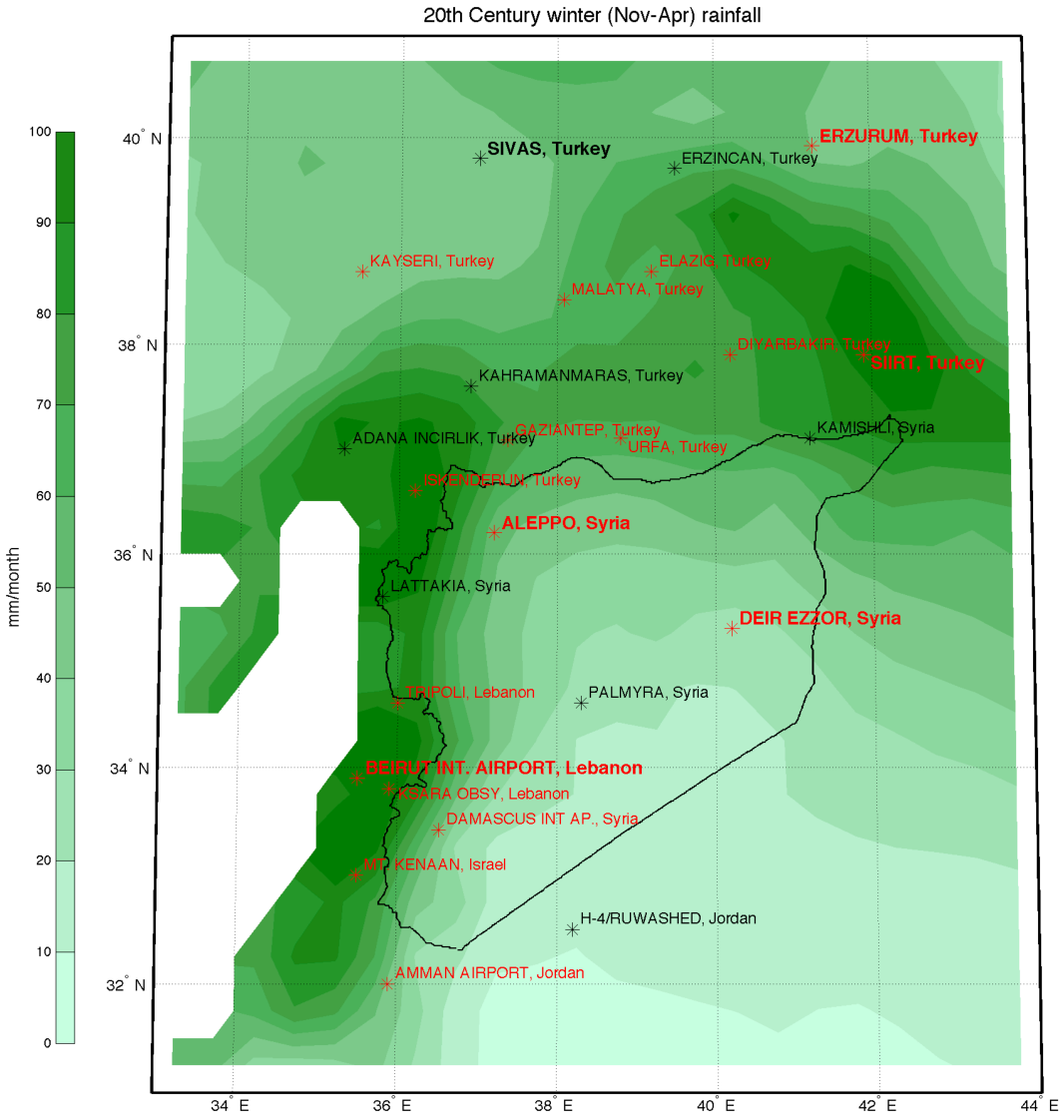

Figure 5.7: Trends based on linear fits to observed (GHCN) stations in the greater Fertile Crescent (see Data and Methods for station selection criteria). Station records are of varying length (accompanying timeseries are shown in Fig. 5.8). Green shading indicates the CRU 3.1 winter (Nov-Apr) precipitation climatology (1901-2008). Red labels indicate drying trends and bold indicates statistical significance ($p<.1$).

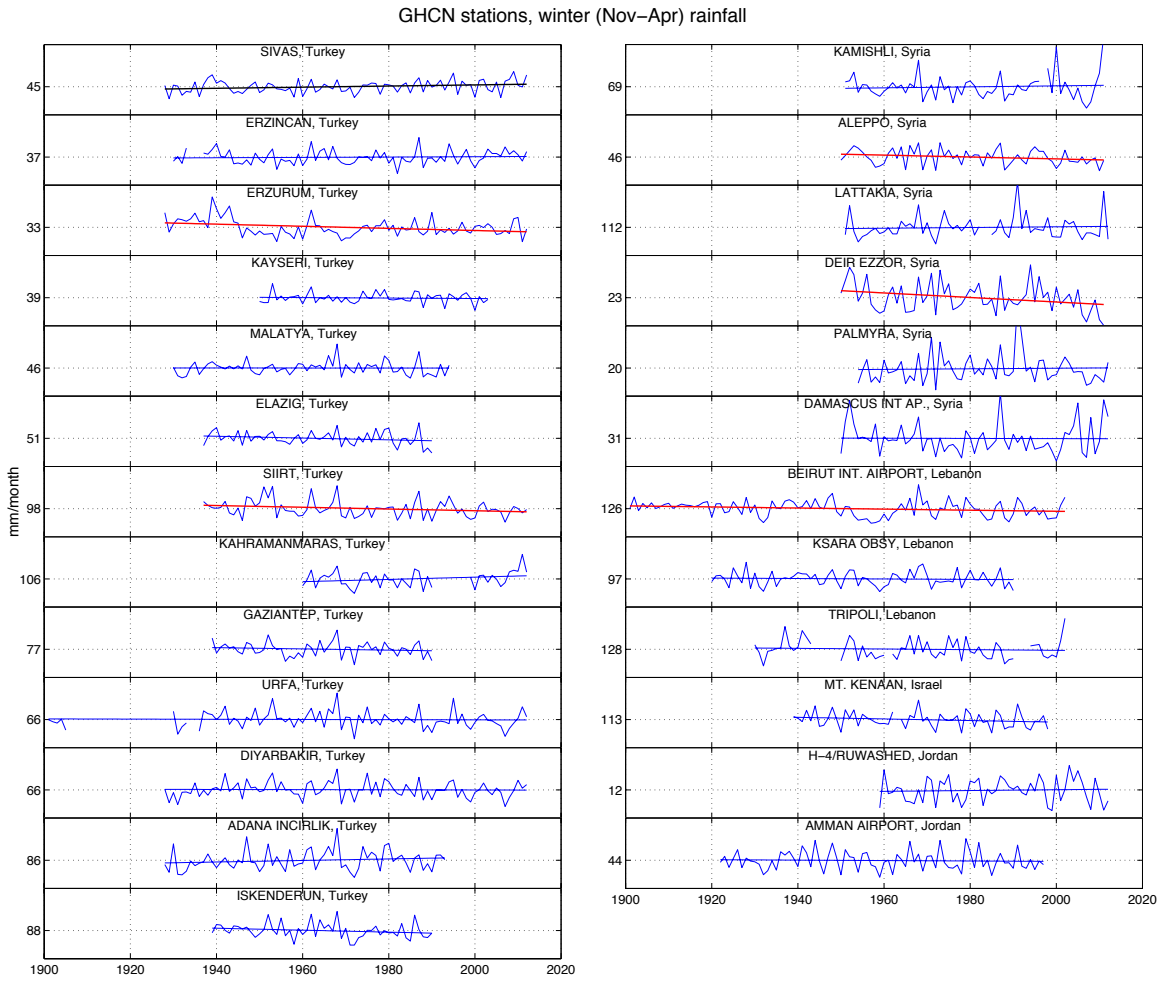

Figure 5.8: Rainfall trends based on linear fits to observed (GHCN) stations in the greater Fertile Crescent (see Data and Methods for station selection criteria), six-month winter (Nov-Apr). Climatological values are labeled on the y-axis. Red and black lines indicate statistically significant ($p<.1$) drying and wetting trends, respectively.

In addition to the long-term reduction in winter precipitation Syria has also seen a significant ($p<.01$) positive trend in annual near-surface air temperature (Fig. 5.2(d)) based on the CRU data. The change over the 109 years is slightly larger during the summer half year (1.2 degrees) than during winter (0.9 degrees) and both linear trends are significant ($p<.01$) (Fig. 5.9). The summer trend is particularly important as this is the season of highest evaporation and winter crops such as wheat are also strongly dependent on reserves of soil moisture (Trigo et al., 2010). Reductions in winter precipitation and increases in summer evaporation both reduce the excess of precipitation over evaporation

that sustains soil moisture, groundwater and streamflow.

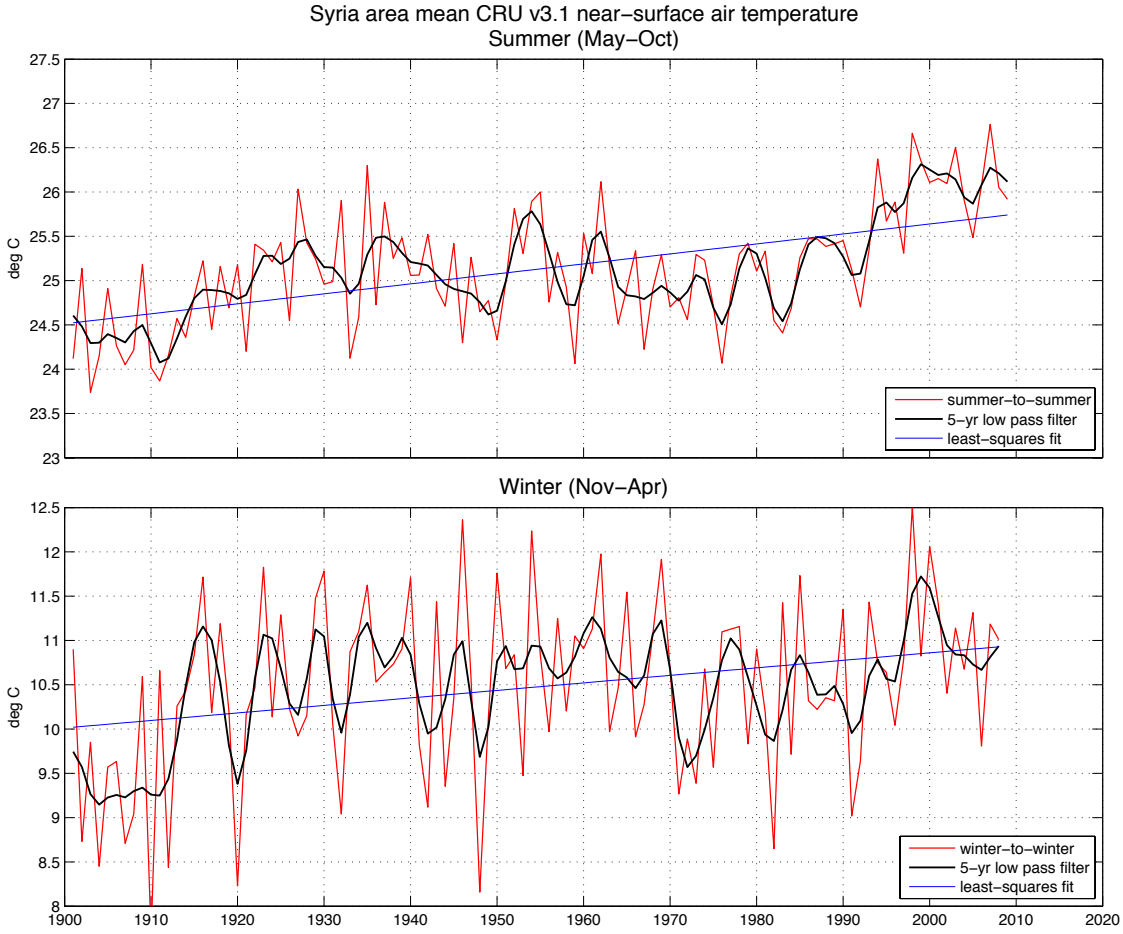

Figure 5.9: Observed summer (May-Oct) and winter (Nov-Apr) near-surface temperature for the Syria area mean, CRU 3.1 data, with 5-year Butterworth low-pass filter (black) and least squares fit (blue).

It is apparent from Figure 5.2 that the century-long, statistically significant trends in precipitation, and temperature point toward a key contribution to the recent severe drought from long-term trends, suggesting anthropogenic influence. In order to quantify the increased likelihood of an extreme three-year Syrian drought, such as the one from 2006/7-2008/9, we estimate the portion of Syrian precipitation reduction due to the long-term trend and separate it from the residual, presumably natural, variability. We estimate the trend contribution by regressing the running three-year mean of observed (CRU) six-

month winter precipitation onto the observed annual global atmospheric carbon dioxide (CO_2) mixing ratios from 1901-2008 (Etheridge et al., 1996; Keeling et al., 2001). We then remove the CO_2 fit from the total observed winter precipitation timeseries (Fig. 5.10(a)) and construct frequency distributions of the total and residual timeseries (Fig. 5.10(b)). The resulting residual timeseries was tested using a Kolmogorov-Smirnoff (K-S) test and found not to be normally distributed ($p<.05$), so we applied gamma fits to the distributions. The difference in the total and residual distributions is significant ($p<.06$), also based on a K-S test. Removing the mean from each distribution and then repeating the K-S test indicates a not significant ($p<.3$) difference in the shape of the distributions, indicating that the difference between the two is due almost entirely to the difference in the means. Thresholds are shown at 2, 2.5 and 3 standard deviations (σs) below the residual mean (Fig. 5.10(a)(b)). When combined, natural variability and CO_2 forcing are seen to be much more likely to produce the most severe 3-year droughts than natural variability alone. Events exceeding a 2σ threshold occur twice as often (6 versus 3) and events exceeding 2.5σ occur 2.5 times more often (5 versus 2). For the residual alone no values exceed 3σ whereas the addition of the CO_2-related trend is able to produce the 3σ drought of 2006/7 to 2008/9. Based on the gamma distribution fits a 3σ event – i.e. this drought – became much more likely with the additional drying due to the long-term trend.

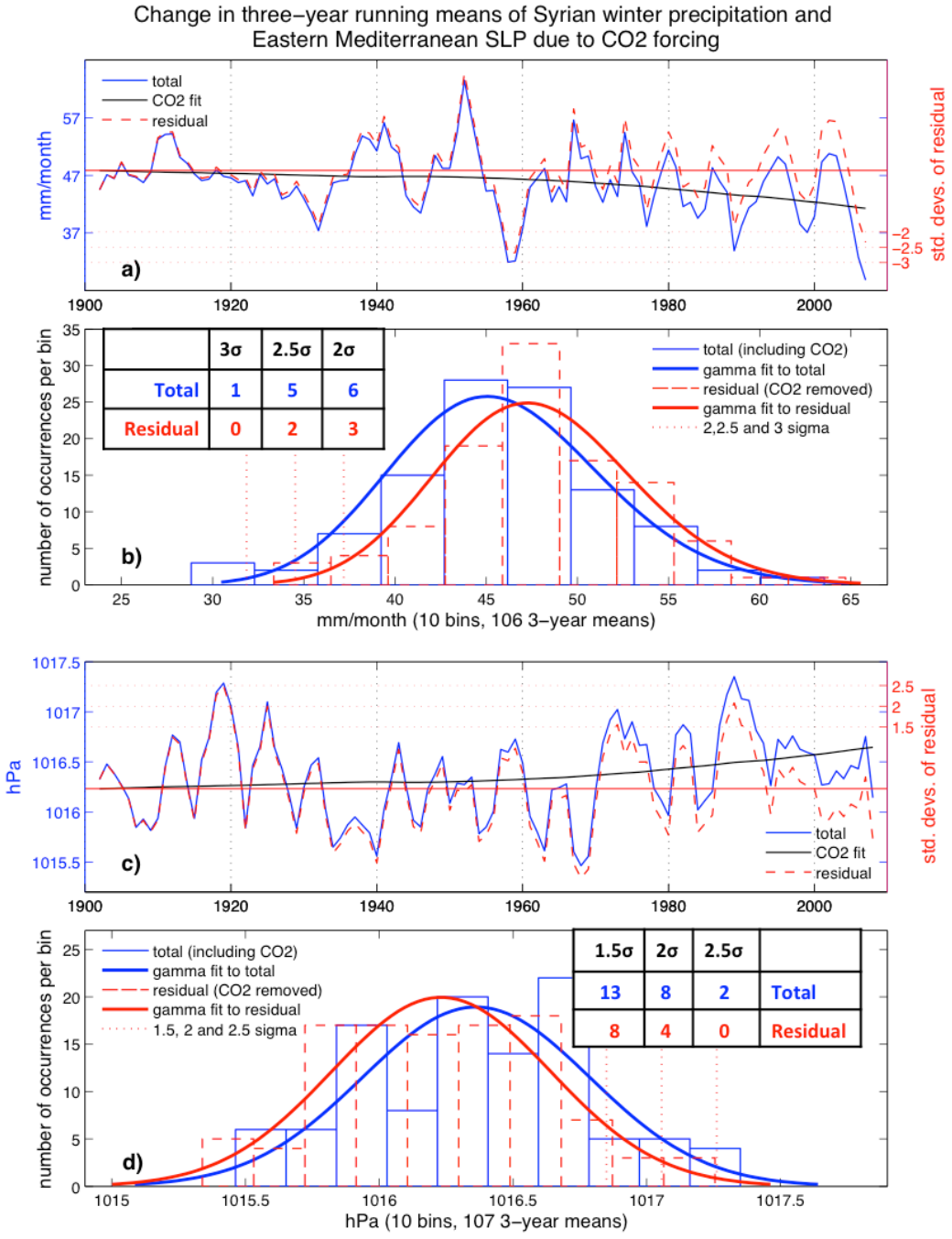

Figure 5.10: Three-year running mean six-month winter Syrian precipitation (CRU3.1) and Eastern Mediterranean SLP (20th Century Reanalysis) for the 20th Century. Shown are the total 3-year running means (blue), the CO2 fits from regression (black), and the difference between these (residual, dashed red). Frequency distributions include gamma fits and sigma thresholds of the residual timeseries (red dotted lines). The table indicates the number of occurrences of exceeding the residual thresholds for the actual (which includes any CO_2 effect) and residual (with CO_2 effect removed) time series.

5.5 Mechanisms of the Syrian drought

We conclude that the addition of a long-term drying trend is needed to account for the duration and severity of the recent drought. That the long-term trend is consistent with the time history of anthropogenic climate forcing and that there is no similar trend attributable to natural causes begins to make the case for anthropogenic influence, a case that can be supported by additional modeling, theoretical and observational evidence.

Consistent with the observed negative winter precipitation trend in Syria over the 20th Century (Fig. 5.2(a)), we concluded in Chapters 2 and 3 that human-induced precipitation change has already begun in the Mediterranean region, is more clearly dominant in the EM, and is very likely to intensify (also see Giorgi and Lionello, 2008). In these chapters we used a signal-to-noise maximizing EOF technique to extract the precipitation response signal common to CMIP3 and to CMIP5 models and concluded that increased anthropogenic forcing primarily caused the recent drying in the EM. Hoerling et al. (2012) showed that a drier Mediterranean results in experiments using atmospheric models forced with rising sea-surface temperatures in the tropical Pacific and Indian oceans, a likely consequence of anthropogenic climate change. Furthermore, CMIP3 and CMIP5 coupled climate models overwhelmingly agree that the EM region will become drier in the future as greenhouse gas concentrations rise (IPCC, 2007; Giorgi and Lionello, 2008), and a study using a high-resolution model able to resolve the complex orography of the region concluded that the Fertile Crescent is likely to disappear by the end of the 21st Century as a result of anthropogenic climate change (Kitoh et al., 2008).

Theoretical mechanisms for drying subtropical regions under a warming global climate include both a thermodynamic component related to increased moisture-carrying capacity in a warmer atmosphere (Held and Soden, 2006; Seager et al., 2010), and a dynamical component involving an expanding Hadley Cell (Lu et al., 2007) and a poleward migration of the midlatitude storm tracks (Wu et al., 2011; Yin, 2005) and more local processes specifically involving the Mediterranean storm track (Trigo et al., 2010; Giorgi and Lionello, 2008; Bengtsson et al., 2006; Lionello and Giorgi, 2007; Ziv et al.,

2013). A poleward migration, weakening or suppressed development of the winter storms that enter Syria from the EM could mean a reduction in winter rainfall, with potentially dire consequences for agriculture. Much of Syrian precipitation depends on cyclogenesis in the region of the Cyprus low and is associated with cold air outbreaks from Europe (Trigo et al., 2010). A detailed analysis of the large-scale atmospheric conditions present during the record dry 2007/08 winter (DJFM) using the NCEP/NCAR reanalysis (Trigo et al., 2010; Kalnay et al., 2006) concluded that anomalous high surface pressure inhibited synoptic activity over the EM, and was accompanied by dry advection from the east and northeast that significantly reduced precipitable water and convective instability.

The mechanisms cited in the previous paragraph all imply a rise in sea level pressure (SLP) in the Mediterranean, especially the Eastern Mediterranean (EM SLP), as a consequence of anthropogenic climate change. Observationally-based data from the Twentieth Century Reanalysis (Compo et al., 2011) show an increase in EM SLP since 1901, although the linear trend is only marginally significant ($p<.14$) (see Fig. 5.10(c)). Prior to the winter of 2009/10 40 years had elapsed since the last recorded winter with SLP more than one standard deviation below the 1901-70 mean (Fig. 5.11(b)) while in the prior 70 winters SLP regularly fell below this threshold. Distributions of observed three-year running means of winter EM SLP over the EM, as with Syrian precipitation above, indicates a similar difference between the total and residual after the CO_2 fit is removed (Fig. 5.10(c)). Extreme three-year high-pressure events increase in frequency and intensity under the CO_2 forcing and the most extreme events ($>2.5\sigma$ above the residual mean) only occur when the strong NAO-related natural variability and the CO2 forcing combine (Fig. 5.10(d)).

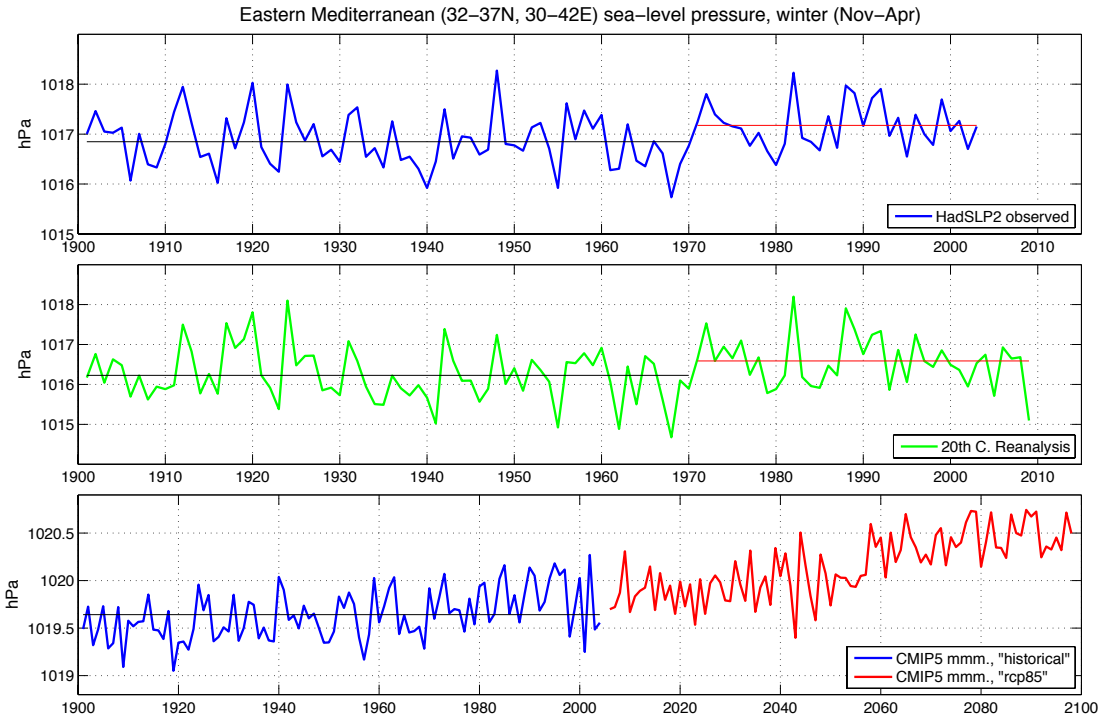

Figure 5.11: Timeseries of area-mean Eastern Mediterranean sea-level pressure for six-month winter (Nov-Apr). a) observed HadSLP2, b) 20th Century Reanalysis and c) CMIP5 multimodel mean (15 models, see Table S1) for the 20th Century "historical" simulations and 21st Century rcp85 projections.

5.6 CMIP5 model simulations and projections

Analysis of the newly available CMIP5 simulations also points to the importance of anthropogenic forcing in the drying of the eastern Mediterranean. A comparison of Syrian winter precipitation from 1950 to 2004 in the 20th Century CMIP5 runs (15 models) with CRU observations shows improvement over the CMIP3 models, though both mean rainfall and year-to-year variability are still underestimated (Fig. 5.12). The CMIP5 20th Century multi-model mean gives a reduction in rainfall over Syria between 1901 and 2005 of 3-9% (Fig. 5.13), compared to the CRU decrease of 2-10% (Fig. 5.2(a)). The projection for the 21st Century (2006-2099) is a 17-30% reduction in winter precipitation for Syria due to the increased radiative forcing (Fig. 5.13). In order to better characterize the uncertainty in the models' projections of future drying, we compare 54-year winter trends using all available CMIP5 models, one run each, for the preindustrial

control, the historical simulations and the rcp85 projections to the observed trend from 1951-2004 (Fig. 5.14). The goal here is to determine long-term trend, sufficiently long to minimize any trend that could be due to natural multidecadal variability. The observations however are more uncertain prior to 1950, so we chose 54-year trends beginning in 1951 and ending in winter 2004/05 because this is the last year of the modeled historical simulations. In choosing this length it is acknowledged that 54 years is not entirely sufficient to remove all natural variability. Additionally, 1951-2004 is the period during which we would expect the response to forcing to begin to emerge, rather than during the first half of the 20th Century, as this is the period during which the atmospheric CO_2 concentration has increased the most (see Fig. 5.10). In the bottom panel (Fig. 5.14) we see that the distribution of modeled 54-year winter trends is Gaussian and centered on zero, indicating equal likelihood of dry and wet trends under no external transient forcing, and that the observed winter trend from 1951-2004 is within but not centered in the distribution. A possible implication is that at least a portion of the observed trend is externally forced. When we examine the distribution of model-simulated trends from 1951-2004 (middle panel) the observed trend is closer to the center. Because the observed trend represents only one possible iteration of a 54-year trend in nature, which could be due at least in part to residual low-frequency natural variability, it is impossible to know with certainty how much of its agreement with the model-simulated distribution from 1951-2004 is due to external forcing. However, the agreement is sufficiently good to give us some confidence in the future projections. In the top panel, under rcp85 forcing, the distribution shifts dramatically. Few of the models project 54-year wetting trends during the 21st Century and most of the projected trends are more severe than the observed trend from 1951-2004. Although the sign of the model trend projections is not unanimous, the consensus is overwhelmingly in favor of robust future drying of the Fertile Crescent, and many of these projections are for more severe drying than that observed since 1951.

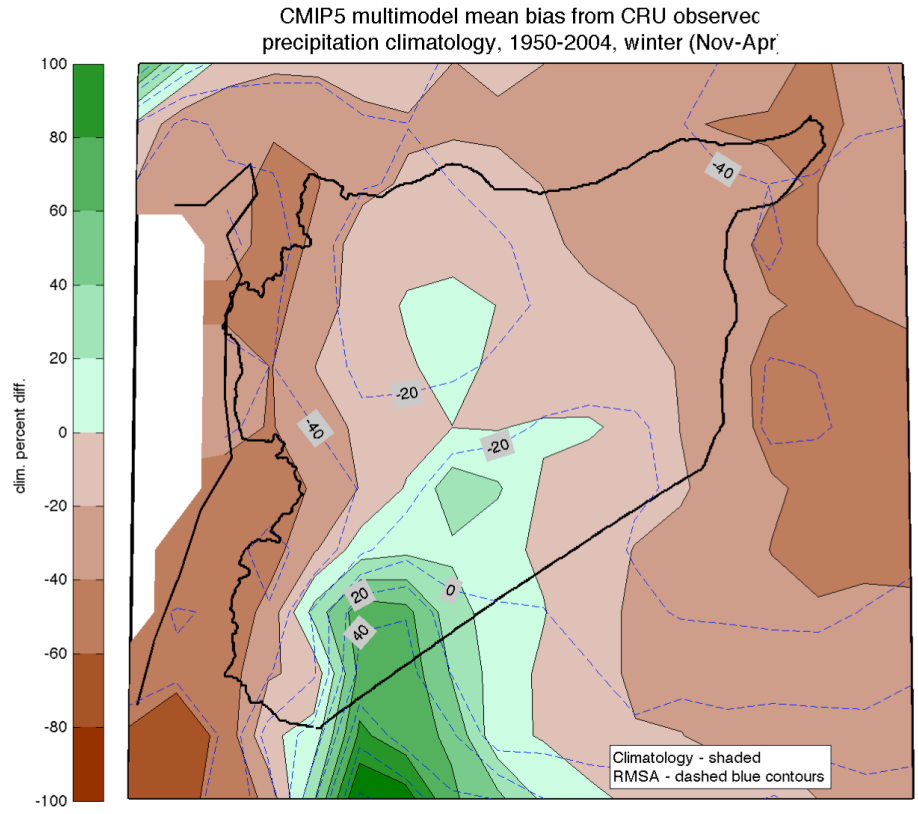

Figure 5.12: Difference, expressed in percent, between the CMIP5 multimodel mean (15 models, see Table 5.1) and observed CRU3.1 winter precipitation from 1950-2004. Climatology difference is shaded and the winter-to-winter root mean square anomaly (RMSA) is shown in dashed blue contours.

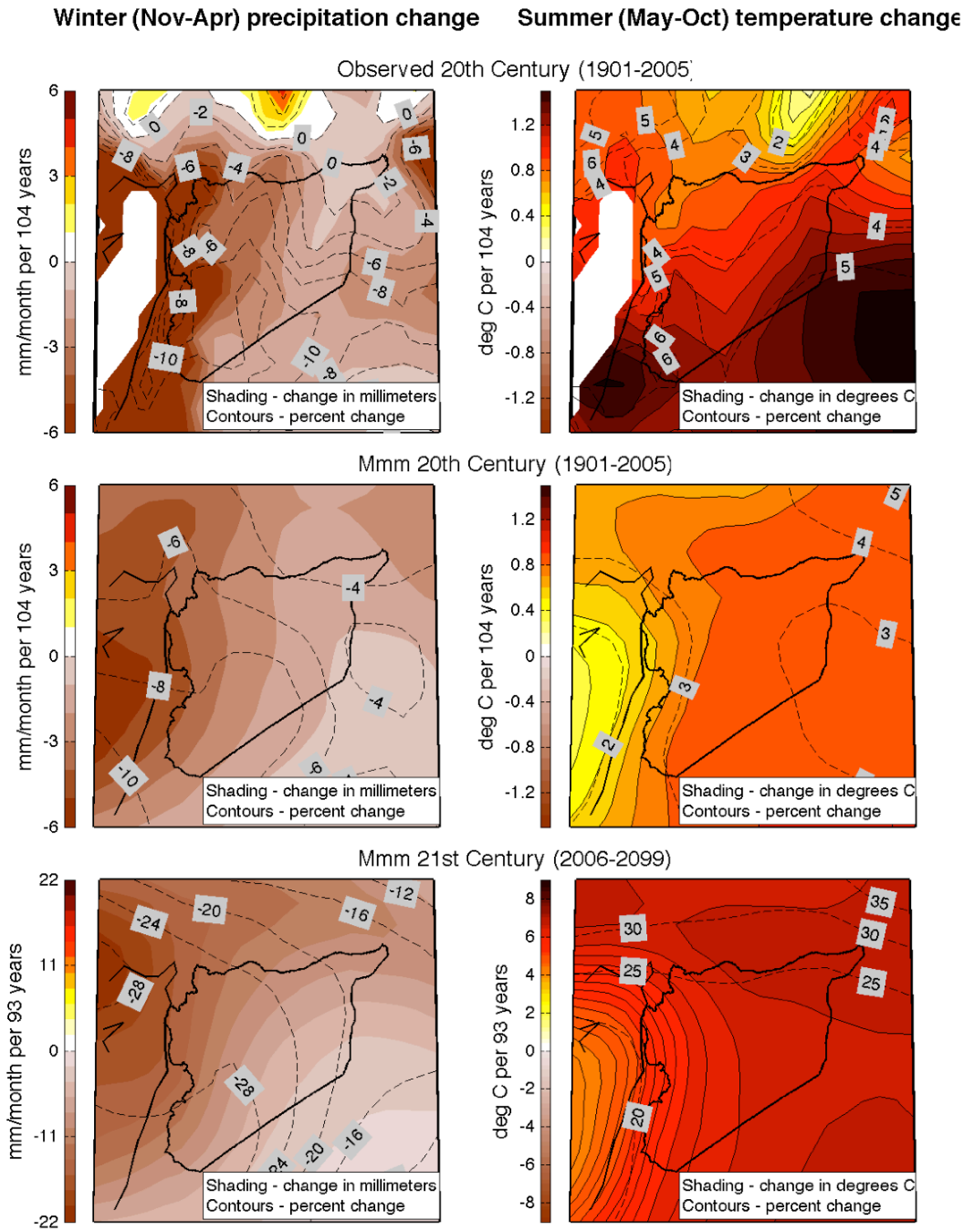

Fig: 5.13: Observed (CRU3.1) and CMIP5 multimodel mean of the winter (Nov-Apr) precipitation (left) and summer (May-Oct) temperature (right) change from 1901-2005 and 2006 to 2100, based on a linear least squares fit. The rcp8.5 was used for the 21st Century model projections. Shading represents change in actual units (mm/month and degrees C) and the dashed contours represent percent change from the beginning of the 20th and 21st Centuries respectively.

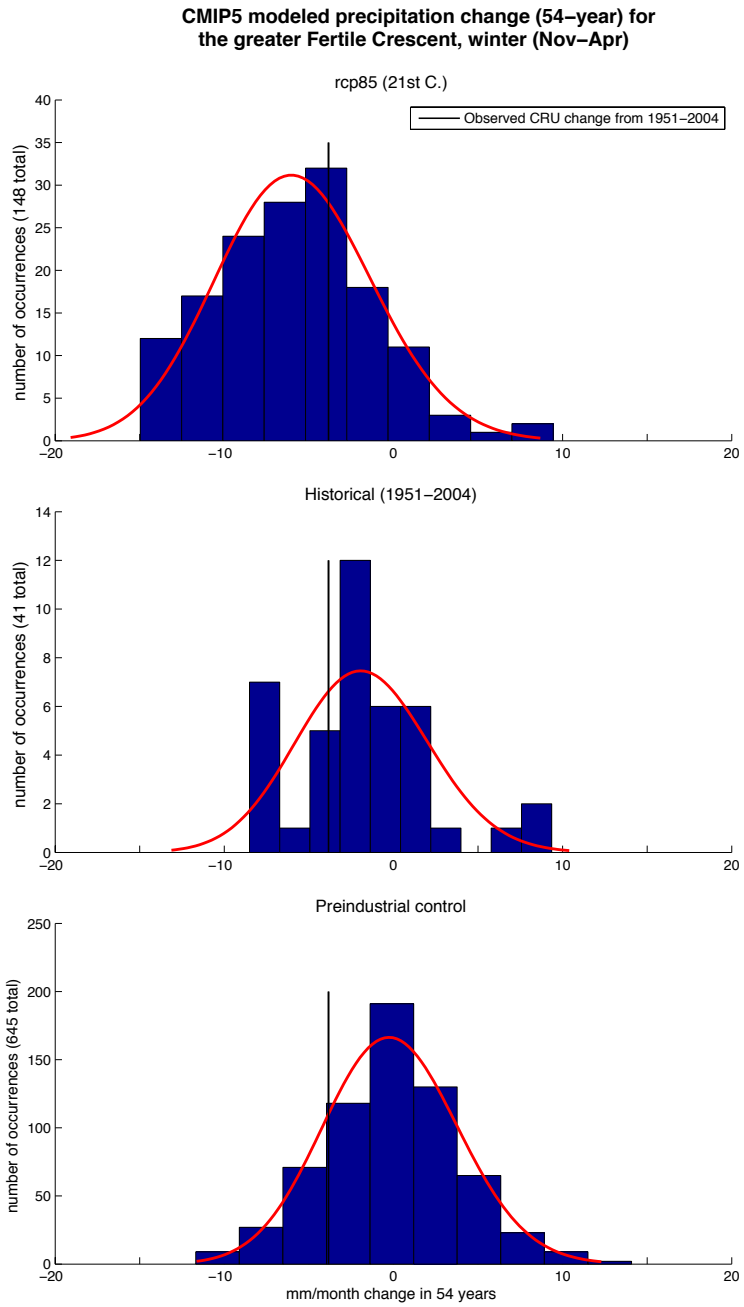

Fig: 5.14: Distributions of CMIP5 model simulations and projections of six month winter (Nov-Apr) rainfall trends, 54 years in length, as compared with the observed (CRU 3.1) trend from 1951-2004 represented by the black line. Trends are change based on a linear least squares fit to the area mean of the greater Fertile Crescent domain, here described as 32 to 40N latitude, 34 to 44E longitude (see Fig. 5.7). The bottom panel represents 54-year trends in the preindustrial CMIP5 simulations (with no transient external forcing) using 43 models (15 trends each, 54 years in length). The middle panel represents historical trends from 1951-2004 using 41 models. The top panel represents rcp85 21st Century model projected trends using 37 models (4 trends each, 54 years in length). Red curves indicate a gamma fit to the distributions.

The 20th and 21st Century changes in summer (May-Oct) temperature are also shown in Figure 5.13, at right. The models simulate an increase of .5 to .9°C over the 20th Century, as compared with .6 to 1.1°C for the observations, and project an increase of 5-7°C for the 21st Century, implying a huge increase in potential evaporation, strongly drying the soil.

The CMIP5 model-projected drying of the EM is consistent with the recent observed Syrian precipitation and EM SLP change. The CMIP5 multimodel mean of area-averaged EM SLP, though biased high over the 20th Century, agrees with the observations in trending upward during the century (Fig. 5.11). This positive trend continues strongly through the 21st Century (Fig. 5.11(c)).

More generally, the projection for the 21st Century under increased greenhouse gas forcing is for an increase in surface pressure and anticyclonic tendency, a reduction in the frequency and strength of cyclones in the EM, and a reduction in winter precipitation in Syria. The recent drought, so exceptional in its severity and persistence in the context of the 20th Century, is projected to become the rule in the 21st Century.

5.7 Conclusions

In the first decade of the 21st Century Syria was subjected to an especially severe and prolonged drought, with the 2006-2009 period being the driest three years in at least a century. Though droughts occur periodically in Syria due to natural causes, it is unlikely that the recent drought would have been so extreme absent the century long drying trend that added to the usual natural oscillations in rainfall. Here we estimated that the long-term trend made a drought of such severity as the recent one several times more likely. We then argued that the long-term trend was a consequence of human interference with the climate system. The similarity of the trend to the increase in greenhouse gas concentrations and the absence of any natural forcing with similar temporal structure is one strand of the evidence. Other strands bring in climate theory and model simulations. Fortunately for this line of argument, the Eastern Mediterranean is a region where models compare well with 20th Century observations for both climatology and trend. It is also one of the rare regions where the anthropogenic precipitation signal has already emerged

from the natural "noise". In Chapter 2 we showed that for the Mediterranean as a whole the dominant signal is still multidecadal variability associated with the NAO, and then in Chapter 3 that over much of the EM and for precipitation in Syria in particular the NAO signal is secondary. The strong agreement between observations and climate model simulations in century-long trends in precipitation, temperature and sea level pressure adds confidence to the conclusion that the recent drought has an anthropogenic component, and that future projections of continued drying for Syria are reliable.

Climate is but one perturbation that can contribute to unrest, and there were less severe droughts that occurred in the 20th Century that did not result in civil unrest. The 21st Century drought however devastated Syrian agriculture, resulting in food shortages, widespread unemployment, and the collapse of rural social structure. The drought's impacts were exacerbated by depleted groundwater, and by government policy that turned away from support of agriculture and rural populations. Rural life in northeast Syria became untenable, leading to mass migration to the urban peripheries. This influx of as many as 1.5 million people to the flood of Iraqi refugees strained urban services to a breaking point. Anger at the inability or unwillingness of the government to ameliorate conditions sparked the 2011 uprising in Syria that evolved into a pervasive civil war.

We have here pointed to a connected path running from human interference with climate to drought to conflict. This path is in a landscape encompassing natural cause of drought, the heavy burden of 1.5 million refugees from the Iraq war, government policies promoting unsustainable agricultural practice, and the failure of the government to address the suffering of a displaced population. The abundance of history books on the subject tells us that war can never be said to have a simple or unique cause. The Syrian conflict, now civil war, is no exception. Still, when a displaced Syrian farmer was asked if this was about the drought, she replied: "Of course. The drought and unemployment were important in pushing people toward revolution" (New York Times editorial by Friedman 2013). Droughts are a natural, recurring feature of Syrian climate, but without the added anthropogenic forcing it is unlikely this drought would have been so severe and as long lasting. "When the drought happened, we could handle it for two years, and then we said, 'It's enough'" (Friedman 2013). Such persistent, deep droughts are projected to be commonplace in a warming world. Will the Fertile Crescent, a locus of the origins of

agriculture and the beginnings of our civilization, be allowed to devolve into a sand-strewn monument to civilization's advance?

5.8 Data and Methods

In this chapter the winter and summer seasons are represented by the six-month periods November through April and May through October, respectively. To construct timeseries of Syria area means, only those gridboxes in which more than half of the gridbox area is Syrian were included. The area mean EM is here defined by the domain 32-37N, 30-42E. Three datasets were used for observed precipitation, the University of East Anglia (UEA) Climate Research Unit (CRU) version 3.1 (New et al., 2000; Jones and Harris 2008) and Global Precipitation Climatology Centre (GPCC) v6 (Schneider et al., 2008) gridded (.5 degree by .5 degree horizontal resolution) precipitation data sets and the Global Historical Climatology Network (GHCN) beta version 2 station precipitation data (Vose et al., 1992). In the case of the gridded datasets, the uncertainty is much larger in the early half of the century, when the available stations were much more sparse, particularly for Syria. However, these are the best available precipitation datasets, to the best of our knowledge, with which to determine the century-long trend for this region. For corroboration of long-term six-month winter trends we examined station data that met the following criteria: stations 1) greater than fifty years in length, from first value to last, 2) that extended beyond 1990, and 3) that contained five or fewer missing years. The UEA CRU 3.1 was also used for observed surface temperature. For sea-level pressure we used the Twentieth Century Reanalysis Project, with a horizontal resolution of 2 degrees by 2 degrees (Compo et al., 2011). We used 15 CMIP5 global climate models (see Table 5.1) to be assessed in the upcoming Intergovernmental Panel on Climate Change (IPCC) Fifth Assessment Report for multimodel mean calculations. For intermodel comparisons we used all available models, one run each. For the preindustrial control runs we used the first 200 years of each model, for the 20th Century we used the "historical" simulations and for the 21st Century model projections we used the Representative Concentration Pathway experiment "rcp85", with an increase in radiative forcing of 8.5W/m^2 by 2100 (Taylor et al., 2012). To compare with 20th Century observations and to examine model-projected changes in six-month winter precipitation for Syria over the 21st Century we

first linearly interpolated the models to a common .5 by .5 horizontal grid (the same grid as the CRU observations). To determine the change we applied a linear least-squares fit to each model at every gridpoint.

MODEL	Horiz. Res. (lon x lat)	Modeling center
bcc-csm1-1	2.81x2.81	Beijing Climate Center
CCSM4	1.25x.94	National Center for Atmospheric Research
CNRM-CM5	1.41x1.41	Centre National de Recherches Meteorologiques
CSIRO-Mk3-6-0	1.88x1.88	Commonwealth Scientific and Industrial Research Organisation
FIO-ESM	2.81x2.81	The First Institute of Oceanography, SOA, China
GFDL-CM3	2.5x2	Geophysical Fluid Dynamics Laboratory
GFDL-ESM2M	2x2.5	Geophysical Fluid Dynamics Laboratory
GISS-E2-R	2.5x2	Goddard Institute for Space Studies
HadGEM2-ES	1.88x1.25	Met Office Hadley Centre
IPSL-CM5A-LR	3.75x1.89	Institut Pierre-Simon Laplace
MIROC-ESM	2.81x2.81	Model for Interdisciplinary Research on Climate, Univ. of Tokyo
MIROC-5	1.41x1.41	Model for Interdisciplinary Research on Climate, Univ. of Tokyo
MPI-ESM-LR	1.88x1.88	Max Planck Institut
MRI-CGCM3	1.13x1.13	Meteorological Research Institute, Japan
NorESM1-M	2.5x1.89	Norwegian Climate Centre

Table 5.1: CMIP5 models used to construct multimodel means. The first available run of each model was used, one run for each model. Models were linearly interpolated to a common .5 degree by .5 degree horizontal grid for comparison. Only models with available output for preindustrial, historical and rcp85 were included, for consistency, with no more than two models from any one modeling center to reduce bias.

Chapter 6

Conclusions and future directions

In this thesis we examined the relationship between naturally varying and forced precipitation and moisture budget change for the Mediterranean region using observations, reanalyses and comprehensive climate models. We began by using the CMIP3 coupled global climate models to estimate the anthropogenically-forced contribution to the observed Mediterranean drying trend from the 1960s to 2000. Signal-to-noise EOF maximization has been employed to determine the forced precipitation response common to the models, and the observations were then regressed onto this signal. It was found that over most of the Mediterranean region the multidecadal variability of the NAO, in particular the strong positive trend over this period, dominated the total precipitation trend with only a small contribution from the forced response. This was not the case for the eastern Mediterranean, where the influence of the NAO was weaker and the forced response more clearly evident. Based on model projections of the 21st Century (using the A1B scenario), as the forcing due to increasing concentrations of greenhouse gases continues to rise, so will its contribution to Mediterranean winter drying relative to the natural NAO variability. Based on the quasi-linear increase in the signal projected by this model-based estimate, the forced precipitation change could begin to approach the magnitude of observed multidecadal natural variability by the end of the 21st Century, establishing the level of aridity seen in the late 20th Century as the new climate. However if the strength of the natural variability observed in the 20th Century (which could also change in the future) persists, then the path towards this drier climate might not be smooth but involve drier and wetter periods of varying length around a steadily drying mean climate. The models were shown to be able to produce

trends of the magnitude of the observed trend from 1965-1995, but only as unusual events. The observed North Atlantic SLP and Mediterranean winter precipitation trends from 1965 to 1995 were within the overall estimated distributions of those simulated during the 20th Century by the models. This study was performed for the Mediterranean wet season, six-month winter (November-April). This led us to the question of how well the newest generation of models (CMIP5) perform with respect to their simulation of climatology and trend for all seasons. This is covered in Chapter 3.

The work in Chapter 3 focused on the seasonality of the CMIP5 models and their improvement over the previous generation, CMIP3. This previous generation was able to simulate the large-scale climatological features of Mediterranean region precipitation. Increased spatial resolution in the CMIP5, in addition to other model advancements, potentially allows improved representation of the climatological pattern and amplitude associated with the complex physiography and orography of the region. This chapter addressed how well the CMIP5 models simulated the observed Mediterranean precipitation climatology, seasonal cycle and trends, and to what extent we can trust the multimodel mean trends as representing the externally forced trends. We showed that the climatology is generally well simulated in both spatial pattern and seasonal cycle. All models simulated the winter maximum and summer minimum in precipitation but the model mean and median slightly underestimated the amplitude of the seasonal cycle. There was a modest improvement of the CMIP5 climatology over CMIP3, possibly because of improved horizontal resolution. In contrast, the trends of the last half century in the CMIP5 multimodel means and the observations differed significantly, particularly in winter and over the northern Mediterranean region. The CMIP5 multimodel mean trend indicated a modest drying throughout the seasonal cycle, with the strongest drying in the March, April and May spring season. The observed trend, on the other hand, showed a predominantly winter drying, however this may be due to multidecadal natural variability. The modest agreement in spatial patterns between the modeled and observed external trends further reinforced our conclusion from Chapter 2 that the radiatively forced portion of the precipitation trend has only begun to emerge relative to natural variability on multidecadal timescales, but that its influence is likely to grow in the future as the forcing increases. We now shifted the focus of the thesis to the mechanisms of

natural variability and forced moisture budget change.

In Chapter 4 we examined a suite of 15 CMIP5 models as well as the ERA Interim reanalysis to address the following questions. How is the interannual natural variability of the NAO related to the greater Atlantic and Mediterranean moisture budget, and which terms within the moisture budget are most important? How do the patterns of forced and natural NAO-related moisture budget change compare? A prime motivation was to determine the similarities and differences between the mechanisms of natural variability and radiatively-forced change as part of a larger effort to attribute the causes of ongoing hydroclimate change. Can we determine a signature for forced moisture budget change that is distinct from the change associated with NAO variability? We found that during a positive NAO, the resulting poleward shift in both the mean flow and in the transient eddies combined to bring about robust drying of the Mediterranean region, but that the drying was largely due to the shift in the mean flow with the transients providing a modest, offsetting, anomalous moisture convergence. The importance of the mean flow moisture divergence was reflected in the pattern of large-scale subsidence associated with the NAO, with, for a positive NAO, widespread subsidence anomalies across the Mediterranean region and much of Europe and ascent over northwest Europe. For a positive winter NAO the transients dried most of Europe but provided anomalous moistening over the Mediterranean region, despite weaker eddies, opposing the mean flow divergence. We compared the moisture budget changes associated with NAO variability to the changes under global warming over the Mediterranean during winter to facilitate discrimination between the patterns of climate change and climate variability. We found there are similarities and key differences, which include:

Similarities –

- A deficit of P-E over the subtropical North Atlantic and over Iberia, largely due to the contribution from the mean flow divergence, which also dries the greater Mediterranean under forcing and under a positive NAO.
- Drying over the Mediterranean Sea associated with low-level mass divergence.

- Divergence over the subtropical North Atlantic due to the moisture advection, extending into northern Africa and Iberia.

Differences -

- Enhanced evaporation over the Mediterranean Sea, Italy and eastern Europe under climate change, but a modest reduction of evaporation there during a positive NAO,
- A poleward-shifted band of subtropical drying under natural variability relative to the climate change case, which is more strongly tied to the Mediterranean Sea, and total subtropical P-E change that is due mostly to the mean flow contribution, under natural variability and under forcing,
- Divergence by the wintertime transients under climate change over nearly all of Europe and the Mediterranean Sea, but convergence over the Mediterranean and divergence over northern Europe under a positive NAO as the shift in the storms actually opposes the mean.

In Chapter 5 we applied the conclusions from the previous chapters and examined the recent severe and persistent drought in Syria. In the first decade of the 21st Century Syria was subjected to an especially severe and prolonged drought, with the 2006-2009 period being the driest three years in at least a century. Though multiyear droughts have occurred periodically in Syria due to natural causes, it is unlikely that the recent drought would have been so extreme absent the century long drying trend that added to the usual natural oscillations in rainfall. We estimated that the trend made a drought of such severity several times more likely. We then argued that the trend was a consequence of human interference with the climate system. This conclusion was aided by the fact the eastern Mediterranean is a region where models compare well with 20th Century observations for both climatology and trend. As we showed in Chapters 2 and 3, it is also one of the rare regions where the anthropogenic precipitation signal has already emerged from the natural "noise". For the Mediterranean as a whole the dominant signal is still multidecadal variability associated with the NAO, but for much of the eastern Mediterranean and for precipitation in Syria in particular the NAO signal is secondary.

The strong agreement between observations and climate model simulations in century-long trends in precipitation, temperature and sea level pressure added confidence to the conclusion that the recent drought had a significant anthropogenic component, and that future projections of continued drying for Syria are reliable. The drought devastated Syrian agriculture, resulting in food shortages, widespread unemployment, and the collapse of rural social structure. The drought's impacts were exacerbated by depleted groundwater, and by government policy that turned away from support of agriculture and rural populations. Rural life in northeast Syria became untenable, leading to mass migration to the urban peripheries. This influx of as many as 1.5 million people to the flood of Iraqi refugees strained urban services to a breaking point. Anger at the inability or unwillingness of the government to ameliorate conditions helped spark the 2011 uprising in Syria that evolved into a pervasive civil war. Droughts are a natural, recurring feature of Syrian climate, but without the added anthropogenic forcing it is unlikely this drought would have been so severe and as long lasting. Such persistent, deep droughts are projected to be commonplace in a warming world.

In summary, this thesis work has added clarity to our understanding of the relationship between naturally-varying and forced hydroclimate change for the greater Mediterranean region and provided some key results with respects to the questions posed in the Introduction. These results include:

1) The influence of global warming on Mediterranean drying has begun to emerge relative to the large natural multidecadal variability associated with the NAO and is likely to increase in the future.
2) The CMIP5 models perform well in their simulation of Mediterranean precipitation climatology, but fail to simulate the seasonality of the observed trend over the latter half of the 20th Century. This could be related to differences in multidecadal variability that in observation produces stronger winter drying. The model winter drying is modest, likely because the anthropogenic forcing has only begun to emerge from the large natural variability.
3) For interannual natural variability of the NAO as related to the greater Atlantic

and Mediterranean moisture budget, the contribution from the mean flow and the mass divergent component of that are shown to be most important, as with trend. The transients however actually provide modest convergence over the Mediterranean during a positive NAO whereas under forcing they diverge moisture. This forced moisture divergence by the transients over the Mediterranean has a different pattern than the clear sea-land signature of the climatology.

4) There are differences in the patterns of forced and natural NAO-related moisture budget change that include the sign of the Mediterranean evaporation anomaly, the latitudinal extent of the band of subtropical drying, and the aforementioned difference in the sign of the divergence by the transients.

5) Last, the recent drought in Syria was shown to be an important contributing factor in the uprising that has led to civil war, and the drought was estimated to have been more severe and persistent due to the contribution from the emerging influence of climate change.

This work highlights the need for a better understanding of the relationship between hydroclimate variability and change and the associated mechanisms, in order to increase predictive capacity of future change. Many countries are already water-stressed, and further drying would only increase that stress, particularly for agriculture and water resources. The findings of this thesis makes clear that there is still much work to be done, some of which includes determining the implications for water resources, agriculture and ecosystems. In addition to using global climate models, reanalyses and observations, tools such as regional models and downscaling can be utilized to determine climate impacts at regional and local levels.

Bibliography

Albala-Bertrand, J. M., 1993: Political Economy of Large Disasters. Oxford: Clarendon Press.

Allan, R., and T. Ansell, 2006: A new globally complete monthly historical gridded mean sea level pressure dataset (HadSLP2): 1850–2004. *J. Clim.*, **19 (22)**, 5816–5842.

Allen, M. R., and L. A. Smith, 1997: Optimal filtering in singular spectrum analysis. *Phys. Lett. A.,* **234 (6)**, 419–428.

Barnes, J., 2009: Managing the Waters of Baath Country: The Politics of Water Scarcity in Syria. *Geopolitics*, **14**, 510-530.

Barnston, A. G., and R. E. Livezey, 1987: Classification, Seasonality and Persistence of Low-Frequency Atmospheric Circulation Patterns. *Mon. Weather Rev.*, **115(6)**, 1083–1126.

Bengtsson, L., K. Hodges, and E. Roeckner, 2006: Storm tracks and climate change. *J. Clim.*, **19**, 3518–3543.

Berrisford, P., P. Kallberg, S. Kobayashi, D. Dee, S. Uppala, A. J. Simmons, P. Poli, and H. Sato, 2011a: Atmospheric conservation properties in ERA-Interim. *Quart. J. Royal Meteor. Soc.*, **137**, 1381–1399.

Berrisford, P., et al., 2011b: The ERA-Interim archive version 2.0. Tech. rep., European Centre for Medium Range Weather Forecasts, ERA report series No. 1, 23 pp.

Blade, I., B. Liebmann, D. Fortuny, G. J. van Oldenborgh, 2012: Observed and simulated

impacts of the summer NAO in Europe: implications for projected drying in the Mediterranean region. *Clim. Dyn.*, **39**, 709–727, doi:10.1007/s00382-011-1195-x

Chang, E. K. M., Y. Guo, and X. Xi, 2012: CMIP5 multimodel ensemble projection of storm track change under global warming. *J. Geophys. Res.*, **117**, D23118, doi:10.1029/2012JD018 578.

Chang, P., R. Saravanan, L. Ji, and G. C. Hegerl, 2000: The effect of local sea surface temperatures on atmospheric circulation over the tropical Atlantic sector. *J. Clim.*, **13(13)**, 2195–2216.

de Châtel, F., Jan. 2010: Mining the Deep. *Syria Today*.

Chou, C., J. D. Neelin, C. Chen, and J. Tu, 2009: Evaluating the 'rich-get-richer' mechanism in tropical precipitation change under global warming. *J. Clim.*, **22**, 1982–2005.

Compo, G. P., et al., 2011: The Twentieth Century Reanalysis Project. *Quarterly J. Roy. Meteorol. Soc.,* **137**, 1-28, doi:10.1002/qj.776.

Cook, E., R. D'Arrigo, and M. Mann, 2002: A Well-Verified, Multiproxy Reconstruction of the Winter North Atlantic Oscillation Index since A.D. 1400. *J. Clim.*, **15**, 1754–1764.

Cullen H. M., and P. B. de Menocal, 2000: North Atlantic influence on Tigris-Euphrates streamflow. *Int. J. Clim.* **20(8)**, 853–863.

Dee, D., et al., 2011: The ERA-Interim Reanalysis: Configuration and performance of the data assimilation system. *Quart. J. Roy. Meteor. Soc.*, **137**, 553–597.

De Schutter, O. 7 Sept. 2010: UN Special Rapporteur on the right to food: Mission to Syria from 29 August to 7 September 2010. United Nations. Available at http://www2.ohchr.org/english/issues/food/docs/SyriaMissionPreliminaryConclusions_070920 10.pdf.

Deser, C., A. Phillips, V. Bourdette, and H. Teng, 2011: Uncertainty in climate change projections: the role of internal variability. *Clim. Dyn.,* **38**, 527–546, doi:10.1007/s00382-010-0977-x.

Dunkeloh, A., and J. Jacobeit, 2003: Circulation dynamics of Mediterranean precipitation variability 1948–98. *Int. J. Clim.*, **23(15)**,1843–1866.

Erian, W., April 2011: Drought Vulnerability in the Arab Region. ACSAD and ISDR. Available at http://reliefweb.int/sites/reliefweb.int/files/resources/Full_Report_3074.pdf.

Etheridge, D. M., L. P. Steele, R. L. Langenfelds, R. J. Francey, J. M. Barnola, and V. I. Morgan, 1996: Natural and anthropogenic changes in atmospheric CO2 over the last 1000 years from air in Antarctic ice and fire. *J. Geophys. Res.* **101**, 4115-4128.

FAO, WFP, UNDP, WHO, UNICEF, IOM, 27 Aug. 2008: First Draft: Drought Assessment Mission 3. Available at http://www.faoiraq.org/images/word/Drought%20Assessment%20Mission%20Syria.pdf.

Feldstein, S. B., 2002: The recent trend and variance increase of the annular mode. *J. Clim.*, **15(1)**, 88–94.

Foreign Agricultural Service, Official USDA Estimates. http://www.fas.usda.gov/psdonline/psdQuery.aspx

Friedman, T., May 18 2013: Without Water, Revolution *New York Times* Available at: http://www.nytimes.com/2013/05/19/opinion/sunday/friedman-without-water-revolution.html?pagewanted=all&_r=0

Gillett, N., H. Graf, and T. Osborn, 2003: Climate change and the north Atlantic oscillation. The north Atlantic oscillation: climatic significance and environmental impact. e. a. J. W. Hurrell, *Geophys. Mono.*, **134**

Gillett, N. P., and J. C. Fyfe, 2013: Annular mode changes in the CMIP5 simulations,

Geophys. Res. Lett., **40**, 1189–1193, doi:10.1002/grl.50249.

Giorgi, F., 2006: Climate change Hot-spots. *Geophys. Res. Lett.*, **33**, L08 707.

Giorgi, F., and P. Lionello, 2008: Climate change projections for the Mediterranean region, *Global Planet. Change*, **63**, 90–104, doi:10.1016/ j.gloplacha.2007.09.005.

Held, I. M., and B. J. Soden, 2006: Robust responses of the hydrological cycle to global warming. *J. Clim.,* **19(21)**, 5686–5699.

Hinnebusch, R., 2012: Syria: from 'authoritarian upgrading' to revolution? *Int. Aff.,* **88.1**, 95-113.

Hoerling, M. P., J. W. Hurrell, and T. Y. Xu, 2001: Tropical origins for recent North Atlantic climate change. *Science,* **292(5514)**, 90–92

Hoerling, M. P., J. Eischeid, J. Perlwitz, X. Quan, T. Zhang, and P. Pegion, 2012: On the increased frequency of Mediterranean drought, *J. Clim.*, **25**, 2146–2161, doi:10.1175/JCLI-D-11-00296.1.

Hurrell, J. W., 1995: Decadal trends in the north-atlantic oscillation - regional temperatures and precipitation. *Science,* **269(5224)**, 676–679

Hurrell, J. W., Y. Kushnir, G. Ottersen, and M. Visbeck, 2003: An overview of the North Atlantic Oscillation. The North Atlantic Oscillation: climatic significance and environmental impact. e. a. JW Hurrell. *Geophys Mono.*, **134**, 1–35

Hurrell, J. W., et al., 2006: Atlantic climate variability and predictability: A CLIVAR perspective. *J. Clim.*, **19(20)**, 5100–5121

Intergovernmental Panel on Climate Change (IPCC), 2007: Climate Change 2007: The Physical Science Basis. Contribution of Working Group I to the Fourth Assessment Report of the Intergovernmental Panel on Climate Change, edited by S. Solomon et al., 996 pp., Cambridge Univ. Press, Cambridge, U. K.

Integrated Regional Information Networks (IRIN), 2 Sept. 2009: SYRIA: Drought driving farmers to the cities. (IRIN, Damascus, Syria).

IRIN, 24 Nov. 2009: SYRIA: Drought Response Faces Funding Shortfall (IRIN, Damascus, Syria).

IRIN, 17 Feb. 2010: SYRIA: Over a million people affected by drought. (IRIN, Damascus, Syria).

Jacobeit, J., A. Dunkeloh, and E. Hertig, 2007: Mediterranean rainfall changes and their causes, in Global Change: Enough Water for All?, edited by J. Lozan et al., pp. 195–199, Wiss. Auswertungen, Hamburg, Germany.

Jones, P., and I. Harris, 2008: CRU Time Series (TS) High Resolution Gridded Datasets, http://badc.nerc.ac.uk/view/badc.nerc.ac.uk__ATOM__ dataent_1256223773328276, Clim. Res. Unit, Univ. of East Anglia, Norwich, U. K.

Keeling, C. D., et al., 2001: Exchanges of atmospheric CO_2 and $^{13}CO_2$ with the terrestrial biosphere and oceans from 1978 to 2000. I. Global aspects, SIO Reference Series, No. 01-06, Scripps Institution of Oceanography, San Diego, 88 pages. http://scrippsco2.ucsd.edu/data/in_situ_co2/monthly_mlo.csv

Kalnay E, et al., 1996: The NCEP/NCAR 40-year reanalysis project. *Bull. Am. Meteorol. Soc.,* **77**, 437–471.

Kelley, C., M. Ting, R. Seager, and Y. Kushnir, 2012a: The relative contributions of radiative forcing and internal climate variability to the late 20th century winter drying of the Mediterranean region, *Clim. Dyn.*, **38(9–10)**, 2001–2015, doi:10.1007/s00382-011-1221-z.

Kelley, C., M. Ting, R. Seager, and Y. Kushnir, 2012b: Mediterranean precipitation climatology, seasonal cycle, and trend as simulated by CMIP5. *Geophys. Res. Lett.,* **39,** L21703, doi:10.1029/2012GL053416.

Khadour, Y., and M. Kafa, 2009: Discussion of Random and Informal Settlements in Damascus. *Geo. Spat. Inf. Sci.*, **12(4)**, 289-295. doi: 10.1007/s1180600901009.

al-Khalidi, A., S. Hoffmann, and V. Tanner, 11 June 2007, Iraqi Refugees in the Syrian Arab Republic: A Field-Based Snapshot. (Brookings Institute, Washington DC).

Khawaja, M., 2002: Internal migration in Syria: Findings from a national survey. (Fafo Institute for Applied International Studies, Oslo, Norway). http://almashriq.hiof.no/general/300/320/327/fafo/reports/375.pdf.

Kitoh, A., A. Yatagai, and P. Alpert, 2008: First super-high-resolution model projection that the ancient "Fertile Crescent" will disappear in this century. *Hydrol. Res. Lett.,* **2**, 1–4.

Kushnir, Y., W. A. Robinson, P. Chang, and A. W. Robertson, 2006: The physical basis for predicting Atlantic sector seasonal-to-interannual climate variability. *J. Clim.*, **19(23)**, 5949–5970

Kushnir, Y., and J. M. Wallace, 1989: Low-Frequency Variability in the Northern Hemisphere Winter: Geographical Distribution, Structure and Time-Scale Dependence. *J. Atmos. Sci.*, **46**, 3122–3143. doi: http://dx.doi.org/10.1175/1520-0469(1989)046<3122:LFVITN>2.0.CO;2

Lionello, P., and F. Giorgi, 2007: Winter precipitation and cyclones in the Mediterranean region: future climate scenarios in a regional simulation. *Adv. Geosci.,* **12**, 153–158. doi:10.5194/adgeo-12-153-2007.

Lu, J., G. A. Vecchi, and T. A. Reichler, 2007: Expansion of the Hadley cell under global warming. *Geophys. Res. Lett*, **34(6)**, doi:10.1029/ 2006GL028443

Mariotti, A., 2010: Recent changes in the Mediterranean water cycle: a pathway toward long-term regional hydroclimatic change? J. Clim., 23(6), 1513–1525, doi:10.1175/2009JCLI3251.1

Mariotti, A., and A. Dell'Aquila, 2012: Decadal climate variability in the Mediterranean

region: roles of large-scale forcings and regional processes. Clim. Dyn., doi:10.1007/s00382-011-1056-7

Mariotti, A., M. V. Struglia, N. Zeng, and K. Lau, 2002: The hydrological cycle in the Mediterranean region and implications for the water budget of the Mediterranean Sea. *J. Clim.*, **15**, 1674–1690.

Mariotti, A., N. Zeng, J. Yoon, V. Artale, A. Navarra, P. Alpert, and L. Li, 2008: Mediterranean water cycle changes: transition to drier 21st century conditions in observations and CMIP3 simulations. Environ. Res. Lett., 3(4), doi:10.1088/1748-9326/3/4/044001

Massoud, A., 2010: Years of Drought: A Report on the Effects of Drought on the Syrian Peninsula. (*Heinrich Böll Stiftung*, Berlin, Germany).

Meehl, G. A., et al., 2007: The WCRP CMIP3 multimodel dataset—a new era in climate change research. *B. Am. Meteorol. Soc.* **88(9)**, 1383–1394.

Nakicenovic, N., and R. Swart, 2000: Special report on emissions scenarios. Cambridge University Press, Cambridge.

Nehme, N., 1-2 July 2008: Contribution of Agriculture to the Progress of Economic Reforms in Syria. NAPC. (NAPC, Damascus, Syria). Proceedings No. 27, International Workshop.

New, M., M. Hulme, and P. D. Jones, 1999: Representing twentieth century space–time climate variability. Part 1: Development of a 1961–90 mean monthly terrestrial climatology, *J. Clim.*, **12**, 829–856, doi:10.1175/ 1520-0442(1999)012<0829:RTCSTC>2.0.CO;2.

New, M., M. Hulme, and P. D. Jones, 2000: Representing twentieth century space-time climate variability. Part 2: development of 1901–96 monthly grids of terrestrial surface climate, *J. Clim.*, **13**, 2217–2238, doi:10.1175/1520-0442(2000)013<2217:RTCSTC>2.0.CO;2.

Office for the Coordination of Humanitarian Affairs (OCHA), 29 Sept. 2008: Syria Drought Appeal (United Nation, New York, NY). Available at http://unocha.org/cap/appeals/syria-drought-appeal-2008.

Osborn, T. J., 2004: Simulating the winter North Atlantic Oscillation: the roles of internal variability and greenhouse gas forcing. *Clim.Dyn*. **22(6–7)**, 605–623.

Osborn, T. J., K. R. Briffa, S. F. B. Tett, P. D. Jones, and R. M. Trigo RM, 1999: Evaluation of the North Atlantic Oscillation as simulated by a coupled climate model. *Clim. Dyn*., **15(9)**, 685–702.

Previdi, M., and B. G. Liepert, 2007: Annular modes and Hadley cell expansion under global warming. *Geophys. Res. Lett*., **34(22)**, doi:10.1029/2007GL031243

Rodriguez, A., H. Salahieh, R. Badwan, H. Khawam, 2010: Groundwater Use and Supplemental Irrigation in Atareb, Northwest Syria. ICARDA Social Science Paper No.7.

Salamini, F., H. Ozkan, A. Brandolini, R. Schafer-Pregl, and W. Martin, 2002: Genetics and geography of wild cereal domestication in the Near East. *Nat. Rev. Genet*., **3(6)**

Salman, M., W. Mualla, 2008: Water Demand Management in Syria: Centralized and Decentralized Views. *Water Policy,* **10**, 6.5, doi:10.2166/wp.2008.065.

Schneider, E. K., L. Bengtsson, and Z. Z. Hu, 2003: Forcing of Northern Hemisphere climate trends. *J. Atmos. Sci*., **60(12)**, 1504–1521.

Schneider, U., T. Fuchs, A. Meyer-Christoffer, and B. Rudolf, 2008: Global precipitation analysis products of the GPCC. Global Precipitation Climatology Centre (GPCC), DWD, Internet publication: 1–12

Schwartz, F. W., and M. Ibaraki, 2011: Groundwater: A resource in decline. *Elements*, **7**, 175–179.

Seager, R., and N. Henderson, 2013: Diagnostic computation of moisture budgets in the

ERA-Interim Reanalysis with reference to analysis of CMIP-archived atmospheric model data. *J. Clim.*, in press.

Seager, R., H. Liu, N. Henderson, I. Simpson, C. Kelley, T. Shaw, Y. Kushnir, and M. Ting, 2013: Causes of increasing aridification of the Mediterranean region in response to rising greenhouse gases. *J. Clim.*, submitted.

Seager, R., et al., 2007: Model projections of an imminent transition to a more arid climate in southwestern North America. *Science,* **316(5828)**, 1181–1184.

Seager, R., N. Naik, and G. A. Vecchi, 2010: Thermodynamic and dynamic mechanisms for large-scale changes in the hydrological cycle in response to global warming. *J. Clim*, **23(17)**, 4651–4668.

Shadid, A., 23 June 2011: Syria's Ailing Economy Poses a Threat to Assad *New York Times* Available at http://www.nytimes.com/2011/06/24/world/middleeast/24damascus.html?_r=1.

Shindell, D. T., R. L. Miller, G. A. Schmidt, and L. Pandolfo, 1999: Simulation of recent northern winter climate trends by greenhouse-gas forcing. *Nature,* **399(6735)**, 452–455.

Simpson, I., T. A. Shaw, and R. Seager, 2013: A diagnosis of the seasonally and longitudinally varying mid-latitude circulation response to global warming. *J. Atmos. Sci.,* submitted.

Solh, M., 27 Sept. 2010: Tackling the drought in Syria. *Nature Middle East,* doi:10.1038/nmiddleeast.2010.206.

Solomon, S., D. Qin, M. Manning, Z. Chen, M. Marquis, K. B. Avery, M. Tignor, and H. L. Miller, (eds.) 2007: IPCC, 2007: climate change 2007: the physical science basis. Contribution of working group I to the fourth assessment report of the intergovernmental panel on climate change

Taylor, K. E., 2001: Summarizing multiple aspects of model performance in a single

diagram, *J. Geophys. Res.*, **106(D7)**, 7183–7192, doi:10.1029/ 2000JD900719.

Taylor, K. E., R. J. Stouffer, and G. A. Meehl, 2012: An overview of CMIP5 and the experiment design, *Bull. Am. Meteorol. Soc.*, **93(4)**, 485–498, doi:10.1175/BAMS-D-11-00094.1.

Thompson, D. W. J., J. M. Wallace, and G. C. Hegerl, 2000: Annular modes in the extratropical circulation. Part II: Trends. *J. Clim*, **13(5)**, 1018–1036.

Thompson, D. W. J., S. Lee, and M. P. Baldwin, 2003: Atmospheric processes governing the Northern Hempisphere Annular Mode/North Atlantic Oscillation. The North Atlantic Oscillation: climatic significance and environmental impact. e. a. J.W. Hurrell. *Geophys. Mono.*, **134**, 81–112.

Ting, M. F., Y. Kushnir, R. Seager, and C. H. Li, 2009: Forced and Internal Twentieth-Century SST Trends in the North Atlantic. *J. Clim.*, **22(6)**, 1469–1481.

Trigo, I. F., T. D. Davies, and G. R. Bigg, 2000: Decline in Mediterranean rainfall caused by weakening of Mediterranean cyclones. *Geophys. Res. Lett.*, **27**, 2913–2916.

Trigo, R. M., C. Gouveia, and D. Barriopedro, 2010: The intense 2007–2009 drought in the Fertile Crescent: Impact and associated atmospheric circulation, *Agric. Meteorol.*, **150**, 1245–1257, doi:10.1016/j. agrformet.2010.05.006.

USDA Foreign Agricultural Service. Production, Supply and Distribution Online Database. Available at http://www.fas.usda.gov/psdonline/psdQuery.aspx

United Nations High Commissions for Refugees (UNHCR), 8 Oct. 2010: Iraqi refugees in Syria reluctant to return to home permanently: survey. (United Nations, Geneva, Switzlerland). Available at http://www.unhcr.org/4caf376c6.html.

Venzke, S., M. R. Allen, R. T. Sutton, and D. P. Rowell, 1999: The atmospheric response over the North Atlantic to decadal changes in sea surface temperature. *J. Clim.*, **12(8)**, 2562–2584.

Vose, R. S., et al., 1992: The Global Historical Climatology Network: long-term monthly temperature, precipitation, sea level pressure, and station pressure data. ORNL/CDIAC-53, NDP-041. Carbon Dioxide Information Analysis Center, Oak Ridge National Laboratory, Oak Ridge, Tennessee.

Werrell, C., and F. Femia, Feb. 2013: The Arab Spring and Climate Change. Center for American Progress.

Woollings, T., 2010: Dynamical influences on European climate: an uncertain future. *Phil. Trans. R. Soc. A*, **368**, 3733–3756, doi:10.1098/rsta.2010.0040

Wu, Y., R. Seager, M. Ting, N. Naik, and T. Shaw, 2012: Atmospheric circulation response to an instantaneous doubling of carbon dioxide. Part I: Model experiments and transient thermal response in the troposphere. *J. Clim.*, **25**, 2862–2879.

Wu, Y., R. Seager, M. Ting, N. Naik, T. Shaw, 2012: Atmospheric circulation response to an instantaneous doubling of carbon dioxide. Part II: Atmospheric transient adjustment and its dynamics. *J. Clim.*, **26**, 918.

Wu, Y., M. F. Ting, R. Seager, H. Huang, and M. Cane, 2011: Changes in storm tracks and energy transports in a warmer climate simulated by the GFDL CM2.1 model. *Clim. Dyn.*, doi:10.1007/ s00382-010-0776-4

Yin, J. H., 2005: A consistent poleward shift of the storm tracks in simulations of 21st century climate. *Geophys. Res. Lett.* **32(18).**

Zappa, G., L. C. Shaffrey, K. I. Hodges, P. G. Sansom, and D. B. Stephenson, 2013: A multi-model assessment of future projections of North Atlantic and European extratropical cyclones in the CMIP5 climate models. *J. Clim.*, in press.

Ziv, B., Y. Kushnir, J. Nakamura, N. H. Naik,, and T. Harpaz, 2013: Coupled climate model simulations of Mediterranean winter cyclones and large-scale flow patterns. *Nat. Hazard Earth Sys.*, **13**, 779–793.